Tampere University

Jan Sindelar

MECHANICAL TESTING AND IN VITRO DEGRADATION OF COMPOSITE MATERIALS FOR BONE TISSUE ENGINEERING

Faculty of Medicine and Health Technology
Master of Science Thesis
July 2022

ABSTRACT

Jan Sindelar: Mechanical Testing and in vitro Degradation of Composite Materials for Bone Tissue Engineering
Master of Science Thesis
Tampere University
Master's Degree Programme in Biomedical Sciences and Engineering
July 2022

Mechanical testing is one of the most common and most performed characterization methods when studying scaffolds for tissue engineering. Knowledge of the mechanical properties of tissue engineering scaffolds is important since unsuitable mechanical properties are likely to lead to implant failure and possibly even to the damage of surrounding tissues. This is even more of importance for implants in load bearing applications.

Static mechanical testing is simple to perform and commonly used. However, for many materials, it does not provide information about their behaviour under long-term sustained or dynamic loads. Creep-recovery, stress relaxation, and dynamic testing are used to assess such behaviour. However, as it is complicated, it is not commonly performed.

In this thesis, static, dynamic, and creep-recovery testing was performed to assess the complex mechanical behaviour of two composite materials that are being developed for bone tissue engineering. The composites consist of a biodegradable, thermoplastic polymer matrix and a bioceramic filler. Poly-L-DL-lactide was used as a matrix in both composites and bioactive glass 13-93 was used as a filler in one composite and β-tricalcium phosphate in the other. Tensile and compression mechanical testing was performed. Specimens of porous scaffolds were used for compression testing and compact plates for tensile testing. Mechanical properties were assessed over the course of 12 weeks of in vitro degradation in a TRIS buffer solution. Additionally, ion release from the porous scaffolds was measured.

Strength and mass retention were evaluated for the degradation period. Creep and recovery and dynamic testing confirmed that both materials showed strong viscoelastic behaviour and their mechanical behaviour was changing considerably during cyclic dynamic testing, however, less strongly in the case of the β-tricalcium phosphate containing composite.

Results obtained from mechanical testing can be used for mathematical modelling to perform finite element analysis and create constitutive models. Such models and simulations can then be used to aid the design of the final tissue engineering scaffolds.

Keywords: mechanical testing, viscoelasticity, composite, bone tissue engineering

PREFACE

This thesis was done for the Biomaterials and Tissue Engineering and the Bioceramics, -glasses, and -composites groups.

I would like to thank my supervisors prof. Minna Kellomäki, prof. Jonathan Massera and M.Sc. Mart Kroon for providing me an interesting topic and guidance for my work. I would also like to thank Agata Szczodra, who taught me glass preparation and processing, buffer preparation, and principles of in vitro degradation, as well as ran the ICP-OES measurements for me. Mart Kroon, who taught me composite extrusion and compression moulding and did some of the extrusions with me. Olli Korhonen who introduced me to supercritical CO_2 foaming and assisted me with my first trials, and finally, to my colleagues from both research groups for help, advice, and support during the thesis process.

Tampere, 31. July 2022

Jan Sindelar

CONTENTS

1. INTRODUCTION 1
2. BIOMATERIALS FOR TISSUE ENGINEERING 3
   2.1 Biodegradable polymers 3
      2.1.1 Natural biodegradable polymers 4
      2.1.2 Synthetic biodegradable polymers 4
   2.2 Bioceramics 6
      2.2.1 Bioactive glasses 7
   2.3 Composites 7
      2.3.1 Porous scaffolds for bone tissue engineering 8
3. MECHANICAL TESTING 10
   3.1 Fundaments of mechanical testing, uniaxial static testing 10
   3.2 Modes of loading 15
      3.2.1 Tensile testing 16
      3.2.2 Compression testing 16
      3.2.3 Torsion 17
      3.2.4 Bending 18
      3.2.5 Shear 18
   3.3 Time-dependent behaviour, dynamic testing 18
      3.3.1 Viscoelasticity, creep, and stress relaxation 19
      3.3.2 Cyclic loading and fatigue 22
4. MATERIALS AND METHODS 26
   4.1 Sample preparation 26
      4.1.1 Bioactive glass preparation 26
      4.1.2 Composite Extrusion 27
      4.1.3 Supercritical CO_2 foaming 27
      4.1.4 Compression Moulding 28
      4.1.5 Specimens for mechanical testing 29
   4.2 In vitro degradation 30
   4.3 Mechanical Testing 31
      4.3.1 Static testing 32
      4.3.2 Creep-recovery testing 32
      4.3.3 Dynamic testing 32
   4.4 Water Absorption and Mass Loss Analysis 33
   4.5 Ion release analysis 33
5. RESULTS AND DISCUSSION 34
   5.1 In vitro degradation 34
      5.1.1 Changes in pH and water uptake 34
      5.1.2 Strength and mass retention 36
   5.2 Ion release 37
   5.3 Mechanical testing 39
      5.3.1 Static testing 39

5.3.2 Creep-recovery testing 44
5.3.3 Dynamic testing 47
5.3.4 Confined compression testing 51
6. CONCLUSION 54
REFERENCES 56
A. COMPLETE STRESS-STRAIN CURVES I
A.1. Tensile testing i
A.1.1. Week 0 i
A.1.2. Week 4 ii
A.1.3. Week 8 iii
A.1.4. Week 12 iv
A.2. Unconfined compression testing v
A.2.1. Week 0 v
A.2.2. Week 4 vi
A.2.3. Week 8 vii
A.2.4. Week 12 viii
A.3. Confined compression ix
A.3.1. Week 0 ix
A.3.2. Week 4 x
A.3.3. Week 8 xi
A.3.4. Week 12 xii

LIST OF FIGURES

el***Figure 1.*** *A comparison of typical stress-strain curves of various materials [3]..... 11*
Figure 2. *Tangent and secant modulus of elasticity [1]..... 12*
Figure 3. *Stress-strain curve of a porous material, with the first maximum compressive strength, indicated as point 3. Modified from [67] 12*
Figure 4. *Stress-strain diagram with curves showing typical behaviour in a static tensile test of plastics with important stress and strain values marked. 1) hard and brittle polymer that breaks without yielding. 2) and 3) Ductile material that exhibits/does not exhibit significant strain hardening after yield. 4) Rubber-like material that breaks at high strains without a prior decrease in stress. Subscripts indicate: y = yield, m = maximum; ultimate strength; b = break. Modified from [64]..... 13*
Figure 5. *Proportional limit and offset yield point with 0.2% offset [1] 14*
Figure 6. *Comparison of true and engineering stress and strain in a static tensile test. Ultimate tensile strength peak cannot be seen in the true stress-strain curve [1]..... 15*
Figure 7. *Some of the most common modes of mechanical testing [3]..... 15*
Figure 8. *Confined compression testing configuration [1]..... 17*
Figure 9. *Most common constitutive models for viscoelastic creep-recovery and stress relaxation testing [3]..... 21*
Figure 10. *Burgers model of viscoelastic material. It allows modelling of instantaneous deformation and recovery thanks to the serial spring (yellow), retarded creep strain and delayed strain recovery thanks to the parallel spring and dashpot (blue) and permanent ceep and permanent creep strain thanks to the serial dashpot (red) [80]..... 21*
Figure 11. *S-N diagram with a Wöhler's curve of wood filled PLA composite. Modified with additional comments from [86]..... 23*
Figure 12. *Viscoelastic properties that can be obtained from a cyclic testing: Elastic recoverable deformation $\Delta\varepsilon e$, cumulative non-recoverable deformation $\varepsilon creep$, phase angle δ, complex modulus E^*, and storage and loss moduli E' and E".....24*
Figure 13. *Material loaded in the Teflon mould (left). Porous rods of the bioactive glass (top) and β-TCP (bottom) composite. There is non-porous skin on the surface of the rods. 28*
Figure 14. *Drawing with important dimensions of the mould used for compression moulding of the plates. 28*
Figure 15. *Pieces of rods in the mould and moulded plates. 29*
Figure 16. *A: specimens for compression testing punched from cut pieces of the porous rods. Variability in height is due to the manual equipment used for the cutting. B: specimens for tensile testing of the two different composites (top – bioactive glass, bottom – β-TCP)..... 30*
Figure 17. *Changes in the pH value of the degradation medium, presented as mean (n=5). Medium was replaced after every time point for a new one with a pH of 7.4. ..... 35*
Figure 18. *Swelling of the scaffolds and plates during the degradation. Presented as mean ± SD (n=6-22)..... 35*
Figure 19. *Mass and strength retention. A: porous scaffolds, 0.2 % offset yield compressive strength retention shown; B: plates, ultimate tensile strength retention shown. Presented as % of the original mass and strength. Presented as mean values (mass loss: n=6-22, strength loss: n=3-7). 36*

Figure 20. *Cumulative release of ions during degradation. Presented as mean (n=5 for weeks 1 and 2, n=3 for remaining timepoints). For clarity, error bars are not shown.* 38
Figure 21. *Representative stress-strain curves of week 0 compression testing. Representative curves selected from 4 BaG and 4 TCP specimens.* 40
Figure 22. *Representative stress-strain curves of week 0 tensile testing. Tensile strength of the TCP composite is significantly higher (p=0.001). Representative curves selected from 5 BaG and 3 TCP specimens.* 40
Figure 23. *Tensile specimen degraded for 8 weeks and tested beyond 10 % strain without rupture.* 41
Figure 24. *Comparison of stress-strain curves from tensile testing during the degradation. Representative curves for each time point shown.* 42
Figure 25. *Comparison of stress-strain curves from unconfined compression testing during the degradation. Representative curves for each time point shown.* 42
Figure 26. *A: tensile elastic modulus, B: global compressive elastic modulus. Presented as mean ± SD (n=3-7).* 44
Figure 27. *Results from week 8 compression creep-recovery test. All curves have a non-zero slope at the end of the creep phase, indicating the presence of permanent creep, which also results in non-recoverable deformation after the end of the recovery phase.* 45
Figure 28. *Maximum creep strain* εmax *and permanent creep strain* $\varepsilon\infty$ *in compression creep testing. Presented as mean ± SD (n=3-5).* 46
Figure 29. *Maximum creep strain* εmax *and permanent creep strain* $\varepsilon\infty$ *in tensile creep testing. Presented as mean ± SD (n=2-4).* 46
Figure 30. *Changes in peak stress values of the bioactive glass composite during degradation and between cycles 300 and 1000 in a compression test. Presented as mean ± SD (n=3-5).* 48
Figure 31. *Changes in peak stress values of the TCP composite during degradation and between cycles 300 and 1000 in a compression test. Presented as mean ± SD (n=3-5).* 48
Figure 32. *Average percentual drop in stress peak values between cycles 300 and 1000.* 49
Figure 33. *Stress peaks during cyclic loading from the point when the loading waveform stabilized. A representative curve showing behaviour that was shared by all specimens at all time points. The incremental decrease in stress has a decreasing trend.* 50
Figure 34. *Decrease in height of a specimen under cyclic load driven by stress with different peak loads. Under peak loads below yield, the incremental decrease in height between cycles is decreasing [48].* 50
Figure 35. *Representative stress-strain curves from confined and unconfined compression testing.* 53

LIST OF SYMBOLS AND ABBREVIATIONS

BaG	bioactive glass
ECM	extracellular matrix
HA	hydroxyapatite
ISO	
ICP-OES, ICP	inductively coupled plasma optical emission spectroscopy
PBS	polybutylene succinate
PCL	polycaprolactone
PGA	polyglycolide
PIPS	pressure-induced phase separation
PLA	polylactide
PLCL	Poly-lactide-co-caprolactone
PLGA	poly-lactide-co-glycolide
POM	polyoxymethylene
PTC	poly(trimethylene carbonate)
PTFE	polytetrafluorethylene
$scCO_2$	supercritical CO_2
TCP	tricalcium phosphate, β-tricalcium phosphate
TIPS	thermally induced phase separation

A	area
A_0	initial area
°C	Celsius degrees
E	Young's modulus of elasticity
E'	storage modulus
E''	loss modulus
E^*	complex modulus
F	force
L	length
L_0	initial length
N	number of cycles
N_f	number of cycles to failure
S	stress
S_f	stress amplitude
Δ	phase angle
ε	strain
ε_0	strain amplitude
ε_∞, ε_{creep}	permanent creep strain
ε_e	elastic strain
ε_{max}	maximum strain
ε_T	true strain
σ	stress
σ_T	true stress
σ_0	stress amplitude

1. INTRODUCTION

Mechanical testing is one of the main characterization methods for tissue engineering scaffolds. It is performed at some stage of the development on nearly all materials and structures since suitable mechanical properties are critical for the success of the implant [1,2]. Each application requires different mechanical properties, and it must be ensured, that the proposed materials and structures of the scaffold match the requirements. Mismatch in mechanical properties is likely to lead to implant failure. Too weak implant might not sustain the applied load and yield or brake, get loose and potentially damage surrounding tissues. Too stiff implant leads to stress shielding. The implant carries all the load and there will be insufficient mechanical stimulation. The lack of sufficient mechanical stimulation then leads to osteolysis. The tissue does not regenerate, and the implant may even loosen and thus fail [2,3]. Moreover, cells can sense the stiffness of the substrate they adhere to, and it affects their fate. An implant with unsuitable stiffness for a particular application might not support cell attachment, differentiation and proliferation so well, as an implant with suitable stiffness would [1,2].

Uniaxial static mechanical testing is the fundamental and most common, often the only performed type of mechanical testing, as it is relatively simple to perform and analyse [3,4]. However, many materials show very different mechanical behaviour when they are subject to sustained load over long periods of time or when they are subject to cyclic loads, such as many movements of our body, including walking, breathing and heartbeat [3]. Behaviour under such conditions cannot be predicted based on static testing [3,5]. Elastic, time-independent behaviour is assumed during static testing, and it describes well the behaviour of metals. However, many other materials, including most tissues and thermoplastic polymers, exhibit viscoelastic, rather than elastic mechanical behaviour, characterized by creep under sustained load and stress relaxation under sustained deformation [1,3]. Such behaviour is assessed by creep and recovery and stress relaxation testing. Behaviour under cyclic load is assessed by cyclic dynamic testing [6,7]. Yet such tests are difficult to perform and therefore not commonly done. Nevertheless, neglecting the viscoelastic properties and the effect of cyclic loading may also lead to implant failure due to the accumulation of permanent creep deformation or due to fatigue by cyclic loading [2,3].

The aim of this thesis was to perform complex mechanical testing of materials for bone tissue engineering under static and dynamic conditions. Static, creep-recovery, and cyclic dynamic testing were performed in tension and compression. Compression testing was done also as confined compression in addition to traditional unconfined compression. It may allow to better estimate in situ performance of the tissue engineered scaffolds as they are usually implanted into at least partially confined places [8,9]. All tests were done at simulated physiological conditions in a water bath at 37 °C because the mechanical behaviour of used materials is heavily dependent on temperature. Tests were performed at 4 time points during a 12-week in vitro degradation. In addition, ion release and change in the pH of the buffer solution was measured at week 1 and 2 and then every two weeks.

2. BIOMATERIALS FOR TISSUE ENGINEERING

Over the past decades, there has been a growing interest and need for the development of novel tissue regeneration solutions. Due to the ageing population, the survival time of many implants from biostable materials, that focus on the replacement of tissue function, is becoming insufficient [10]. Therefore, the interest in new implant development has shifted from tissue replacement to tissue regeneration that can be achieved by tissue engineered products. Instead of biostable nearly inert materials, biodegradable and especially bioactive materials are used and often combined with cells or growth factors to achieve desired therapeutic effect [10,11]. With successful tissue engineered products, also another pressing problem can be solved. In many situations, damaged tissue cannot heal itself and implants replacing its function are unavailable or have a poor survival rate. Small blood vessels and large bone defects are examples of such situations. Currently, they are mostly treated with autografts and allografts [12–14]. However, such solutions have many limitations. There is a limited number of sites from where autografts can be harvested, and the harvest can cause donor site morbidity. There is low availability of allografts, and they pose a risk of transfer of infection or rejection by the immune system. Therefore, tissue engineering products that provide temporary support and aid the native tissue regeneration present an optimal solution [12–14].

The main materials used nowadays for tissue engineering scaffolds are biodegradable polymers and bioceramics [2,15]. Besides offering structural support they also degrade in the environment of the human body, fulfilling one of the main requirements of tissue engineering products, that they should degrade and be replaced by native tissues as part of the healing process [2,13,16]. Many natural polymers and bioceramics also enhance the healing process. Usually, composites are used, as there is no ideal material with all the required properties, such as sufficient strength, optimal degradation time and promotion of tissue healing. By combining different materials, a suitable product that has the required properties can be made [2,15].

2.1 Biodegradable polymers

Biodegradable polymers are a large group of polymeric materials that can be decomposed by natural processes either in nature or in the human body. They feature a wide range of properties that can be combined and tailored to fit the desired application. Many can be processed using traditional processing techniques and using different materials,

structures ranging from soft hydrogels to tough, rigid, structures can be prepared. There are two main groups of biodegradable polymers: natural and synthetic. Natural polymers occur naturally in nature, and they are produced by living organisms, while synthetic polymers, despite being made from naturally occurring monomers, are made by synthetic polymerization techniques [2,17,18]. Not only their origin but also their properties are different. Many natural polymers feature bioactivity, but they are mechanically rather weak, and their preparation is complicated and often features high batch to batch variation. Synthetic biodegradable polymers are usually thermoplastic, and therefore they can be processed by traditional melt processing techniques [2]. However, they are not bioactive, and they can only act as a structural component of the scaffold. They are inert and do not promote healing in any way. Therefore, they are usually used as a part of a composite or for applications where tissue adhesion is not important [2].

2.1.1 Natural biodegradable polymers

Natural biodegradable polymers comprise two main groups of materials: polysaccharides and proteins. They degrade mostly by enzymatic degradation by specific or non-specific enzymes. They are derived from natural sources such as plants, fungi, microorganisms, or animals. Many of them are natural constituents of the human extracellular matrix (ECM) and have binding sites for cells and other ECM components [2,17,19]. They also generally have various functional groups that allow chemical and enzymatic modifications. Such modifications can even further increase tissue regeneration capabilities or that can be used to improve their mechanical properties or to create smart materials, such as injectable, in situ gelling hydrogels or self-healing materials. They are also usually hydrophilic, and some have high water-binding capabilities [2,19,20]. However, they are difficult to process because of their complicated chemical structures and low degradation temperatures. Furthermore, due to the complex extraction process, they feature high batch-to-batch variations. As their degradation is mostly facilitated by enzymes, it can also differ between individuals and the degradation rate is more difficult to predict than in the case of synthetic polymers [20,21].

2.1.2 Synthetic biodegradable polymers

Synthetic biodegradable polymers are synthesized by traditional polymerization techniques, such as ring-opening polymerization or condensation polymerization. They are mostly synthetized from naturally occurring monomers that are usually obtained by fermentation of saccharides, but they can be also petroleum-based [2,22,23]. Because they are thermoplastic, they can be processed by traditional melt processing methods such

as extrusion or injection moulding. Various shapes, such as rods, plates, sheets, fibres, screws, films, micro- and nanospheres or porous scaffolds can be made relatively easily when compared to natural polymers [2,16,18,24]. They can be also electrospun and 3D printed. Polylactide (PLA), one of the synthetic biodegradable polymers is considered one of the most easily printable materials for 3D printing [24,25]. Most synthetic biodegradable polymers are aliphatic polyesters, such as polylactide (PLA), polyglycolide (PGA), polybutylene succinate (PBS), polycaprolactone (PCL), poly(trimethylene carbonate) (PTC), or poly(p-dioxanone) [2,19,22,26–28]. All these materials have distinct properties. Combining them into copolymers and blends provides opportunities to finely tune the mechanical properties and degradation rate. Therefore, most available products from biodegradable polymers are made from either copolymers or blends. PGA is highly crystalline, brittle, hydrophilic, and fast degrading in vivo, while the other materials are hydrophobic and rather slowly degrading. It is usually used as the main material of fast resorbing sutures or as a part of copolymers and blends to increase their degradation rate [18]. PLC and PTC are highly ductile, and they are used in blends to increase elasticity and malleability [26,27]. PLA is the most widely available and most common biodegradable polymer. It is synthesized by ring-opening polymerization from lactide – a dimer of lactic acid. It exists as two stereoisomers – L and D. Only the L isomer is naturally occurring [18]. Poly-L-lactide is semicrystalline, with a glass transition temperature of 60 °C and melting temperature of 180 °C. Its methyl groups make it hydrophobic, which causes slow degradation. It may take 2-6 years to fully degrade, which is not suitable for most clinical applications [29,30]. The degradation rate can be increased by copolymerization of L-lactide with D-lactide. Copolymers of poly-L-lactide with poly-DL or D-lactide are the most commonly used PLA copolymers that combine only stereoisomers of PLA. If the portion of DL-lactide or D-lactide is more than 15%, the resulting polymer is fully amorphous. If the degradation rate needs to be further increased, poly-lactide-co-glycolide (PLGA) is commonly used [16,18]. Poly-lactide-co-caprolactone (PLCL) is another common copolymer for applications that require higher elasticity [27]. Synthetic biodegradable polymers degrade by hydrolysis and their monomers, such as lactic acid in the case of PLA, can be metabolised by the human body [30]. They degrade mostly by bulk degradation – homogenously throughout the whole structure, as opposed to surface degradation of materials like ceramics. Usually, autocatalytic degradation also happens if bigger bulk of the material is used – acidic monomers trapped inside the structure increases the degradation rate and the bulk degrades faster inside than on the surface [31]. Unlike natural polymers, synthetic polymers behave as nearly inert. They do not bind with surrounding tissues, but a fibrous capsule is formed around implants made

from synthetic polymers upon implantation as a result of foreign body reaction [2]. Therefore, in applications where binding with surrounding tissues is desired, bioactivity needs to be introduced. Composite and hybrid materials are then used, that contain besides the nearly inert synthetic polymers also natural polymers, bioactive ceramics, or bioactive glasses [2,32].

2.2 Bioceramics

Bioceramics are inorganic materials especially important in, but not limited to, bone tissue regeneration. The group of bioceramic materials includes nearly inert bioceramics, bioresorbable calcium phosphate ceramics, bioactive glasses, and glass-ceramics that are partially crystallized glasses [33]. Nearly inert bioceramics, such as aluminium oxide, zirconium oxide or titanium oxide are used for permanent implants such as parts of joint prosthesis but generally not for tissue engineering as they are not biodegradable [33,34].

Calcium phosphate ceramics are used because their composition is similar to the inorganic part of bone tissue and due to their osteoconductivity [34]. The main calcium-phosphate ceramics are hydroxyapatite (HA), tricalcium phosphate (TCP) and biphasic calcium phosphate, which is a mixture of HA and TCP [33,34]. Hydroxyapatite is the inorganic phase of the bone tissue. For use in bone tissue regeneration, natural HA can be derived from coral or bovine bone. More commonly, it is prepared synthetically. When implanted, it degrades and is eventually remodelled to native hydroxyapatite [34,35]. TCP, on another hand, is less stable, more soluble, and more widely used [34,36,37]. Calcium phosphate ceramics are used mainly as bone cement, fillers, spacers and as a coating on metallic implants to enable bonding with the native tissue [34,35]. They are also used as fillers in composite materials with the polymeric matrix to improve mechanical properties and introduce bioactivity [38–40].

Tricalcium phosphate, $Ca_3(PO_4)_2$, exists in three polymorphic forms: α, α’ and β, with a Ca to P molar ratio of 1.48. β-TCP is rhomboedral and stable at room temperature, α and α’ are high-temperature forms with monoclinic and hexagonal crystal structures, respectively. β-TCP transforms at 1125°C to α-TCP, which transforms to α’-TCP at 1430°C. α’-TCP exists only above this temperature, while α-TCP can be cooled down without changing to β. Both α and β variants are used, however, α-TCP is less stable and more reactive and soluble, and it is mostly used as a powder for the preparation of bone cement. β-TCP is the most commonly used form of TCP and is used in various applications and in various shapes, such as powder, granules and micro- or microporous structures [36,37,41].

TCP is synthesized by various methods at high temperatures. Most commonly, it is prepared from calcium deficient hydroxyapatite at ≥800 or ≥1125°C, yielding β- and α-TCP respectively. Other methods include heating of amorphous calcium phosphate or by reaction of solid precursors, such as $CaHPO_4$ and $CaCO_3$ at high temperatures around 1000°C [36,41,42].

2.2.1 Bioactive glasses

Bioactive glasses have been of great interest in the recent decades because of their bioactivity and osteostimulative properties. The first bioactive glass was discovered in 1969. It was found that ions that are released from the dissolving glass function as growth factors and attract osteoprogenitor cells and thus stimulate bone tissue growth [43].

The mechanism of bone growth stimulation by bioactive glass has two ways. One is direct bone tissue growth on the interface between the glass and the host tissue. Upon implantation, as a result of dissolving ions, a silica gel layer is formed on the surface of the implanted glass. Amorphous calcium phosphate precipitates on the layer and crystalizes into natural hydroxyapatite that triggers new bone tissue formation by osteoblasts [15,43]. The other is the action of the dissolved ions, released from the glass. They attract osteoprogenitor cells, stimulate differentiation into mature osteocyte phenotype, and trigger apoptosis of cells incapable of differentiation [15,43]. It is a process referred to as osteostimulation that is superior to the osteoconductive property of phosphate ceramics, that only provide an interface for migration and proliferation of the osteoprogenitor cells [34,43,44].

2.3 Composites

There are many requirements that materials for tissue engineering should meet and very often, individual materials cannot meet them. The most common of such requirements is the combination of bioactivity and sufficient strength and compliance [22,32]. Many natural polymers support cell attachment and proliferation, but they do not have sufficient strength for applications in hard tissue reconstructions [17]. Bioactive glasses have osteostimulative properties and sufficient compressive strength, but they are hard and brittle and have low tensile strength and low resistance to dynamic loads [14]. Synthetic polymers are relatively easy to process, but they may not have sufficient strength and stiffness and they behave as nearly inert, as described previously [2,22,32,45]. However, if glass particles are introduced into a matrix of natural or synthetic polymer, the benefits of both materials can be combined, and shortcomings overcome [2]. A scaffold made from hydrogel with dispersed glass particles features bioactivity, osteostimulation, and

sufficient strength for less demanding applications [46,47]. By the introduction of glass particles into the matrix of synthetic polymer, strength and stiffness are increased, and osteostimulation is introduced, while keeping the relatively simple processability of the polymer [2,18,45]. In addition, unwanted permanent deformation by creep is reduced [48–50]. Therefore, especially for scaffolds for bone tissue engineering, composites and hybrids are the most common materials [51,52]. The difference between composite and hybrid materials is in the interactions between the constituents. While composite materials are a physical mixture and their properties are the combination of properties of the constituents, hybrid materials may have completely new properties caused by interactions between the constituents on a molecular level [53]. One of the most important applications of composites as scaffold materials is bone tissue engineering because of the demands for high strength and osteostimulation or at least osteoconduction, as described previously. Therefore, some approaches to bone tissue engineering composite scaffolds will be reviewed.

2.3.1 Porous scaffolds for bone tissue engineering

For applications that do not require high strength, hydrogels with dispersed particles of bioactive glass or ceramics are researched. Their advantage is a combination of natural polymer that might contain binding sites for cells and bioactive filler that might attract them, maximizing the regeneration effect [47]. However, they are not suitable for all applications because they are relatively weak. For such applications, porous structures are developed, where the main structural material is either a synthetic biodegradable polymer or bioactive ceramic, especially glass. 3D printed ceramic structures are used for scaffolds where the ceramic is the main component. The main shortcoming of bioactive ceramics is their brittleness and low fracture toughness [14,54]. Therefore, they may be combined with other materials to overcome these issues. A hydrogel may be cast around the ceramic structure to provide a temporary structure for cell attachment and possibly also deliver stem cells to enhance tissue healing [55]. The glass structure can be coated with a synthetic biodegradable polymer. By such an approach, load-bearing capability, strength, and toughness are increased dramatically, and brittle behaviour was changed to non-brittle, ductile. The main means of improvement of the load-bearing capability is the healing of microcracks present in the ceramic structure by the coating and preventing them from propagation [14,54]. Another approach is a composite with a matrix from a synthetic biodegradable polymer and a filler of bioceramic particles. Various methods are used to create porous scaffolds from such composite. The main ones are solvent casting with particle leaching, electrospinning, 3D printing, and thermally or pressure-

induced phase separation (TIPS/PIPS) [56–58]. Particularly 3D printing and PIPS with supercritical CO_2 are of great interest, as they do not rely on toxic solvents and therefore supress the risk of toxic residues in the final scaffold [58,59].

Supercritical CO_2 ($scCO_2$) foaming by PIPS or TIPS can produce foam without using any solvent. Supercritical liquid occurs at high temperature and pressure and has properties of both liquid and gas. They have a density of a liquid, which gives them a high solvent power, but they are compressible like a gas, and their density can be therefore regulated by pressure. They have also low viscosity like gases, which gives them a high mass diffusivity [60,61]. The supercritical $scCO_2$ foaming process begins with a saturation of the polymer with the supercritical gas at high pressure and temperature. Then it is brought to a supersaturated state by either increasing the temperature (TIPS) or decreasing the pressure (PIPS). It starts the nucleation of the pores and their growth. It is driven by the difference between temperature and glass transition temperature, and therefore it can be controlled by heating or depressurization rate to produce scaffolds with desired pore size [62].

3. MECHANICAL TESTING

Mechanical properties are one of the most important properties of scaffolds for tissue engineering and orthopaedic implants. Mechanical testing is almost always performed during their development. Many types of mechanical testing exist, here the most common are reviewed.

3.1 Fundaments of mechanical testing, uniaxial static testing

The most common and most basic way to evaluate material response to external load is static testing, usually done in uniaxial tension or compression. Uniaxial tension or compression applied to a homogenous specimen produces theoretically homogenous stress distribution, and the test can be easily controlled and results easily interpreted [1]. The specimen is subject to a loading ramp, and the force applied by the instrument as well as displacement of the specimen is recorded. To obtain material properties independent of specimen dimensions, stress and strain are calculated [1,3]. The true stress in the material can be calculated by dividing the load (F in N) by cross-section (A in mm^2):

$$\sigma_T = \frac{F}{A} \tag{1}$$

However, as the determination of real-time cross-section is difficult or impossible to carry out, engineering stress, that is calculated using an initial cross-section is generally used:

$$\sigma = \frac{F}{A_0} \tag{2}$$

True strain at point i, also referred to as logarithmic strain is calculated as an integral from original length L_0 to a length L_i:

$$\varepsilon = \frac{dL}{L} = \int_{L_0}^{L_i} \frac{dL}{L} = \ln\left(\frac{L_i}{L_0}\right) \tag{3}$$

However, similarly as in the case of stress, engineering strain, calculated as deformation as a portion of the original length, is generally used:

$$\varepsilon = \frac{\Delta L}{L_0} = \frac{L - L_0}{L_0} \tag{4}$$

It can be expressed as dimensionless, but most commonly, it is presented as a percentual value [1].

In static testing, a ramp with a constant rate is applied. Stress, strain, force, and displacement ramp can be used to drive the test in theory. However, most commonly, the test is driven by displacement, as specified by ISO standards. For plastics, it is the only standardized option for static testing, for metals also stress ramp is standardized [63–65]. A strain ramp is not commonly used, because it is difficult to be precisely controlled by the machine when the strain rate response of the material is not known [63]. The test is stopped when the specimen breaks or when certain chosen conditions are met (e.g., the test reached a pre-set strain value) [65]. The measurements done during the static test are plotted as a stress-strain diagram with strain on the x-axis and stress on the y-axis [1,3]. A typical stress-strain diagram for various kinds of material is shown in Figure 1.

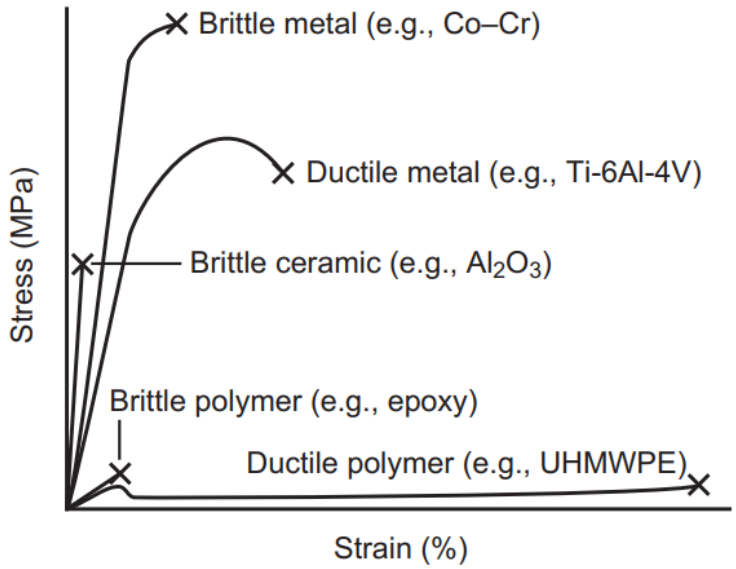

Figure 1. *A comparison of typical stress-strain curves of various materials* [3]

Stiffness and strength are the main material properties that can be obtained from the stress-strain curves. Stiffness is characterized by the Young's or elastic modulus E, which is the slope of the initial linear part of the stress-strain curve. Many materials exhibit a clear nearly linear part of the stress-strain curve between the beginning of the test and the onset of plastic deformation. Such behaviour is described by Hook's law for the relationship between stress σ and strain ε using Young's modulus E [1]:

$$\sigma = \epsilon \cdot E \tag{5}$$

However, many materials, especially plastics behave in a more complex way without a clear linear region. In such cases, tangent or secant modulus of elasticity is used. As

seen in Figure 2, the tangent modulus is a slope of the stress-strain curve at a given point, while the secant modulus is a slope of a line between the origin and a given point on the curve. Alternatively, it can be also calculated as the linear regression of the curve between the origin and a given point [1,65].

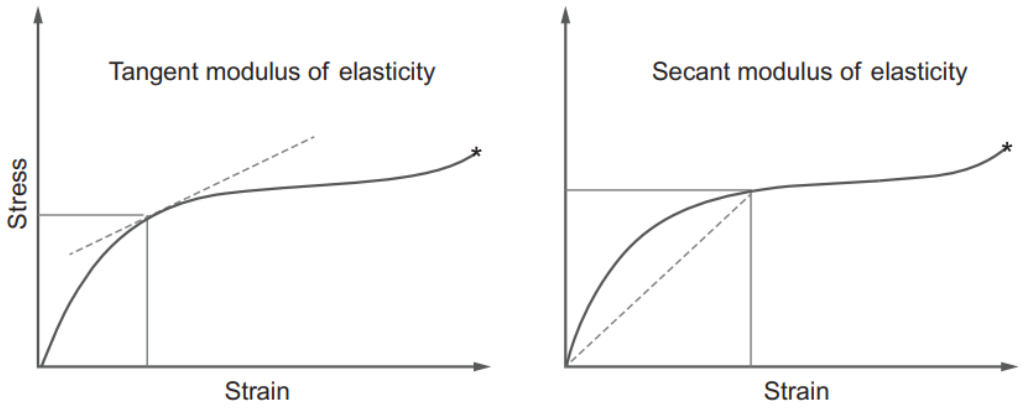

Figure 2. *Tangent and secant modulus of elasticity* [1]

Strength can be described as a stress value at which the material starts failing. Two types of strength are identified, ultimate and yield strength.

Ultimate strength, sometimes (e.g., in ISO standards) referred to as just strength, is considered the highest stress value before ultimate failure and breaking of the test specimen. For plastics, that often exhibit large deformations and strain hardening before failure, the first local maximum in stress value is considered as tensile strength and the highest stress value during the test as compressive strength according to ISO 527 and ISO 604 standards, respectively [64,65]. For porous materials, that may exhibit many local maximum stress values in a compression test, as they fail and collapse non-homogenously, the first local maximum is referred to as first maximum compressive strength [66].

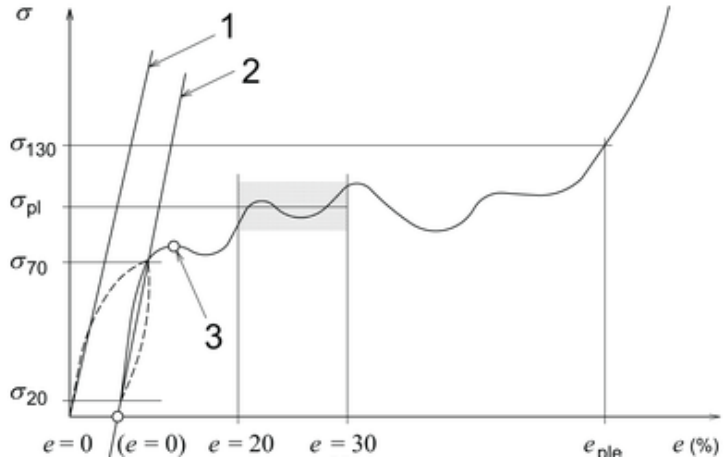

Figure 3. *Stress-strain curve of a porous material, with the first maximum compressive strength, indicated as point 3. Modified from* [67]

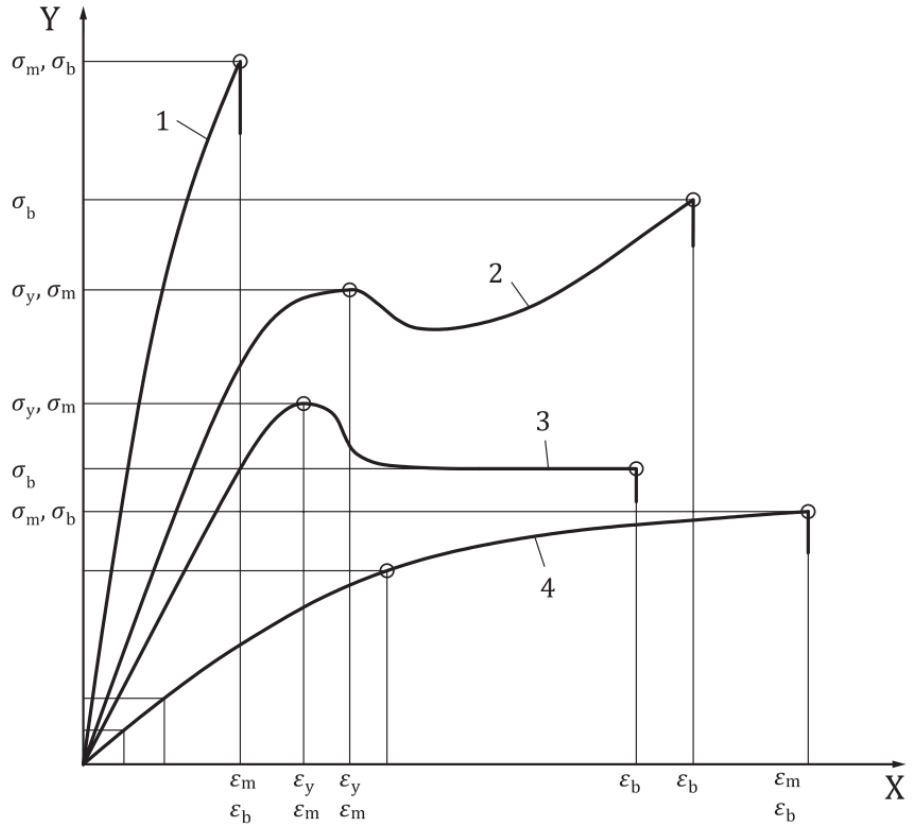

Figure 4. *Stress-strain diagram with curves showing typical behaviour in a static tensile test of plastics with important stress and strain values marked. 1) hard and brittle polymer that breaks without yielding. 2) and 3) Ductile material that exhibits/does not exhibit significant strain hardening after yield. 4) Rubber-like material that breaks at high strains without a prior decrease in stress. Subscripts indicate: y = yield, m = maximum; ultimate strength; b = break. Modified from* [64]

Yield strength is the stress value at which the deformation changes from elastic to plastic. For some materials, yield strength can be easily obtained from the stress-strain curve, because a local peak in engineering stress appears, followed by a decrease and a subsequent increase as strain hardening during plastic deformation starts to occur, as seen in Figure 4. This is typical behaviour for many metals. However, for many highly ductile materials, such as aluminium or thermoplastics, there is no clear point that can be identified as yield strength [1,3]. For some materials, two methods of yield determination are used: proportional limit and offset yield point. Proportional limit is a point, where the stress-strain curve changes from linear to decreasing slope [1]. Offset yield point is obtained so, that a line with the slope of Young's modulus (and therefore parallel to the initial linear part of the stress-strain curve) is constructed from a set point on the strain axis, usually at a value of 0.2 %, as seen in Figure 5. A point where it intersects with the stress-strain curve is then considered offset yield point. It is a stress value, that causes 0.2 % of nonlinear deformation, which is for many materials also plastic, non-recoverable deformation [1,3]. However, most thermoplastic materials have more complicated stress-

strain behaviour. They generally do not have a clear linear region in the stress-strain curve. Also, the linearity or non-linearity of their stress-strain curve does not provide information on whether the deformation is recoverable or not. Typically, they exhibit delayed rather than instantaneous recovery of elastic deformation and even deformations in the non-linear part of the stress-strain curve are recoverable [1,5]. Therefore, it is very complicated to correctly find the yield point. The offset method is sometimes used, but the ISO standards for tensile and compression testing of plastics (ISO 527 and ISO 604 respectively) define yield as the first point where an increase in strain occurs without an increase in stress [64,65]. Therefore, for many plastics, the yield and ultimate strength are identical according to this definition. Very brittle materials, such as ceramics and brittle polymers, on the other hand, break without yielding, as seen in Figure 1 [2,5].

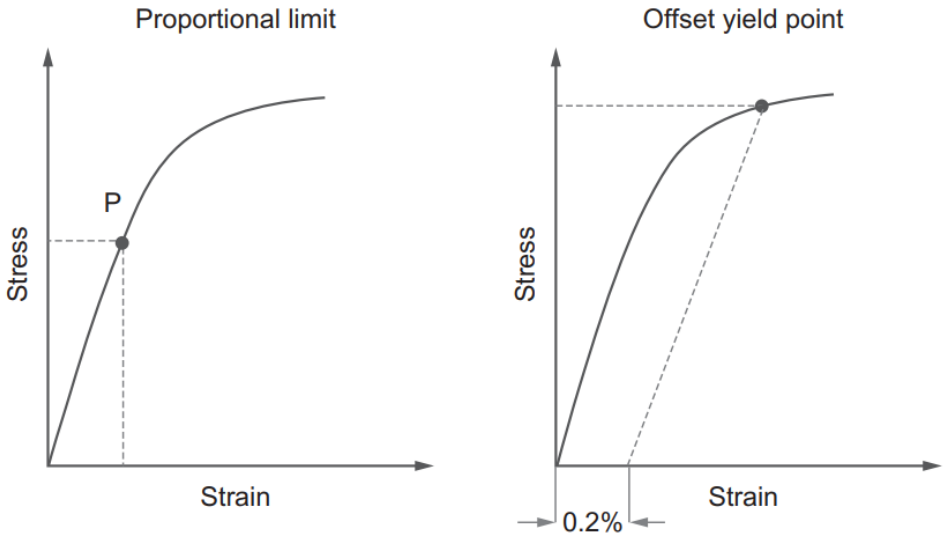

Figure 5. *Proportional limit and offset yield point with 0.2% offset* [1]

It is important to remember, that stress values in these cases are engineering stress values. For ductile materials, engineering stress value decreases significantly after ultimate tensile strength is reached, as it is proportional to force and that is decreasing because the failing material is becoming less stiff until it finally breaks. However, as necking of the specimen occurs, its cross-section decreases dramatically and true stress in the thinnest part of the specimen increases, as seen in Figure 6 [1,3].

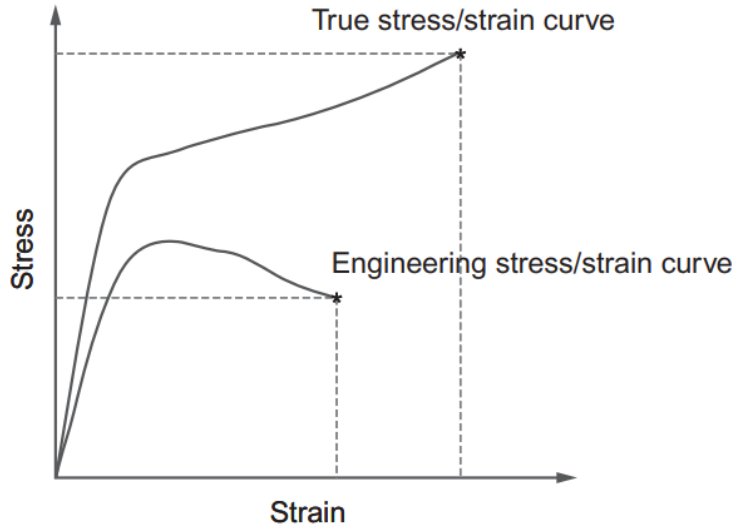

Figure 6. *Comparison of true and engineering stress and strain in a static tensile test. Ultimate tensile strength peak cannot be seen in the true stress-strain curve* [1]

3.2 Modes of loading

Static testing is done in many different modes of loading. The most common is tensile testing, followed by compression testing. Those modes were also used to explain the mechanical testing fundamentals. In this section, the basics of the most used modes will be described.

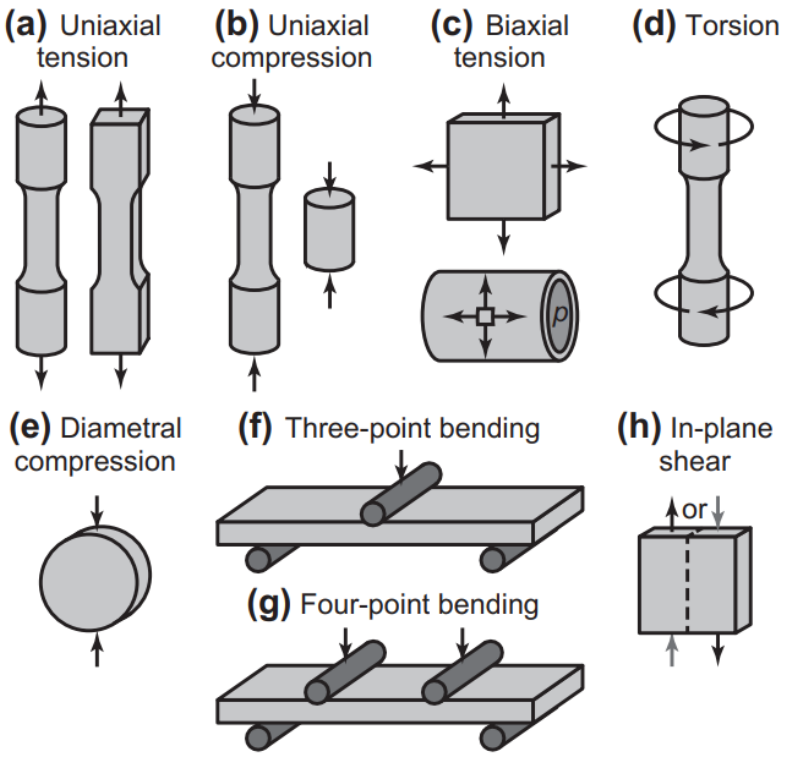

Figure 7. *Some of the most common modes of mechanical testing* [3]

3.2.1 Tensile testing

As mentioned earlier, tensile testing is the most common type of mechanical testing. Uniaxial testing is the most common variant. It is performed so, that a specimen is mounted to two grips that are pulled apart from each other. However, also bi- and triaxial variants are used, where the specimen is pulled by four or six grips in two or three perpendicular directions, respectively [3,68]. The test specimens for the uniaxial tensile test are made in a shape of a dogbone. Such shape ensures, that deformation occurs in the central part of the specimen and not close to the grips, where the material can be affected by the gripping. Flat or round specimens are used for testing metals, for testing of plastics, flat specimens are used. Shapes and dimensions of dogbone samples are specified in standards, usually, there are multiple variants for each material type [63,64]. For multiaxial testing specimens of various geometries are used, for biaxial test mostly crosses, for triaxial tests mostly cubes[68,69].

3.2.2 Compression testing

Compression testing is less common than tensile testing and is most commonly done on materials that are expected to be loaded mostly by compression such as cast iron or on materials that are difficult or impossible to grip for tensile testing [1,3,70]. Such materials include malleable porous structures or hydrogels. Uniaxial, multiaxial, or confined compression can be performed. Uniaxial compression is most common. A sample shaped as a cuboid or cylinder is placed on a plate and pushed by another perpendicular plate. The test is performed until a fracture occurs or until a set value of strain, stress, displacement, or force is reached [1,3,65]. Testing until a set value of strain is more common than the other options because, for many materials, it is difficult to precisely define a fracture of the specimen in compression. Biaxial testing is conducted by compressing a cuboidal specimen in two perpendicular directions [71]. Triaxial testing is done on cylindrical specimens. The flat surfaces are compressed by parallel plates, and the round surface by hydrostatic pressure applied through a membrane [72]. Also, uniaxial diametral compression is used for very hard and brittle materials as a substitution for tensile testing. Uniaxial compression is applied to opposite sides of its round surface, which creates parallel tensile loading due to Poisson’s effect. Diametral tensile strength is an output of this type of test [3,5].

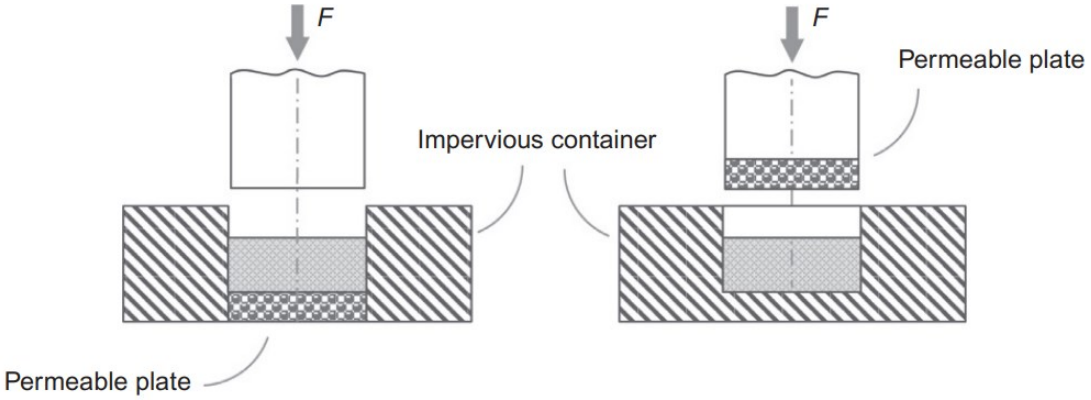

Figure 8. *Confined compression testing configuration* [1]

In confined compression, the specimen is loaded uniaxially, but it is placed in a confined space that restricts the increase of its cross-section (Figure 8). It allows more homogenous stress distribution, and it also corresponds better to in vivo conditions of many medical implants, as they are often at least partially confined [73]. It is also of special interest for testing highly hydrated tissues and materials, such as hydrogels, because it allows taking into account the effect of the fluid flow through and out of the specimen during the test. In such a case, the test is conducted in a liquid environment and either the top or bottom plate of the testing machine is porous and allows a flow of the fluid out of the confined space [1,74,75]. Despite the advantages over plain unconfined compression, it is not commonly performed because it is difficult to perform. To obtain reliable and accurate results, the dimensions of the specimen must be very precise and match the dimensions of the walls of the confining chamber, which is difficult to obtain with many biomaterials [1]. Therefore, it is only established as the standard testing method for mechanical testing of cartilage, where the flow of the interstitial fluid through the dense matrix has a critical impact on the mechanical properties of the tissue [1,75,76]. However, instead of a static test, a creep test is performed, which is described later, and elastic modulus is obtained using a linear viscoelastic model [75].

3.2.3 Torsion

Torsion testing is done on materials of devices that are intended to be loaded by torsion. From medical implants, such devices are typically screws or catheters, not so commonly tissue engineered scaffolds. Cylindrical rods are rotated by their ends in opposite directions, which creates pure shear loading. Due to the geometry, stress and strain values vary from 0 in the middle of the rods to the maximum value on the outer surface [3].

3.2.4 Bending

Bending test, also referred to as flexural test, can be done as a three-point or four-point bending, as seen in Figure 7. Three-point bending is more common, four-point bending is mostly used with brittle materials [3]. It is used to evaluate the mechanical properties of specimens that are difficult to mount for tensile testing. However, flexural loading combines tension/compression with shear loading and both normal and shear stress and strain values vary through the specimen. Along the length of the specimen, between the supports and the point of loading, normal stress increases linearly from the supports to the loading point and shear stress remains constant. Through the cross-section, shear stress increases parabolically from the top and bottom to the neutral plane, that is in the middle for a specimen with a symmetrical cross-section. Normal stress changes linearly from maximum compression in the top plane through zero stress at the neutral plane to maximum tension in the bottom plane [1,3]. Results reported from a bending test are flexural strength and modulus. The flexural strength is higher for three-point bending than for four-point bending, which is higher than the tensile strength of the same material [3,77].

3.2.5 Shear

Shear testing is used to determine the shear strength of both bulk materials and interfaces between materials. In this type of test, opposite parallel pulling forces are applied to opposite ends of the rectangular specimen, creating uniform shear, unlike in torsional test. However, specimen fixation is complicated since the creation of an eccentric load is needed [3].

3.3 Time-dependent behaviour, dynamic testing

In many cases, static testing does not provide sufficient information about the implant's mechanical behaviour. The behaviour of materials is different when they are subject to cyclic loading or constant load than during the one-time load ramp of a static mechanical test. In the first two cases, the behaviour of most materials tends to be time-dependent, while during static testing it is assumed to be time-independent [1,3]. Moreover, thermoplastic polymers tend to have time-dependent behaviour at all times at temperatures near or above their glass transition temperature. And many synthetic biodegradable polymers have glass temperatures low enough, that the body temperature of 37 °C causes time-dependent behaviour [1]. During the static test, the time-dependency is small enough to be neglected, but to predict the mechanical properties of tissue engineering scaffolds and other medical implants made from thermoplastic polymers after they are

implanted, the time-dependency of their mechanical properties needs to be considered [5]. Two mechanisms affect time-dependent behaviour. Fatigue during cyclic loading, which affects all materials, and viscoelasticity during constant load or deformation, which affects especially thermoplastic polymers [2,3].

3.3.1 Viscoelasticity, creep, and stress relaxation

Fully elastic materials (e.g., metals or ceramics), upon application of external load, deform immediately according to their modulus, and upon removal of the load, they recover immediately to their original shape, provided the load was below their yield. Fully viscous materials, such as Newtonian fluids (e.g., water or oil), upon application of external load, keep deforming, flowing in other words, according to their viscosity. Upon removal of the load, they stop deforming (flowing), but remain in their present state, and do not return to their original state. When deformation is the starting point, the stress state in a fully elastic material is proportional to strain value, while in a fully viscous material, it is proportional to stress rate. The coefficients of these relations are elastic modulus and viscosity [3,78,79]. Viscoelastic materials (e.g., polymers and tissues) combine both dependencies. Their stress is dependent both on strain value and rate. When loaded, they exhibit immediate elastic deformation according to their modulus, followed by creep. Creep is deformation under constant load. The rate of creep decreases asymptotically to zero for most viscoelastic solids and to some constant value for viscoelastic fluids and some solids, which is referred to as permanent creep. Upon removal of load, part of the elastic deformation is recovered instantaneously, while the recovery of the rest of the elastic deformation and of the creep deformation is delayed. The viscoelastic deformation recovery happens at decreasing rate. For liquids and some solids, the deformation is approaching asymptotically to a certain value of permanent deformation, while it is approaching zero for other solids. It has to be noted, that the permanent deformation, in this case, is not plastic deformation due to exceeding the yield limit, but deformation caused by permanent creep that happens even at very low load magnitudes [3,7,78,79]. Another effect of viscoelasticity is stress relaxation under constant deformation. After the material is deformed to a certain strain and the strain is kept constant, the stress in the material increases to a value determined by its elastic modulus (that for viscoelastic materials is usually dependent on the strain rate of the ramp) and then decreases asymptotically to a certain stress value in the case of viscoelastic solids. In the case of viscoelastic liquids, the rate of the stress decrease is decreasing asymptotically to a certain value and then the stress keeps decreasing at a constant rate to zero. Fully viscous fluids

relax stress immediately, as it is only dependent on strain rate, while fully elastic solids do not relax, and stress remains constant under sustained strain [3,7,78,79].

Various constitutive models are used to model the behaviour of viscoelastic materials in creep-recovery and stress relaxation. The most common ones are Maxwell model, Kelvin/Voigt model, standard linear solid model, and Burgers model [3,80]. Their representation is shown in Figure 9 and Figure 10.

The Maxwell model consists of a spring and a dashpot connected in series. In the creep test, it can model elastic strain and subsequent viscous flow, which is however limited and has a constant rate, which is not the case for solids. It can only model instantaneous recovery, but not delayed recovery as the whole creep deformation represented by the dashpot is unrecoverable. It can also model stress relaxation, however, it shows stress to exponentially decay to zero, which is again not the case for most solids. Therefore, it is mostly only used to model a simplified behaviour of viscoelastic liquids [3,78,81,82].

The Kelvin/Voigt model consists of a spring and a dashpot connected parallelly. It is used to model a simplified behaviour of viscoelastic solids. It can model maximum creep strain and delayed recovery; however, it cannot model instantaneous deformation and recovery and permanent creep because the spring and dashpot are not able to act independently. It cannot be used to model stress relaxation [3,6,78].

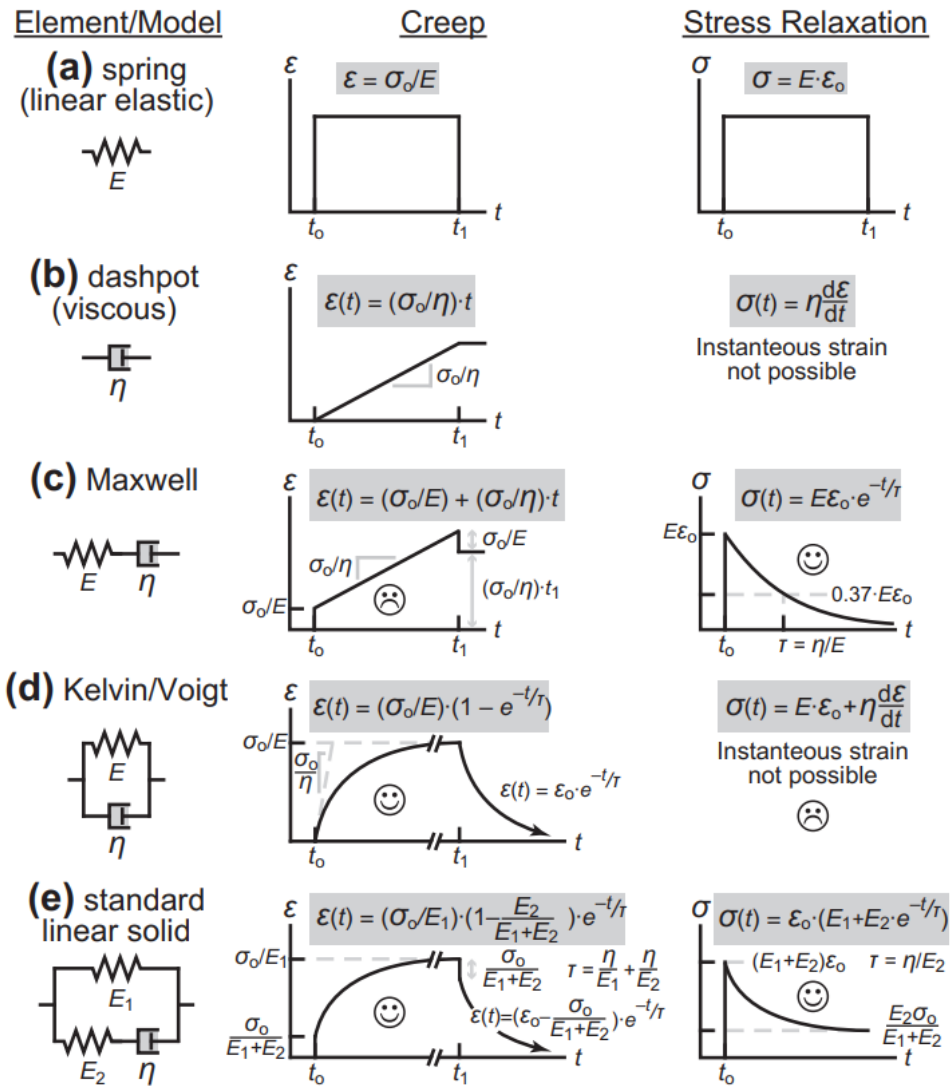

Figure 9. *Most common constitutive models for viscoelastic creep-recovery and stress relaxation testing* [3]

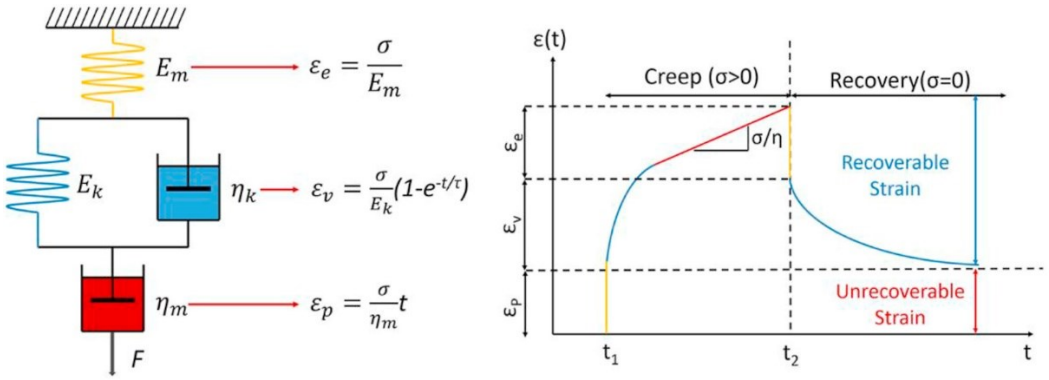

Figure 10. *Burgers model of viscoelastic material. It allows modelling of instantaneous deformation and recovery thanks to the serial spring (yellow), retarded creep strain and delayed strain recovery thanks to the parallel spring and dashpot (blue) and permanent creep and permanent creep strain thanks to the serial dashpot (red)* [80]

The 3-element standard linear solid model consists of a Maxwell model connected parallelly with a spring. It can well approximate creep, recovery, and stress relaxation of most viscoelastic solids. The addition of the parallel spring allows also modelling of both instantaneous deformation and recovery and maximum creep deformation, but similarly to the Kelvin/Voigt model, the standard linear solid model does not model permanent creep [3].

Burgers model consists of Maxwell and Kelvin/Voigt models connected in series. The addition of a spring and a dashpot in series to the Kelvin/Voigt model now allows modelling of both instantaneous deformation and recovery thanks to the spring and permanent creep thanks to the dashpot. It can be used to well approximate the behaviour of almost any plastic material, including polylactide, which shows permanent creep at body temperature [3,49,80].

3.3.2 Cyclic loading and fatigue

Most tissue engineering products are subject to cyclic load when implanted. It is created by voluntary and involuntary periodic movements such as walking, breathing and heartbeat. Under cyclic loading, materials exhibit fatigue and failure occurs at stress levels lower than their yield or ultimate strength as obtained from static testing [3,5,79]. If a scaffold material cannot withstand cyclic load, it is subject to, and it yields, it might lead to its failure [3,79]. Especially bone substitutes are subject mainly to compression loads [51]. If a material yields under compression, its dimensions will be reduced. In the case of a scaffold implanted in the body, it will lead to the loosening of the scaffold in a situation when the bonding with the surrounding tissue has not been created yet. If the scaffold is already bonded with the surrounding tissues, reduction of its unloaded dimensions will lead to the creation of tensile load on the bond in moments when it is not under compressive load. This may lead to the breaking of the bonding and again to the loosening of the implant. A loosened implant then might cause inflammation, tissue damage, pain, and necrosis [83]

Different methods are used to study fatigue under cyclic loading. There are high-cycle fatigue methods, where the material is usually subject to cyclic stress, low-cycle methods that can be driven both by stress and strain, and fracture mechanics methods that study properties of fracture due to fatigue in cyclic loading [79,84,85]. Some will be here briefly reviewed.

Under long-term cyclic loading, the strength of the material is becoming lower with increasing number of cycles until a certain stress value after which it does not decrease anymore. Therefore, there is a stress level under which the material can withstand a

theoretically infinite number of cycles. The relationship between stress and number of cycles to failure is shown in S-N diagrams with number of cycles to failure N_f on the x-axis and stress amplitude S_f on the y-axis, using logarithmic or semi-logarithmic axes. The stress-life curves in the diagram are also known as Wöhler's curves [3,84,86]. It has to be noted, that the stress in the curves is a global engineering stress, not local stress at the failure location. The Wöhler's curves can be made for various scenarios such as first slip, first crack, or failure [84]. An example of a S-N diagram showing a Wöhler's curve of wood filled PLA composite is shown in Figure 11. The asymptote of the curve is the fatigue limit, a stress value under which there is theoretically infinite number of cycles to failure. For stresses above the fatigue limit, the material can withstand only the number of cycles according to the Wöhler's curve. The stress amplitude under which the material can withstand a given number of cycles is fatigue strength, the number of cycles to failure at given stress amplitude is fatigue life [3,84]

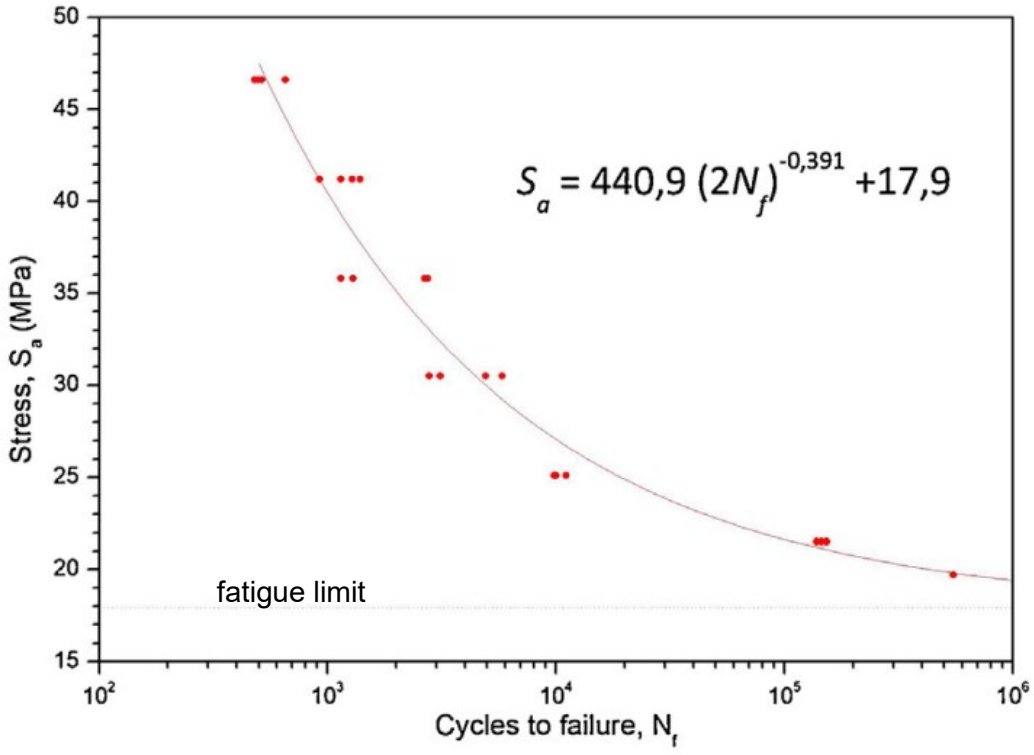

Figure 11. *S-N diagram with a Wöhler's curve of wood filled PLA composite. Modified with additional comments from* [86]

The Wöhler's curve in Figure 11 is fitted as exponential on a semi-logarithmic scale, but often simplified bilinear curve is used. The first linear part shows the limited fatigue section with fatigue strength decreasing with number of cycles, the second linear part shows the fatigue limit and marks the steady-state fatigue section where the fatigue life reached fatigue limit and is not decreasing with number of cycles [87,88]. The main types of stress

waveforms are fully reversed tension-compression with zero mean stress, tension-compression with non-zero mean stress, and pure tension, where the minimum stress value is close to zero, but usually not zero to avoid slack [3,84].

Low cycle fatigue testing is performed at high loads, generally exceeding the yield limit and a low number of cycles is used. Not only stress-driven but also strain driven tests, are used, which allow an analysis of local true stresses [84,85].

For biomaterials, especially polymers, various types of low-cycle testing are also used, that do not focus on the determination of the fatigue life. They can be both stress and strain driven and use both stresses below the yield limit and above [48,89]. They allow, for example, the evaluation of the viscoelastic properties of the material. Hysteresis loops are a common output of such tests [3,48,79]. Elastic materials keep all deformation energy during deformation, and therefore their loading and unloading curves are identical. Viscoelastic materials, however, dissipate part of the energy and their loading and unloading curves form a hysteresis loop. The dissipated energy corresponds to the area inside the loop. The recoverable deformation is seen as the width of the loop. In a stress--driven test, the non-recoverable deformation, such as creep deformation or accumulation of local defects, is seen as a shift of the loops to higher strain values [3,48]. A strain driven test can be used to study stress relaxation [89,90].

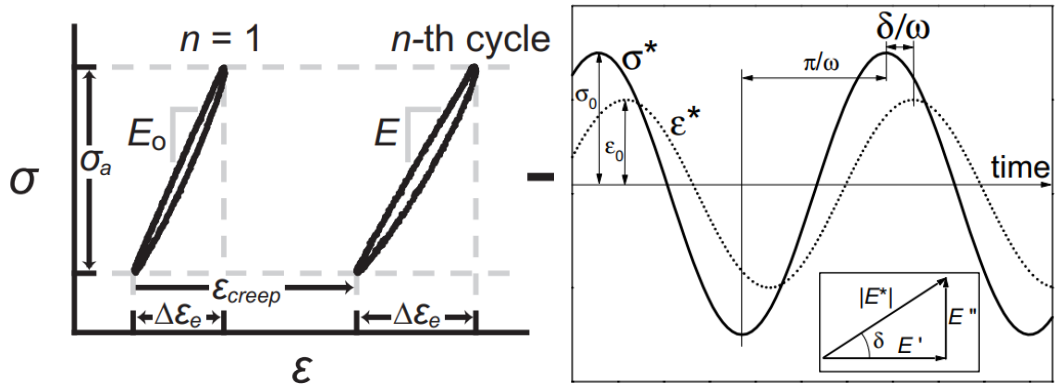

Figure 12. *Viscoelastic properties that can be obtained from a cyclic testing: Elastic recoverable deformation $\Delta\varepsilon_e$, cumulative non-recoverable deformation ε_{creep}, phase angle δ, complex modulus E^*, and storage and loss moduli E' and E".*

Also other viscoelastic properties can be evaluated using a cyclic test with a sinusoidal stress waveform. In a viscoelastic material, the response in strain to the stress is delayed by a phase angle δ. Using the phase angle, complex modulus E^*, storage modulus E' and loss modulus E" can be calculated as follows [2]:

$$E' = \frac{\sigma_0}{\varepsilon_0}\cos\delta \tag{6}$$

$$E'' = \frac{\sigma_0}{\varepsilon_0}\sin\delta \tag{7}$$

$$E^* = \frac{\sigma}{\varepsilon} = \frac{\sigma_0}{\varepsilon_0}exp(i\delta) = E' + iE'' \tag{8}$$

where σ_0 is a stress amplitude and ε_0 is a strain amplitude. The storage modulus represents the elastic behaviour of the material that is in phase with σ_0, while the loss modulus represents the viscous behaviour that is $\frac{\pi}{2}$ out of phase from σ_0 [2,3].

4. MATERIALS AND METHODS

Samples of two composite materials were used for the mechanical testing. As a matrix, poly-L-DL-lactide (PLDLLA) with 70 % L and 30 % DL isomers (Evonik Industries AG, Essen, Germany) was used in both composites. For the two composites, two different fillers were used: bioactive silicate glass 13-93 (BaG) and β-tricalcium phosphate (TCP, Whitlockite, Plasma Biotal Limited, Tideswell, UK). In both compositions, the mass ratio of the matrix to the filler was 70/30. The particle size of the bioactive glass filler was between 36 and 150 µm, and the average particle size of the TCP filler was 27.57 µm. PLDLLA pellets and TCP powder were purchased from their respective manufacturers, bioactive glass was prepared from the raw materials.

Both materials were tested after 0, 4, 8, and 12 weeks of in vitro degradation in TRIS buffer solution. Testing was performed in a water bath at 37 °C. The specimens were porous scaffolds for compression testing and compact 1mm thick plates for tensile testing. Static, dynamic, and creep-recovery testing were performed for both composites at each time point, with the exception of week 12, when dynamic tensile testing was not possible because of a too high amount of permanent creep deformation. The ion release from the porous scaffolds was analysed by inductively coupled plasma optical emission spectroscopy (ICP-OES, further referred to as ICP).

4.1 Sample preparation

The composite material was prepared by melt extrusion. Porous scaffolds were manufactured by supercritical carbon dioxide foaming ($scCO_2$); compact plates were prepared by compression moulding.

4.1.1 Bioactive glass preparation

Bioactive glass 13-93 with the following composition (in wt.-%) was prepared: 53.0 % SiO_2, 20.0 % CaO, 6.0 % Na_2O, 12.0 % K_2O, 5.0 % MgO, and 4 % P_2O_5. Raw materials ($CaCO_3$, K_2CO_3, Na_2CO_3, $(NH_4)H_2PO_4$, MgO (Sigma Aldrich, St. Luis, MO; USA), and Belgian quarz sand) were mixed, melted in a platinum crucible for 3 hours at 1425 °C, and annealed at 520 °C for 4 hours. Then the glass was crushed and milled. The milled glass was sieved and the size range between 36 and 150 µm was used.

4.1.2 Composite extrusion

A twin-screw extruder (Mini ZE 20 x 11.5 D, Neste Oy, Porvoo, Finland) was used to mix the composite. A total of four extrusions were done, two for the TCP and two for the BaG composites. In the first three extrusions, the polymer pellets and filler powder were mixed in the desired ratio of 70/30 before the extrusion and one feeder was used to feed the material to the extruder. In the last extrusion, two feeders were used, and each material was fed separately. The ratio of the matrix and filler was maintained by controlling the ratio of the feeding rates of the feeders. In both cases, both materials were dried in a vacuum chamber at 80° for 8 hours to prevent hydrolytic degradation during the extrusion process. The extruder consisted of a barrel with two 20 mm screws, two intermediate elements and a 10 mm die. There was a breaker plate between the second intermediate element and the die. All elements were heated except the first intermediate element in the first three extrusions. The temperatures had been adjusted during the process to maintain a good quality of the outcoming material and keep the pressure at a steady value between 100 and 1000 bar. The temperature was set to a range from 180 °C at the barrel to 210 °C at the die. The two intermediate elements were heated to 190 and 200 °C. Adjustments were made up to ±10 °C. The melt pressure stayed most of the time around 150 bar, occasionally increasing to values near 400 bar. Only in the third extrusion, the temperature dropped to 130 °C at the barrel and the pressure increased to 700 bar due to a technical problem with the extruder. No impact on the quality of the extruded material was found. The extruded rods were drawn slightly by a conveyor belt. No requirements on the diameter were set, and it varied from 4 to 10 mm. Once the rods cooled on the conveyor belt, they were cut and stored in sealed plastic bags. Before further processing, the material was always dried overnight in a vacuum chamber.

4.1.3 Supercritical CO_2 foaming

The porous scaffolds were prepared by a pressure-induced phase separation of the polymer solution in supercritical carbon dioxide, using a procedure described in detail in [91]. Pieces of the extruded rods were placed inside a custom-made PTFE mould with four shafts, 9 mm in diameter and 72 mm long. About 3 g of material per shaft was used. The mould was placed inside a reactor chamber. The chamber was filled with CO_2 to a pressure of 200 bar and heated to 115 °C. After the temperature reached the desired value, the pressure and temperature were kept for 3200 seconds. Then the reactor was depressurized to 50 bar in 6400 seconds while the temperature was kept constant. The remaining pressure was released manually. Then the mould was removed, cooled down

in a freezer so that it could be handled, and the porous rods were removed. Material loaded into the mould and porous rods are shown in Figure 13.

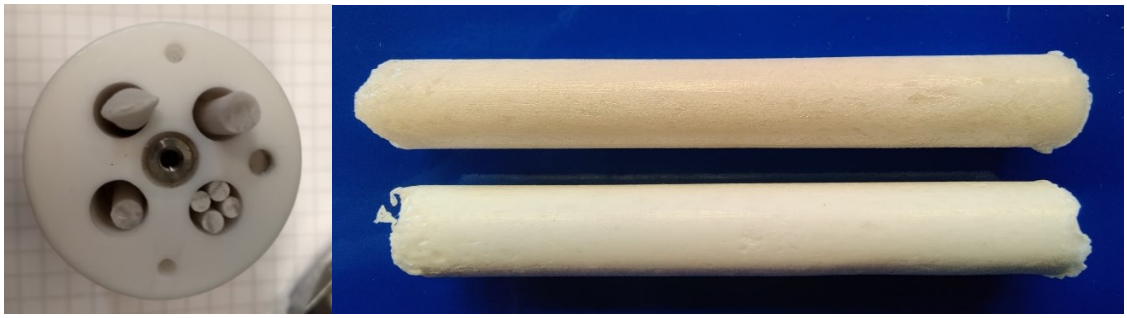

Figure 13. *Material loaded in the Teflon mould (left). Porous rods of the bioactive glass (top) and β-TCP (bottom) composite. There is non-porous skin on the surface of the rods.*

4.1.4 Compression moulding

Non-porous plates were prepared for tensile testing by compression moulding. Rectangular plates were used instead of more usual and standardized dogbone shaped plates because no suitable method was available to cut the complex dogbone shape without significantly affecting the material properties. The used mould consisted of three parts, as seen in Figure 14.

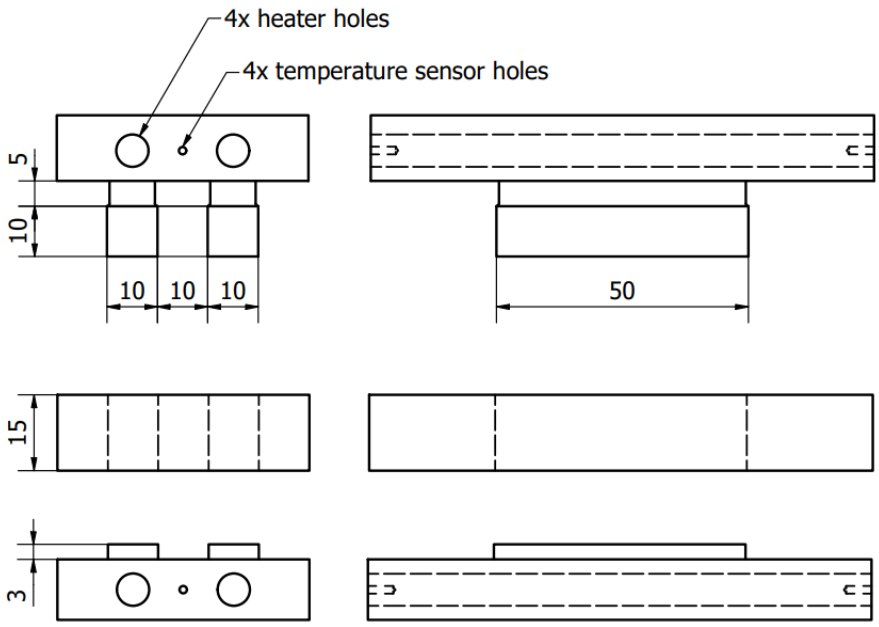

Figure 14. *Drawing with important dimensions of the mould used for compression moulding of the plates.*

The three parts, when put together, formed an assembly with two cavities inside with dimensions of 40x10 mm. The thickness of the plates was controlled by the amount of

material that was put into the cavities. The overlapping sections minimized material outflow from the cavities. The top and bottom parts had holes for heating elements and temperature sensors.

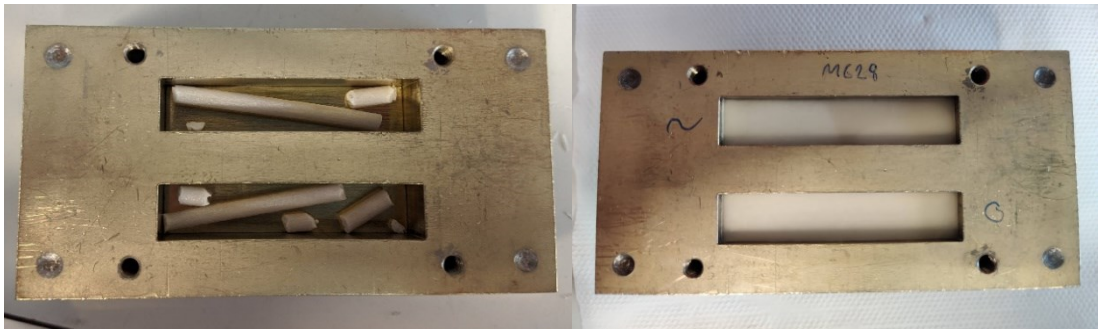

Figure 15. *Pieces of rods in the mould and moulded plates.*

For compression moulding, 748-754 mg of material was placed in each cavity of the assembly without the top part, and then the top part was inserted and closed the cavities. Heating elements and temperature sensors were inserted and the whole assembly was placed inside a pneumatic press equipped with compression plates with a cooling circuit inside. The optimal moulding temperature was found to be 90 °C, slightly below the melting temperature of 100 °C. The mould was heated without pressure applied. When the temperature of the mould reached 70-80 °C, it was pressed to about half of the final pressure, when the temperature of both parts reached 90 °C, it was kept for about 30 seconds and then the mould was pressed to full pressure and kept for about one minute. Then the mould was cooled down until the temperature of both parts was below 30 °C. Then the pressure was released, and the finished plates were removed from the mould. Material loaded to the mould and moulded plates are shown in Figure 15. To remove the plates from the mould, the overflow was scraped from the sides of the mould, and the middle part of the mould was placed in the pneumatic press with supports under it. The top part was then pressed through the middle part to push the plates out. This way, bending and breaking of the plates during demoulding was prevented. Because the TCP composite tended to stick to the mould and the surface of the plates got damaged when demoulding, a silicone release agent (CRC SR Multi, CRC Industries Europe BVPA, Zele, Belgium) was used. It was sprayed on all surfaces of the mould, which came into contact with the moulded material, before moulding and let dry for several minutes. No release agent was used to mould the bioactive glass composite plates.

4.1.5 Specimens for mechanical testing

The specimens for compression testing were prepared from the porous rods prepared by $scCO_2$ with pressure-induced phase separation. Cylinders with a desired 7 mm height

were prepared using a hand saw. The cylinders were then punched using a cylindrical 7 mm punch tool and a hand press to remove the outer non-porous layer of the scaffold. Their dimensions were measured by callipers after incubation before mechanical testing. Both height and diameter of the specimens had relatively high deviations because they were prepared with manual equipment.

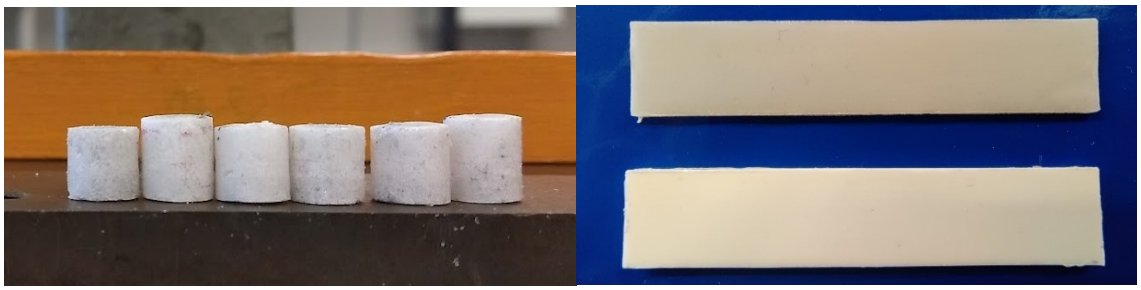

Figure 16. *A: specimens for compression testing punched from cut pieces of the porous rods. Variability in height is due to the manual equipment used for the cutting. B: specimens for tensile testing of the two different composites (top – bioactive glass, bottom – β-TCP).*

The specimens for tensile testing were non-porous plates as they came out from the compression moulding process with dimensions of about 50x10x1 mm. Their dimensions were not modified, only the material overflow was trimmed. Both specimens are shown in Figure 16.

4.2 In vitro degradation

In vitro degradation was done in a TRIS buffer solution. The dimensions and masses of the specimens were varying, but the volume of the solution for each specimen was kept constant – 24.7 ml for plates, and 6.7 ml for porous scaffolds. The ratio of the specimen mass to the medium volume was close to 1:34 (g to ml). TRIS buffer solution was prepared at least one day before immersion by dissolving 1.66 g of Trizma base (Sigma-Aldrich Co. LLC, St. Louis, MO, USA) and 5.72 g of Trizma hydrochloride (Sigma-Aldrich Co. LLC, St. Louis, MO, USA) in 1 l of distilled water under constant stirring. 1 or 2 l of the buffer solution were prepared in one batch. Its pH was measured at (37±0.2) °C after preparation and before every use. Only a buffer with a pH value of 7.40±0.02 was used. The buffer solution was kept in a refrigerator before use for a maximum of four weeks. The buffer was exchanged one and two weeks after immersion and then every two weeks as in [91]. The pH of five specimens from each set (four combinations of specimen type and material) was measured before buffer exchange. A sample of medium from three specimens from both porous scaffold samples was taken for ICP analysis at each buffer change.

4.3 Mechanical testing

Static, dynamic, and creep-recovery testing were performed in tension and confined compression. Static unconfined compression was also performed. Porous scaffolds were used for compression testing, and non-porous plates were used for tensile testing. All tests were done using an Instron Electropuls E1000 (Instron, High Wycombe, UK). Instron WaveMatrix software was used for control of dynamic and creep-recovery testing, Bluehill Universal, developed also by Instron, was used for static testing. All tests were conducted in a water bath with circulating water at 37 °C. The mechanical properties of polymers are largely dependent on temperature, and testing results are only representative for the temperature at which they are performed [1].

For tensile testing, original manual wedge action grips by Instron were used as upper grips, custom made side action grips were used as bottom grips. The length of the specimen between the grips was 25 mm for all tests. Other dimensions were measured for each test separately. The upper grips were tightened carefully so that they did not create significant tensile or compression load. If any load was created, it was removed by moving the crosshead. 1 N preload was used for static and dynamic testing, and 0 N was used as zero state for creep-recovery testing.

For unconfined compression testing, original equipment from Instron – bottom plate and indenter – was used. Custom made equipment was used for confined compression. It consisted of a chamber that was placed on top of the bottom plate of the testing machine and an indenter that was attached to the original indenter from Instron. The chamber had a porous bottom so that the liquid could flow out of the confined testing space. The indenter was machined from polyoxymethylene (POM). Two different chambers were used. One, 3D printed by stereolithography from the Black resin by Formlabs (Formlabs Inc., Somerville, MA, USA) with an inner diameter of 7.33 mm was used for week 0 testing, However, as the diameter of the scaffolds was increasing by swelling during degradation, since week 4, most of them did not fit it this chamber, and a bigger chamber machined from POM was used for those specimens that did not fit. It had an inner diameter of 8.97 mm. As the diameter of each specimen was different, layers of aluminium foil were wound around them so that they fit tightly inside the larger chamber. As aluminium is not as stiff as the material of the chamber and it affected the results, only changes in the behaviour during static testing were evaluated during the degradation.

The height and diameter of each specimen were measured before testing. Before the test, the indenter was moved, so that it touched the top of the specimen and produced a

force about 0.5 N. This condition was used as a zero state for creep-recovery testing. 1 N preload was used for static and dynamic testing.

4.3.1 Static testing

Static testing was performed at a 1 mm/min displacement rate both in compression and tension as in various previous works [89,91,92]. Compression testing was done until 20 % strain, and tensile testing until 5 % strain. These ranges covered the region of elastic deformation and also a large part of plastic deformation. Engineering stress and strain (further referred to as stress and strain) were recorded and used to determine elastic modulus, yield strength and ultimate strength. Elastic modulus was determined by the Bluehill Universal software as the slope of the linear part of the stress-strain curve. Yield strength was determined as 0.2 % offset yield. Ultimate tensile strength was determined according to the ISO 527 standard as the first stress peak, which was in all cases also the global maximum. In the case of compression testing, no type of strength could be easily defined for all time points, other than 0.2 % offset yield.

4.3.2 Creep-recovery testing

Creep and recovery testing was performed both in tension and compression by loading the specimen to 10 N in 1 s and keeping the load for 600 s, and subsequently releasing the load to 1 N in 1 s and keeping it for 600 s. Changes in strain were observed. Maximum creep strain ε_{max} was considered the strain value at the end of the creep phase. Permanent creep strain ε_{∞} was calculated as a difference between the strain value at the end of the recovery phase and the strain value at the point of the ramp before the creep phase when the load was 1 N. This way the elastic deformation created by 1 N load during the recovery phase was subtracted. The load value was selected to be a similar portion of the material strength as in [45,89].

4.3.3 Dynamic testing

Dynamic testing was performed in the elastic region using a sinusoidal strain waveform with 1000 cycles. The parameters of the test were chosen so, that the amount of permanent deformation caused by creep and intrinsic heating was low enough, that it was possible to reach 1000 cycles while maintaining tension/compression during the test. If higher amplitude or frequency had been used, the amount of permanent deformation would have been too high and in the parts of the waveform with the lowest strain, compression specimens would not be loaded and tensile specimens would be loaded by

compression. Such conditions that allowed dynamic testing for all time points of compression testing were frequency of 0.5 Hz and strain oscillating between 2 and 2.4 %. Tensile dynamic testing was done also with a frequency of 0.5 Hz and strain oscillating between 0.076 and 0.124 %. However, with these values, it was only possible to perform static dynamic testing for timepoints at weeks 4 and 8. Non-degraded material and material degraded for 12 weeks showed a too high amount of permanent deformation, and it was not possible to reach 1000 cycles and maintain the original strain waveform without loading the specimens by compression. Therefore, tensile dynamic testing was only performed at weeks 4 and 8.

The first 300 cycles were considered as preloading necessary for the machine to stabilize the waveform. For timepoints where it was possible, changes in stress values between cycles 300 and 1000 were observed.

4.4 Water absorption and mass loss analysis

Water absorption and mass loss were evaluated for each time point. Initial, wet, and dry mass of each specimen was measured. Initial mass was measured before incubation. Wet mass was measured before mechanical testing, immediately after removal from the medium. Before weighing, excess water was dried with tissue paper, so that there were no visible droplets. Dry mass was measured after the tested specimens were dried for one week in a vacuum chamber. It was not measured for specimens where pieces fell off during manipulation or testing. Water absorption was calculated as a difference between wet mass and dry mass. Mass loss was calculated as a difference between initial mass and dry mass. Mass retention was calculated from the dry mass as a percentage of the initial mass.

4.5 Ion release analysis

Samples of 1 ml of the degradation medium were collected before each medium exchange, diluted in 1 M nitric acid solution, and analysed for ion content using an inductively coupled plasma optical emission spectrometer (Agilent Technologies 5110, Santa Clara, CA, USA). The amount of silica, calcium, potassium, sodium, magnesium, and phosphorous ions was measured.

5. RESULTS AND DISCUSSION

5.1 In vitro degradation

Both materials underwent in vitro degradation for 12 weeks in TRIS buffer solution. Changes in mass, mechanical properties, ion release and pH of the degradation medium were measured. Buffer pH measurements and ion release were measured at weeks 1 and 2 and then every 2 weeks. Mechanical testing and mass measurements were done at weeks 0, 4, 8, and 12. Porous scaffolds were tested in compression and compact sheets in tension. It has to be noted that while tensile testing represents the properties of the material itself, compression testing shows the properties of the porous structure as a whole and not the properties of the material. The specimen dimensions are calculated from the whole structure including the pores. Therefore, all properties have to be considered global, specific to the structure, and distinct from the intrinsic properties of the material.

5.1.1 Changes in pH and water uptake

Changes in pH of the degradation medium and swelling of the specimens showed different reactivity of the two fillers, as seen in Figure 17 and Figure 18. While the pH of the medium, where the TCP composite was degrading, did not show any substantial changes in the beginning, and only from week 10 started dropping by less than 0.05, the pH of the medium, where the bioactive glass composite was degrading, increased after every change, suggesting that the bioactive glass is more reactive and dissolves faster.

There was no significant difference between the pH changes of the scaffolds and plates in the case of the TCP composite. No changes in the pH at the beginning in combination with no decrease in mass (Figure 19) showed negligible dissolution of both components. A slight drop in the pH at weeks 10 and 12 shows that the degradation of the polymer reached a phase when the monomers of lactic acid are released. In the case of the bioactive glass composite, there was different behaviour of the porous scaffolds and the plates. There was a higher increase in pH at every medium exchange in the case of the porous scaffolds, most likely due to the higher surface area to volume ratio of the porous structure. The amount of increase of pH of the medium with the plates did not show any clear trend, while the amount of increase of pH of the medium with the porous scaffolds kept increasing until week 8, after which the increase lowered, most likely also because of the onset of PLA degradation phase with a release of acidic monomers.

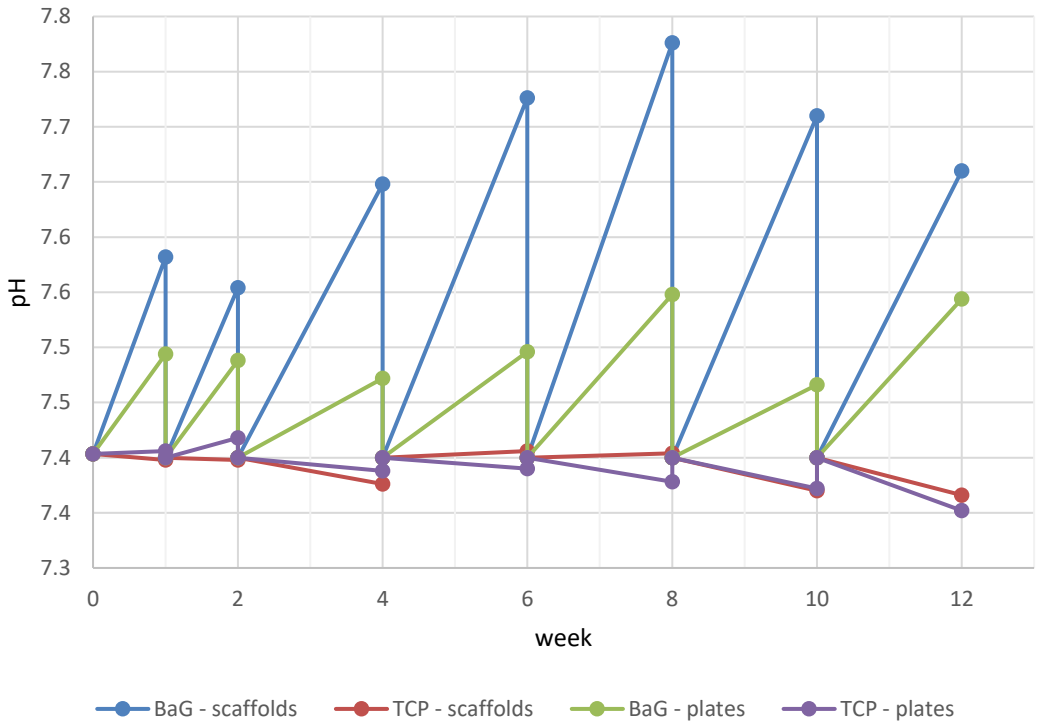

Figure 17. *Changes in the pH value of the degradation medium, presented as mean (n=5). Medium was replaced after every time point for a new one with a pH of 7.4.*

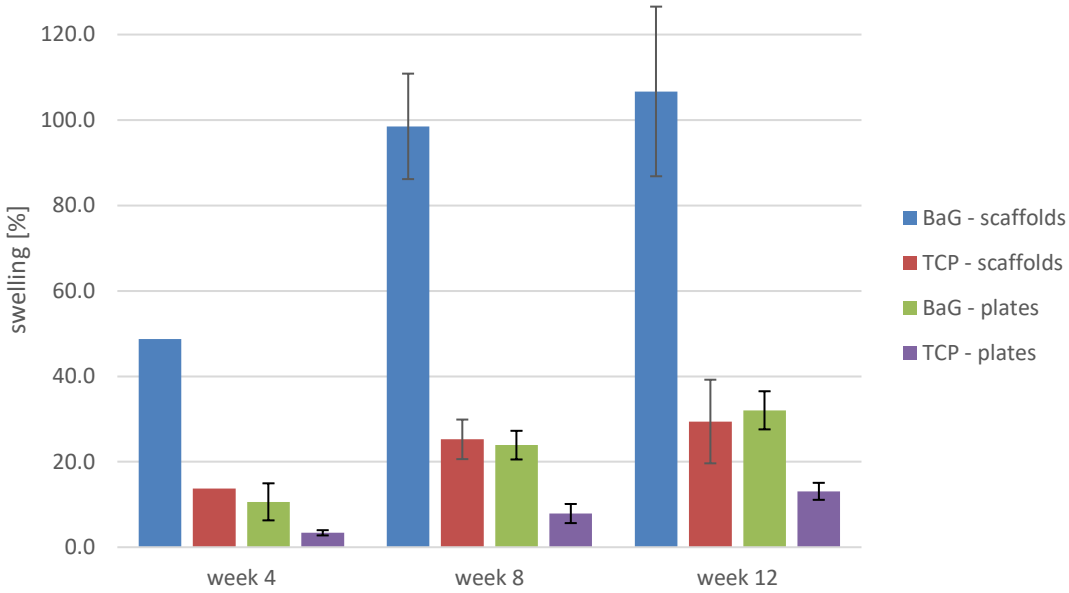

Figure 18. *Swelling of the scaffolds and plates during the degradation. Presented as mean ± SD (n=6-22).*

The higher reactivity of the bioactive glass also affected the swelling behaviour of the composites, which is shown in Figure 18. The bioactive glass composite showed notably higher water uptake than the TCP composite: 3-4 times higher in the case of the porous scaffolds and 2-3 times higher in the case of the plates. Also, the water uptake of the porous scaffolds was considerably higher than the one of the plates. The increased water uptake of the bioactive glass composites material is likely to be due to its faster dissolution confirmed by pH changes and ion release. Dissolved glass particles create micro pores that can be filled with water. Also, the higher degradation of the polymer during the extrusion process due to the reactivity of the glass may have played a role, which would have to be confirmed by molecular mass measurements. The higher water uptake of the porous structure in comparison to the dense is likely due to higher surface to volume ratio of the porous structure and water remaining in the small pores.

5.1.2 Strength and mass retention

Strength and mass retention over the course of the degradation was evaluated. 0.2 % offset yield strength was used as a measure of strength retention of the scaffolds, as it was the only standardized strength type that could be defined for both materials at all timepoints. Ultimate tensile strength was used for the plates, as it is commonly done for tensile testing [29,49,93]. Mass loss was analysed as the difference in mass before incubation and after drying in a vacuum chamber after testing.

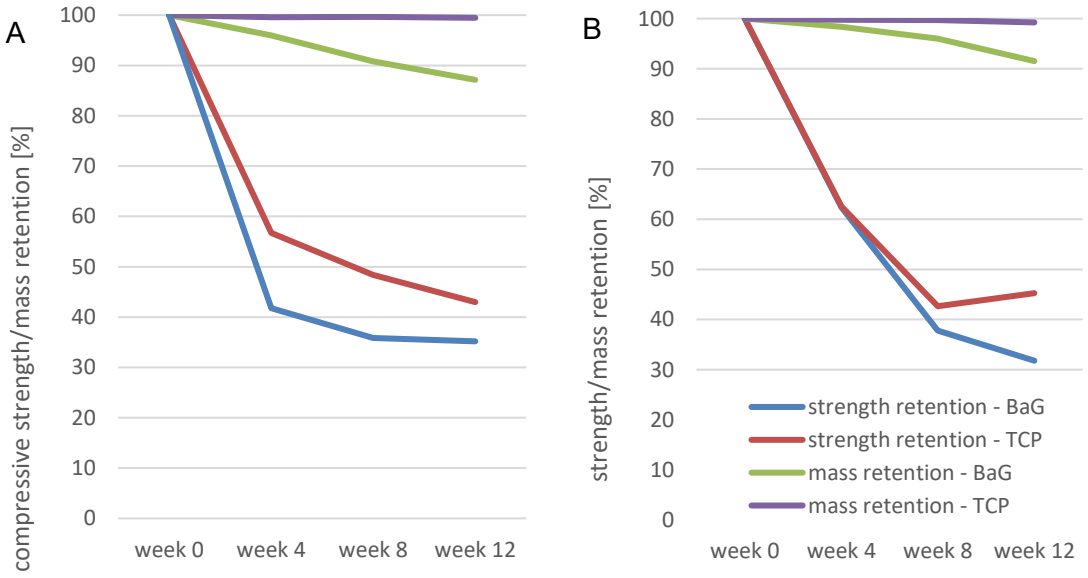

Figure 19. *Mass and strength retention. A: porous scaffolds, 0.2 % offset yield compressive strength retention shown; B: plates, ultimate tensile strength retention shown. Presented as % of the original mass and strength. Presented as mean values (mass loss: n=6-22, strength loss: n=3-7).*

The higher reactivity of the bioactive glass was also shown in strength and mass retention, as seen in Figure 19. While the TCP composite in both forms did not lose more than 1 % of mass over the 12 weeks of degradation, the bioactive glass composite, in the forms of plates and scaffolds, respectively, lost 1.7 and 4 % already during the first 4 weeks and 8.5 and 12.9 % by week 12. However, there were not so distinct differences in the strength retention between the composites. The highest strength loss happened in the cases of both polymers in both forms between weeks 0 and 4 when all materials lost 35-50 % of their ultimate tensile or 0.2 % offset yield compressive strength. It was followed by a smaller loss by week 8. After week 8 followed stagnation with only small changes in strength between weeks 8 and 12. There was practically no difference between the two composites in strength retention of the plates until week 8 and there was only a minor difference at week 12. In the case of the porous scaffolds, there was a noticeable difference already at week 4, but the differences became smaller later. The bioactive glass composite kept about 15 % less of its strength by week 4, 12 % less by week 8 and 8 % less by week 12. These observations are in line with observations of changes in pH and mass retention. The bioactive glass was dissolving faster than TCP and the dissolution was faster from the scaffolds than from the plates, which was seen as a higher increase in pH and higher mass loss. Composites with less filler then became weaker, and therefore the strength retention followed the same pattern as filler dissolution. The differences were, however, smaller because the main load carrier is the polymer matrix. To evaluate whether there were any differences in the polymer degradation, changes in molecular weight would have to be assessed.

5.2 Ion release

Ion release from the porous scaffolds was measured when the medium was changed. The concentration of calcium, silica, sodium, magnesium, potassium, and phosphorous ions in the degradation medium was measured. In the case of the TCP composite, only the concentration of calcium and phosphorous ions was measured as it does not contain the other ions.

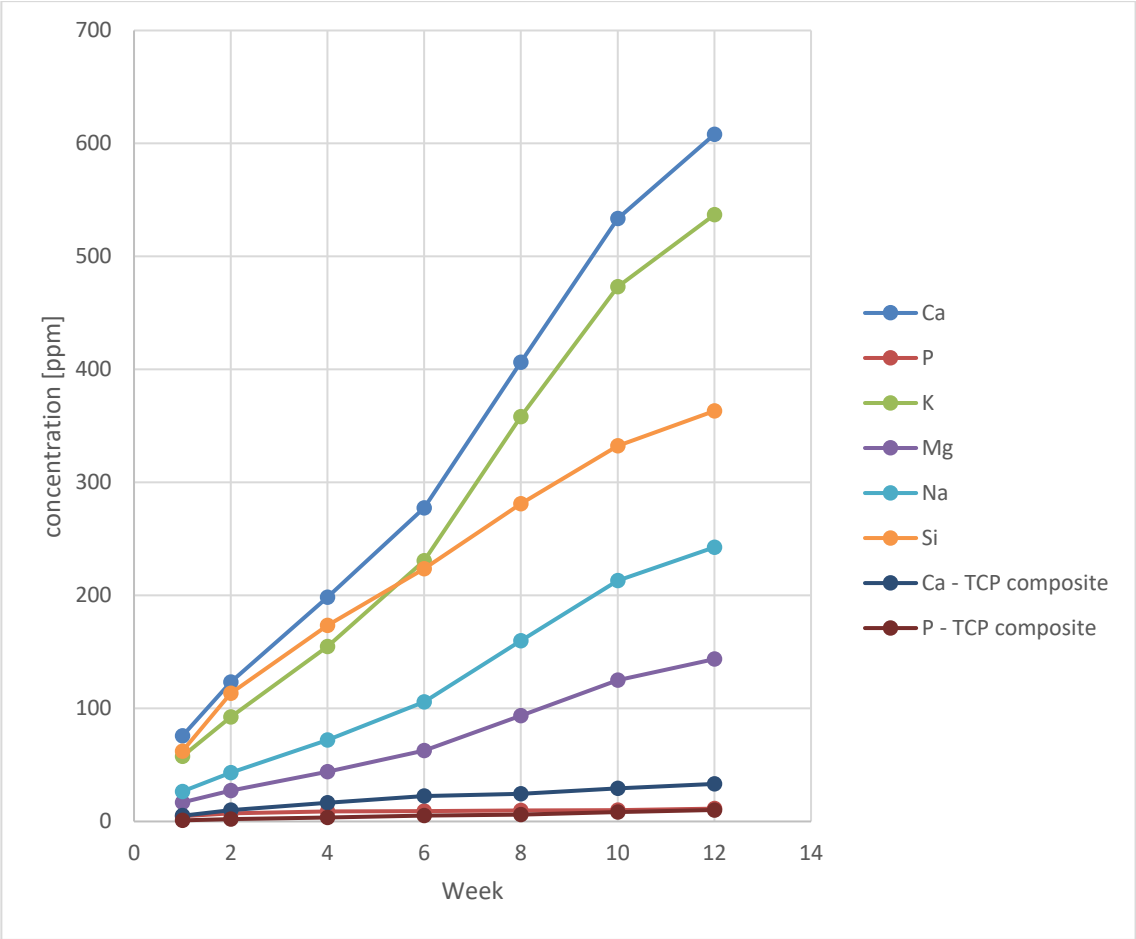

Figure 20. *Cumulative release of ions during degradation. Presented as mean (n=5 for weeks 1 and 2, n=3 for remaining timepoints). For clarity, error bars are not shown.*

The release rate of most ions from the bioactive glass composite followed a similar trend. It dropped between week 1 and 2, then it kept increasing until week 8 and dropped again after week 10. Only the release rate of silica peaked already at week 1 and then it showed a generally decreasing trend. The amount of phosphorous in the 13-93 bioactive glass is very low (4 wt-% of P_2O_5) and therefore also the release of the phosphorous was very low. The release of calcium and phosphorous from the TCP composite was minimal when compared to the bioactive glass composite, confirming markedly higher reactivity of the bioactive glass.

5.3 Mechanical testing

Polylactide is generally brittle at room temperature, which is not ideal for tissue engineering applications. However, this behaviour changes at elevated temperatures and also with degradation [94,95]. In addition to that, also the creep behaviour and performance during cyclic testing changes during degradation [49]. Here, the differences in mechanical behaviour between the two composites and changes during the degradation will be described.

5.3.1 Static testing

Figure 21 and Figure 22 show representative curves of week 0 compression and tensile testing. The compressive strength of both materials was similar, reaching about 10 MPa, which is a value similar to cancellous bone (0.1-16 MPa) [96]. The tensile strength of the TCP composite was significantly higher than in the case of the bioactive glass composite.

The compression behaviour of the scaffolds showed features of a representative porous material [66]. After reaching its first maximum compressive strength, the porous structure failed locally at the weakest point. As the weakest part started collapsing, stress dropped until it collapsed completely and then again increased, as the rest of the structure started bearing the load. Then the next weakest part collapsed, and the pattern repeated in waves, decreasing with every wave.

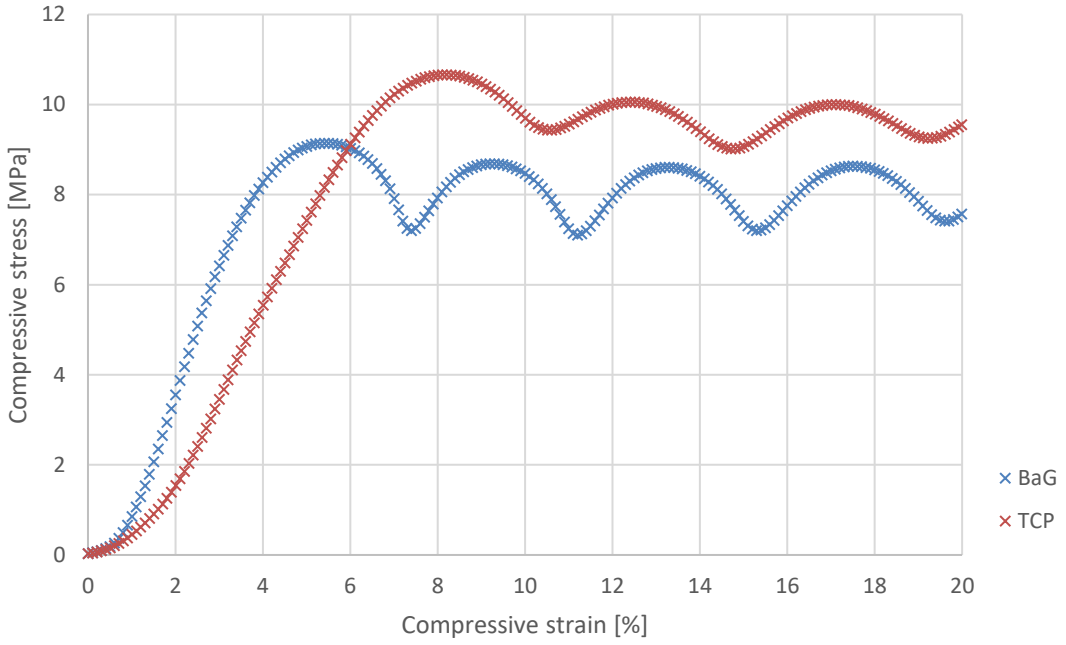

Figure 21. *Representative stress-strain curves of week 0 compression testing. Representative curves selected from 4 BaG and 4 TCP specimens.*

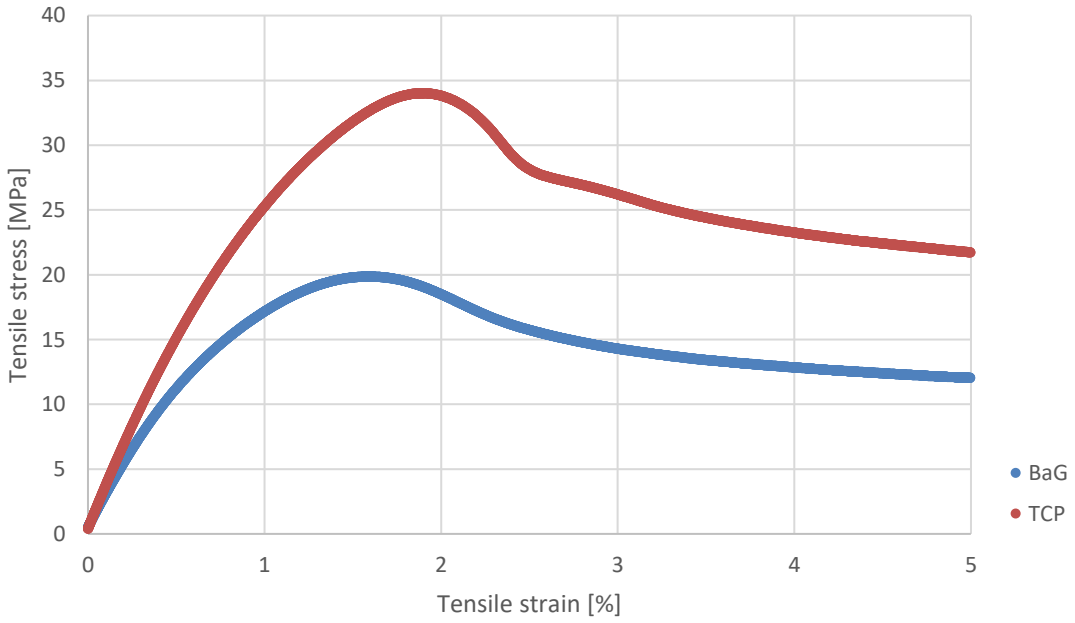

Figure 22. *Representative stress-strain curves of week 0 tensile testing. Tensile strength of the TCP composite is significantly higher (p=0.001). Representative curves selected from 5 BaG and 3 TCP specimens.*

The tensile behaviour of the plates was representative for homogenous ductile polymer. After yield, stress dropped, and necking of the specimen occurred. The strain hardening was not as strong as to cause the stress to rise again above the yield strength value and therefore the ultimate tensile strength was coincident with yield strength. However, the plasticized material kept extending to strains that are multiple times the yield strain without rupture. Some specimens were tested to strains higher than 5 %. Some of them have shown quick failure around 5-10 % strain, probably due to local failures created by non-homogeneous filler distribution, while others started crazing and developing slowly progressing cracks, but they kept extending beyond 10 % strain without ultimate rupture, held together just by small parts of the cross-section. This fracture behaviour did not change during the degradation and can be seen in Figure 23.

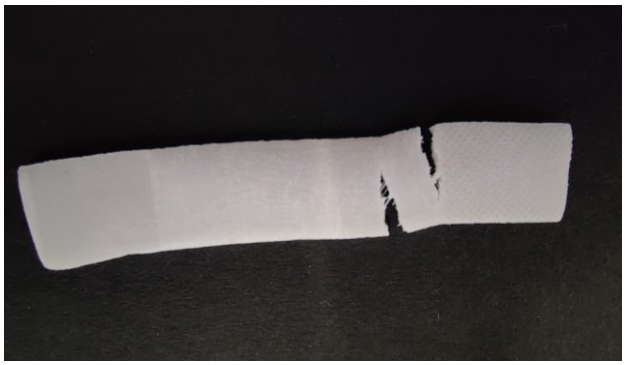

Figure 23. *Tensile specimen degraded for 8 weeks and tested beyond 10 % strain without rupture.*

The changes in behaviour due to degradation during static tensile and unconfined compression testing can be seen in Figure 24 and Figure 25. As shown earlier, the strength dropped dramatically between weeks 0 and 4, then it dropped less between weeks 4 and 8 and did not change significantly between weeks 8 and 12. Also, the shape of the stress-strain curves changed. In tensile testing, the stress peak became less prominent as the plates were degrading, and the subsequent stress drop became smaller. In the case of the bioactive glass composite, starting from week 4, there was no drop but rather a gradual, gentle decrease in stress until crack initiation at strains higher than 5 %. There was also no clearly identifiable yield point, as the slope of the stress-strain curve decreased more gradually before the curve reached the maximum value. Similar behaviour, but with a slightly more prominent stress peak can be seen in the stress-strain curves of the TCP composite starting from week 8.

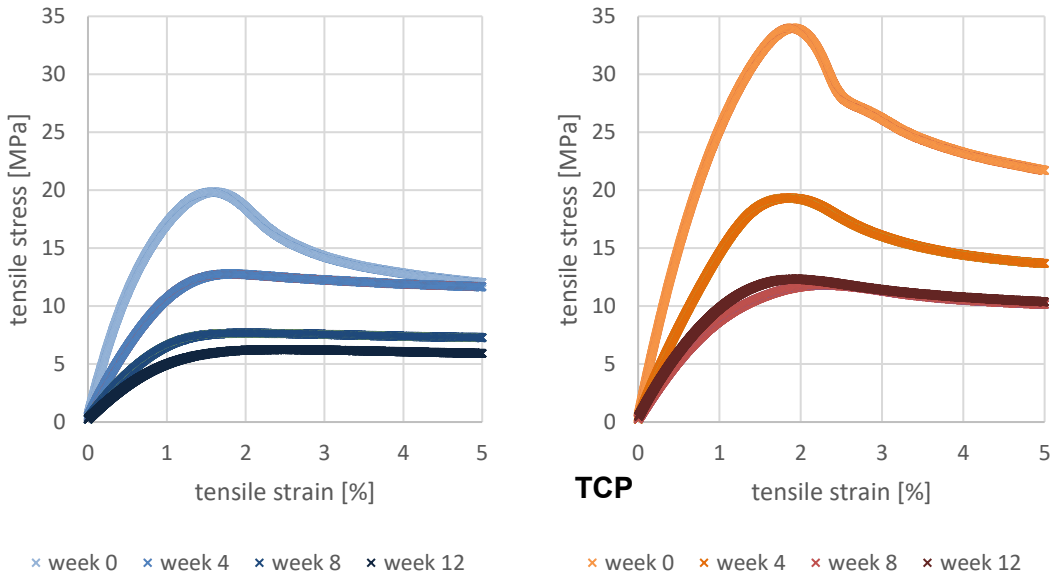

Figure 24. *Comparison of stress-strain curves from tensile testing during the degradation. Representative curves for each time point shown.*

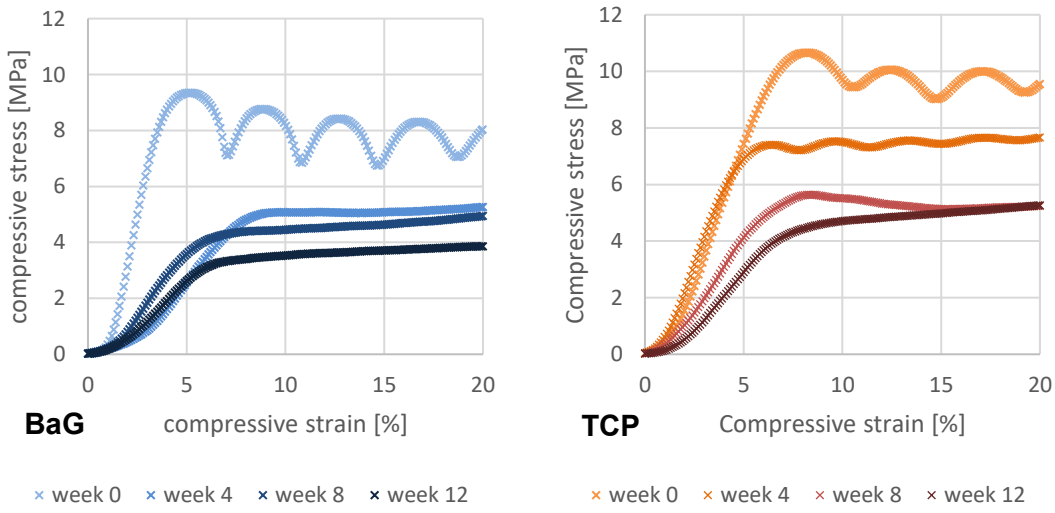

Figure 25. *Comparison of stress-strain curves from unconfined compression testing during the degradation. Representative curves for each time point shown.*

Representative figures of unconfined compression are shown in Figure 25. The shape of the curves was rather variable. However, a clear trend could be observed with a transition between 4 types of behaviour. The first type was a relatively brittle behaviour with many stress peaks with decreasing peak values, which was described earlier and was representative for week 0. The second type was similar; however, the peak values were increasing. The third type exhibited only one peak followed by a moderate decrease in stress, which was however followed by an increase that continued during the rest of the test as the pores became filled. In the fourth type, there was no decrease in stress during the test and therefore also no peak.

In the case of the first and second type of behaviour, the first peak can be defined as first compressive strength, using terminology from ISO 13314 used for porous metals. It can be also defined as yield according to ISO 604 which defines compression testing of plastics. In the case of the third type, the peak matches definitions for both yield and compressive strength according to ISO 604. However, in the case of the fourth type, no kind of strength value could be defined by standards other than 0.2 % offset yield that is not defined in ISO 604. However, as 0.2 % offset yield is the only strength value definable for all time points, it was used as a measure of strength. Unlike in tensile testing, the transition between different behaviours was not homogenous and usually, multiple types of behaviour occurred at the same time point with different specimens. The change was noticeably faster in the case of the bioactive glass composite, showing the higher reactivity. The second, third and fourth type of behaviour were observed at week 4, but only the fourth type occurred starting from week 8. In the case of the TCP composite, even at week 12, one specimen showed a transition between the first and second type (in which case it was not clear whether the stress peaks were increasing or decreasing), while the other specimens showed the third or fourth type behaviours. For a complete picture, all stress-strain curves from all time points can be seen in Appendix A.

Changes in stiffness were also observed. The elastic modulus generally decreased during the degradation. The tensile elastic modulus of the plates decreased substantially between weeks 0 and 4. Then it kept decreasing until week 8, after which the changes were not significant. This behaviour was generally the same for both composites, only the modulus of the TCP composite was higher, with significant differences at weeks 4, 8, and 12 ($p=0.002$, 0.012, 0.013 for weeks 4, 8, and 12, respectively). The global elastic modulus in compression of the porous scaffolds showed a steady decrease in the case of the TCP composite. On the other hand, in the case of the bioactive glass composite, it exhibited a substantial drop only between weeks 0 and 4, which was followed by stagnation. The modulus values generally featured high variation at each timepoint and there were small differences between the two composites. Only at week 12, the difference was found significant ($p=0.024$). It suggests that the material of the filler did not have a very significant impact on the stiffness of the composites. Only the reactivity of the filler materials affected its dissolution which in turn affected mechanical properties at later time points and created bigger differences in stiffness between the materials.

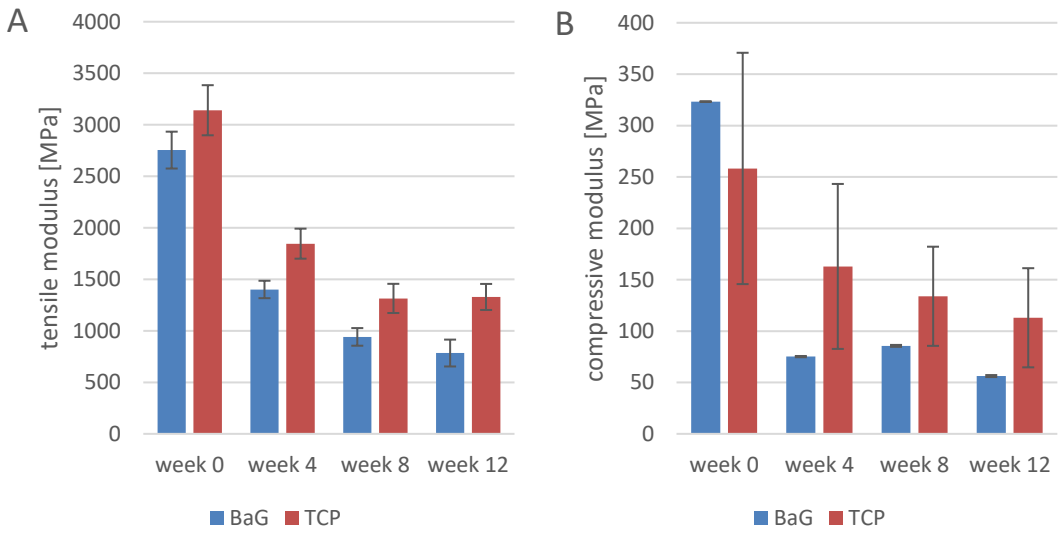

Figure 26. *A: tensile elastic modulus, B: global compressive elastic modulus. Presented as mean ± SD (n=3-7).*

All the noticed changes in mechanical behaviour and properties during the degradation suggest that the mechanical behaviour of both composites was changing to more ductile. Polylactide is brittle at room temperature [97,98], but it becomes more ductile at higher temperatures closer to the glass transition temperature and can become ductile at body temperature [94]. The glass transition temperature of the tested polymer was 68 °C. In tensile testing the behaviour was ductile already at week 0. In compression testing, the porous scaffolds still behaved in a globally brittle manner at week 0, showing behaviour representative for brittle cellular polymer structures. It was similar to the behaviour of PLA tested at room temperature [99] with local failures creating many peaks in the stress-strain curve. However, this behaviour was changed during the degradation, and the absence of peaks showed a transition to a ductile behaviour during the degradation.

5.3.2 Creep-recovery testing

Figure 27 shows the results of creep-recovery testing from week 8. Several phenomena representative for all time points and both materials can be seen in this figure. Both materials exhibit permanent creep, representative for PLA [45], characterized by the non-zero slope of the creep curve at the end of the creep phase and by the presence of permanent, non-recoverable creep strain at the end of the recovery phase. Another observation is, that there is a high variety in the value of creep strain.

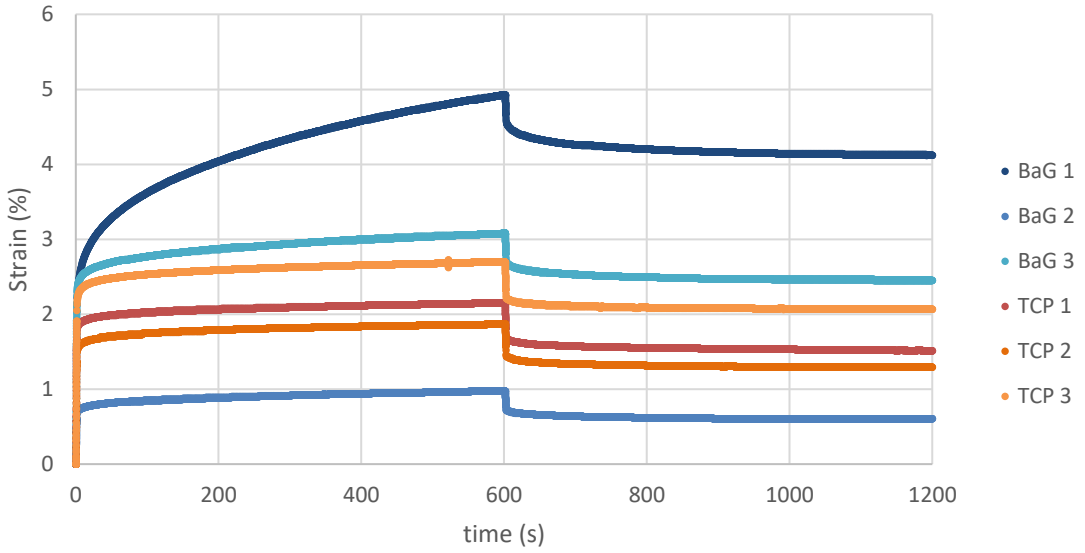

Figure 27. *Results from week 8 compression creep-recovery test. All curves have a non-zero slope at the end of the creep phase, indicating the presence of permanent creep, which also results in non-recoverable deformation after the end of the recovery phase.*

Changes in maximum and permanent creep strain values during the degradation can be seen in Figure 28 for compression testing and Figure 29 for tensile testing. In compression, the trend of the change in maximum and permanent creep strain seemed to be an increase followed by a decrease. However, because of high variations and relatively small sample sizes at weeks 8 and 12, the trend cannot be considered certain. Nevertheless, the initial increase in both values can be seen clearly. It happened between weeks 0 and 4 in the case of the bioactive glass composite and between weeks 4 and 8 in the case of the TCP composite and it was found significant in both cases with the exception of permanent strain of the TCP composite. This may be a sign of a slower dissolution of the TCP filler shown by pH changes and mass retention. The high variations in recorded strain values might be caused by slight variations in specimen dimensions that are caused by their manual preparation. The test was controlled by loading force that would cause slightly different stress levels in specimens with varying cross-sections. Also, the test was conducted at very low loads and deformation and therefore the results are relatively sensitive to various kinds of external effects.

Various tendencies in creep behaviour of PLA and its blends and composites were previously reported. In a 70000 s tensile creep test, pure PLA showed decreased maximum creep strain after 8 weeks that decreased again after 16 weeks. However, PLA-BPS showed increasing maximum creep strain in the same test after 8 and 16 weeks [93]. Elsewhere, pure PLA showed increased maximum creep strain and permanent strain in a tensile 600 s creep 600 s recovery test after 6 months of degradation. In a cyclic test

with the same parameters, the accumulation of permanent strain increased dramatically after degradation and led to rupture after 4 cycles. In the same test, PLA composite with two different grades of graphene nanoplates (GNP) filler showed reduced maximum creep strain after degradation. Permanent creep strain decreased in the case of one of the GNP grades and increased in the case of the other grade. In both cases, the accumulation of permanent strain during a cyclic test increased after degradation but was still very low when compared to pure PLA and did not lead to a rupture during the test [49]. Such mixed results suggest that it is difficult to predict the changes in creep behaviour of polylactide during degradation. It likely depends on the filler material in the case of composites and possibly also on the L and DL ratio in the polylactide and molecular weight of the polymer.

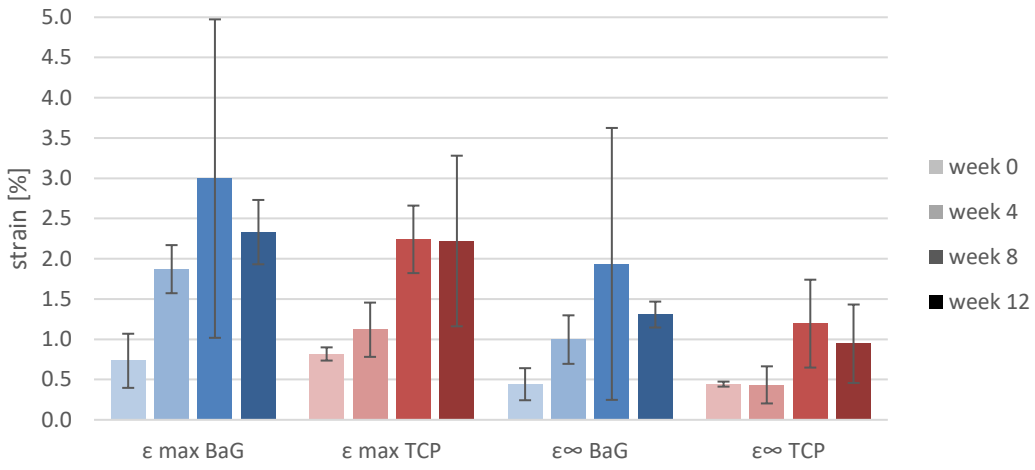

Figure 28. *Maximum creep strain ε_{max} and permanent creep strain ε_{∞} in compression creep testing. Presented as mean ± SD (n=3-5).*

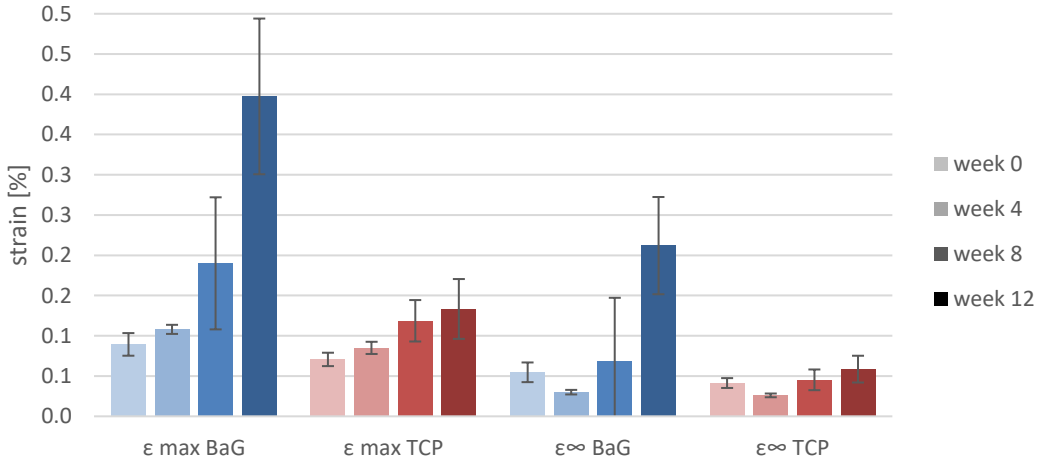

Figure 29. *Maximum creep strain ε_{max} and permanent creep strain ε_{∞} in tensile creep testing. Presented as mean ± SD (n=2-4).*

Because the plates were bending and twisting during degradation, there were not enough specimens to perform creep-recovery testing with the desired number of specimens. Only 2 specimens of the bioactive glass composite were successfully tested at weeks 4 and 8. Therefore, no statistical analysis was performed, and the results from weeks 4 and 8 are only indicative of a probable trend in the degradation and creep behaviour between weeks 0 and 12. They suggest a steady increase of maximum creep strain and a delayed increase in permanent creep strain that appears after week 4 or 8. It is, however, clearly noticeable that the increase in both maximum and permanent creep deformation of the bioactive glass composite between weeks 0 and 12 was much higher compared to the TCP composite. While there is no clear difference between the two materials at week 0, at week 12, both maximum and permanent creep strain values are about thee times higher in the case of the bioactive glass composite, indicating higher reactivity of the bioactive glass and its impact on the change of mechanical properties during the degradation.

5.3.3 Dynamic testing

Dynamic cyclic compression testing was performed with 1000 cycles of sinusoidal strain waveform, using low strains within the elastic region of the materials. However, the testing machine was not tuned properly and needed 200-300 cycles to reach desired strain amplitude and establish the waveform. Therefore, the first 300 cycles were considered as precycling and behaviour between cycles 300 and 1000 was compared. Figure 30 and Figure 31 show peak values of stress at cycles 300 and 1000 for compression testing of the bioactive glass and TCP composite.

In tensile testing, the creep effect was so high, that it was impossible to find suitable parameters to conduct the test. Even a small strain range as 0.076-0.124 % at 0.5 Hz accumulated so much unrecoverable strain during the test, that the unloaded length of the specimen exceeded the lower extreme of the strain waveform, and the loading started producing compression load. Therefore, only compression testing was evaluated.

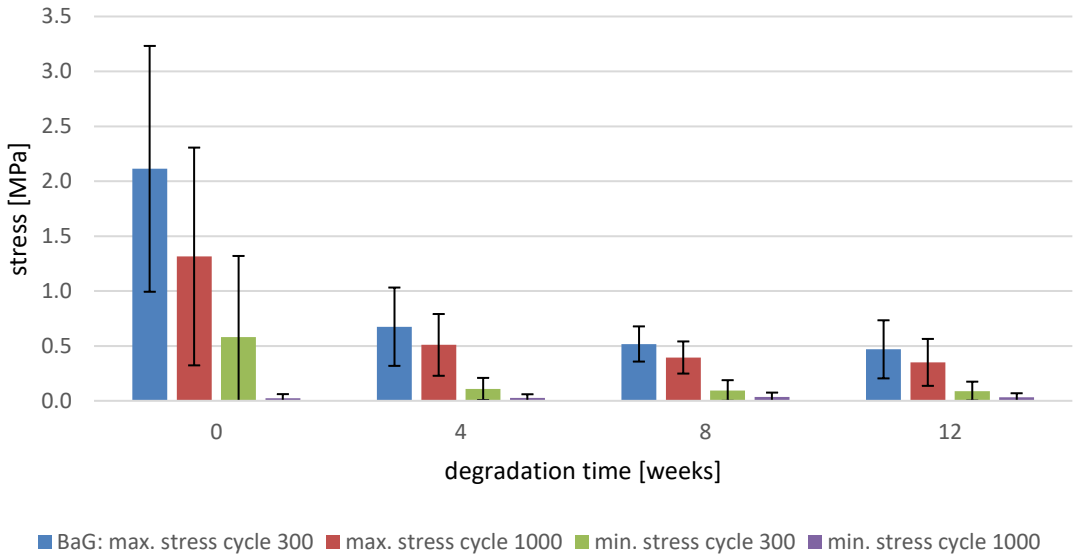

Figure 30. *Changes in peak stress values of the bioactive glass composite during degradation and between cycles 300 and 1000 in a compression test. Presented as mean ± SD (n=3-5).*

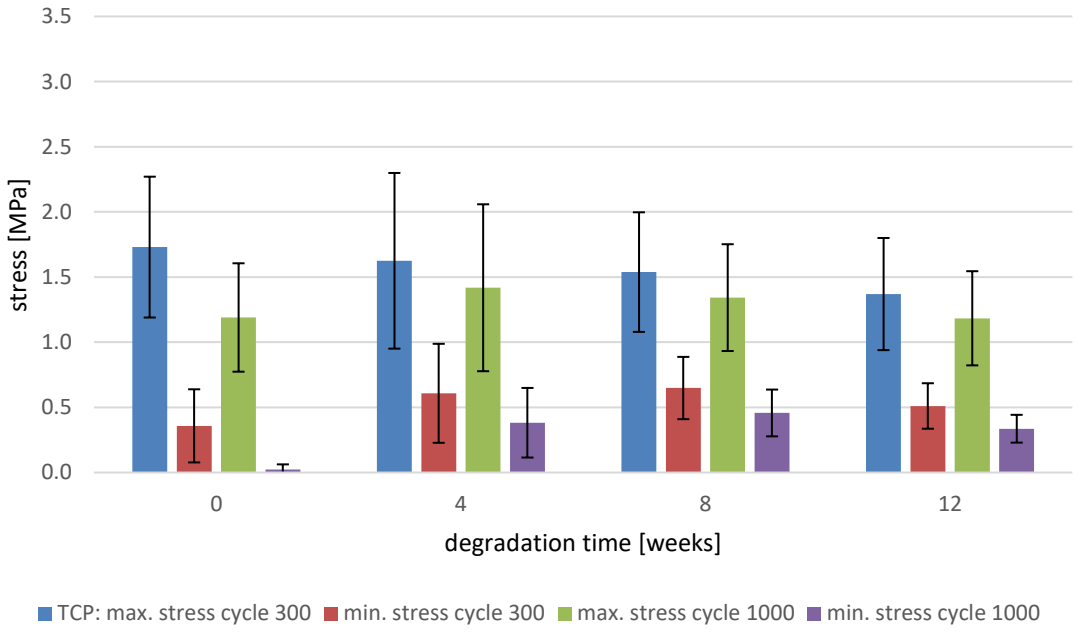

Figure 31. *Changes in peak stress values of the TCP composite during degradation and between cycles 300 and 1000 in a compression test. Presented as mean ± SD (n=3-5).*

In the case of the bioactive glass composite, the peak stress values were decreasing dramatically during the test, especially in the case of non-degraded material, where the maximum stress value decreased by 42 % and the minimum stress by 97 %. During the degradation, the overall stress values were decreasing with decreasing strength of the material. The drop in peak values during the test was becoming smaller at first with degradation, but the drop in minimum stress started to rise again at week 12. The smallest

decrease occurred in week 8. There was no change in the decrease of the maximum value between weeks 4 and 12.

Similar behaviour was observed with the TCP composite, only with smaller decreases in peak values. At time points after degradation, the percentual decrease was about 2x smaller. The biggest decrease in both maximum and minimum stress was observed at week 0, and the smallest at week 8. The percentual decreases in peak stress values are shown in Figure 32.

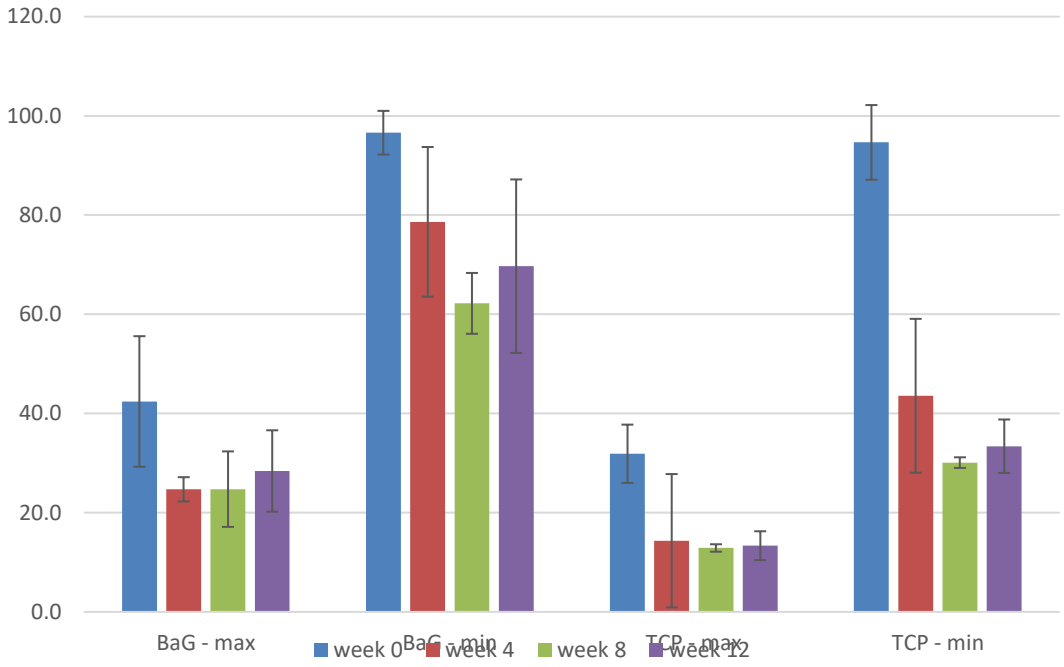

Figure 32. *Average percentual drop in stress peak values between cycles 300 and 1000.*

There are two mechanisms that cause a decrease in stress in the cyclic testing – creep and stress relaxation [3]. The basic form of cyclic testing is tension/compression with load oscillating between tension and compression and the mean load value is zero. Cyclic testing in pure compression or tension can be seen as a combination of creep test and cyclic test with zero mean loads [2]. The dynamic test was driven by strain, but it was strain calculated from the original dimensions. However, due to permanent creep deformation, which was shown during creep-recovery testing, the dimensions of the non-loaded specimen changed. True strain, calculated using the actual length of the unloaded specimen then became smaller, and therefore, also the stress, already lowered by stress relaxation that was happening at the same time, became smaller. Also, the part of creep deformation that is recoverable did not have time to recover completely and was accumulating during the test and appeared as permanent deformation, further lowering the stress.

While stress reduction in the material due to relaxation is not likely to be dangerous for the success of a potential real-life implant, creep can be. If the amount of compression creep deformation is too high, it may produce a tensile load on the interface between the material and the surrounding tissue after the load causing the creep is removed. If the strength of the newly formed connection between the implant and the surrounding tissue is not high enough before cyclic loading of high magnitudes such as walking is enabled, the permanent changes due to fatigue and creep, caused by the cyclic loading, may lead to implant failure.

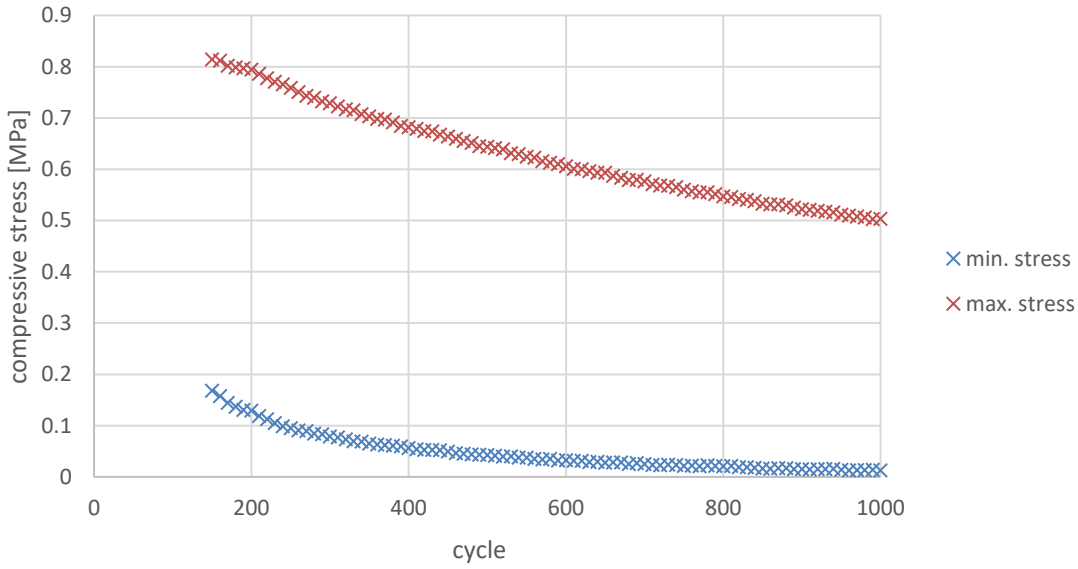

Figure 33. *Stress peaks during cyclic loading from the point when the loading waveform stabilized. A representative curve showing behaviour that was shared by all specimens at all time points. The incremental decrease in stress has a decreasing trend.*

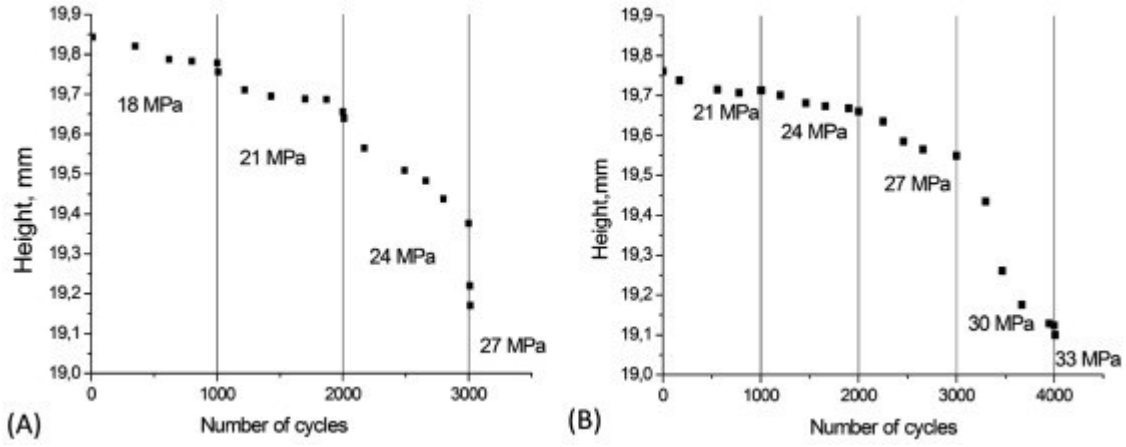

Figure 34. *Decrease in height of a specimen under cyclic load driven by stress with different peak loads. Under peak loads below yield, the incremental decrease in height between cycles is decreasing* [48].

However, the decrease in stress in strain-driven test (Figure 33) or increase in non-recoverable deformation in a stress-driven test performed by Senatov et al. (Figure 34)

shows a decreasing trend in cyclic testing [48]. Therefore, a preload can reduce the decrease in implant height that would be high enough to create a substantial tensile load on the implant-tissue interface. In practice, static preload can be achieved by using an implant slightly larger than the cavity where it is implanted.

Because of the fact that the machine reached the specified amplitude only after 200-300 cycles due to improper tuning, the hysteresis behaviour was not evaluated. Most of the changes in the hysteresis behaviour happened during the first cycles, but since the stress amplitude was not constant, there are too many factors affecting the shape of the hysteresis loops and proper evaluation is not possible.

5.3.4 Confined compression testing

Only static testing was done in confined compression. The deformations created during dynamic and creep testing are too low and to achieve an effect of the confinement, more precise equipment would be necessary. It would have to have an adjustable diameter of the confining chamber so that it perfectly matches the diameter of each specimen. With the current equipment, described earlier, it was not even possible to produce reliable results of static testing during the degradation. They were affected by the difference between the mechanical properties of the original material of the chambers and the aluminium foil that was used to adjust the diameter of the chamber so that it matched the specimen. Therefore, only changes in mechanical behaviour, and especially differences between the behaviour in confined and unconfined compression will be described and no numerical values will be presented for confined compression testing. Comparison of behaviour only can nevertheless suggest how would a porous scaffold behave in situ in a situation where it would be partially or fully confined.

Figure 35 shows a comparison of stress-strain curves from confined and unconfined compression at all time points. At week 0, the confined scaffold tested in confined compression showed clearly different behaviour. Repeating sudden collapses typical for unconfined compression testing were accompanied by local bursts in diameter, which are however prevented in unconfined compression. Therefore, rather homogenous compacting took place. In the case of the bioactive glass, the initial pseudo linear region was followed by a distinct yield, followed by a decrease in stress, a relatively short plateau, and a subsequent increase in stress as the pores had been mostly filled. The TCP composite did not exhibit a clear yield and there was no decrease in stress during the test.

Between weeks 0 and 4, the behaviour of the bioactive glass composite changed noticeably. At week 4, its stress-strain curve was nearly linear from the beginning of the test until 20 % strain. At week 4, it reached a similar stress value at 20 % strain as unconfined

compression testing. At weeks 8 and 12, some specimens produced nearly linear stress-strain curves, while others exhibited slight yield dividing two nearly linear parts of the curve. In both weeks, the stress values appeared lower than in the case of unconfined compression. The behaviour of the TCP composite was similar at weeks 4 and 8. It reached substantially higher stress values than in unconfined compression. The stress-strain curves showed yield, followed by a decrease in the slope of the curve, but not in the stress value. Subsequently, the slope increased again. At week 12, the TCP composite behaved similarly to the bioactive glass composite, with a nearly linear stress-strain curve. It however reached substantially higher stress values.

The behaviour in confined compression shows signs of stronger change to elastic behaviour. Often, there is no distinct yield starting already from week 4. A recognizable onset of compaction, characterized by an increase in the slope of the stress-strain curve can only be seen at week 8 in the case of the TCP composite and at week 0 in the case of the bioactive glass composite.

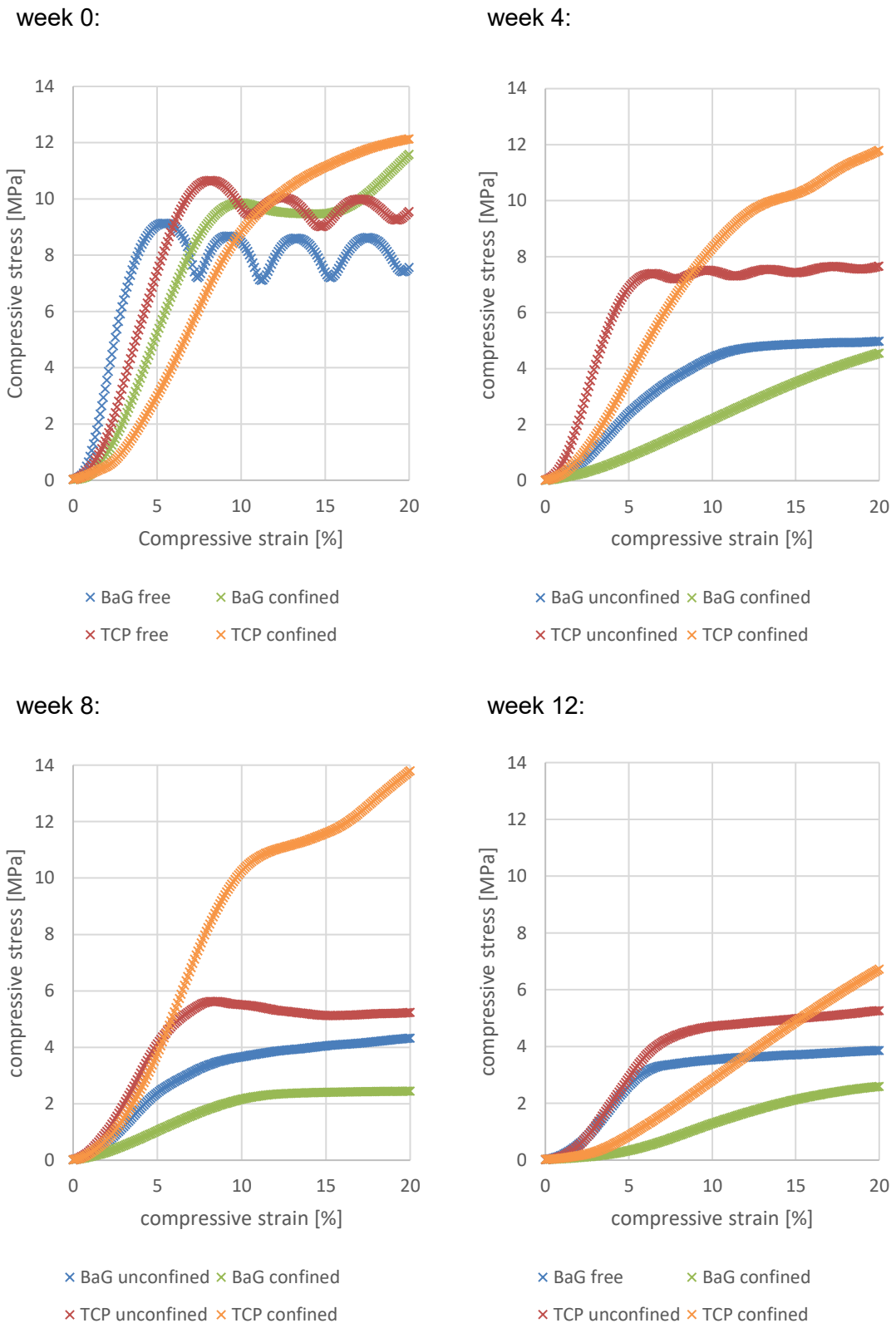

Figure 35. *Representative stress-strain curves from confined and unconfined compression testing.*

6. CONCLUSION

Mechanical testing of composite materials with two different fillers was performed. Bioactive glass 13-93 and β-tricalcium phosphate were used as the fillers, while poly-L-DL-lactide 70/30 was used as a matrix in both composites. Static, dynamic, and creep-recovery testing were performed in tension, and confined and unconfined compression to evaluate the behaviour of the materials in different situations. All tests were done at 4 time points throughout 12-week in vitro degradation in TRIS buffer solution. Changes in mechanical behaviour during the degradation and differences between the two composites were observed.

Changes in pH, mass retention, and ion release during the degradation confirmed the expectation that the bioactive glass is more reactive than the β-TCP and dissolves faster. In all tests, the changes in the behaviour of the β-TCP composite were smaller than in the case of the bioactive glass composite.

In static testing, the TCP composite showed significantly higher tensile strength, but the compressive strength and both tensile and compressive moduli were comparable before degradation. However, during the degradation, the differences between the composites became larger due to the faster dissolution of the bioactive glass. PLA is known to be brittle at room temperature, however, at 37°C, the tested material was ductile in tensile testing at all time points, and in compression testing, the global behaviour of the porous structures changed from brittle to ductile during the degradation.

Creep-recovery testing showed that both composites feature creep behaviour reported previously for PLA and its composites, characterized by a permanent creep with a substantial amount of nonrecoverable creep strain. In accordance with that, the behaviour of both materials changes considerably when they are subject to cyclic load. Due to a combination of creep and stress relaxation, the same strain load produced substantially lower stress levels in the material after 700 cycles. The TCP composite however showed a higher creep resistance and reached a lower maximum and permanent creep values. Also, the drop in stress values during the cyclic testing was lower.

Confined compression testing was performed in addition to traditional unconfined compression testing. Custom made equipment that is being developed was used. Because the equipment could not produce reliable confinement to specimens with varying diameters, especially at low deformations, it was used only for static testing and only the shape of the stress-strain curves was analysed as the numerical values are not precise

enough for comparison. The confinement however caused a very distinct change in material behaviour during compression testing.

It is not possible to clearly say which material is better. The strength of the TCP composite is in all cases higher or at least comparable to the bioactive glass composite and has better creep resistance. However, its degradation might be too slow for many applications. The bioactive composite degrades faster and it is bioactive, and therefore promises better support of tissue regeneration. Both materials can be chosen depending on what property is considered the most important for a particular application.

To further investigate the properties of the materials, a stress-driven cyclic test with a proper tuning of the machine performed before the testing can be done to study hysteresis and cyclic creep behaviour. In a stress-driven test, it would be also possible to perform tensile testing of the sheets, which was not possible in a strain-driven test due to too quick accumulation of permanent strain. Besides 0.2 % offset yield, it was not possible to identify any other well-defined type of strength of the porous scaffolds that would be applicable at all timepoints. At time points later during the degradation, the collapsing of the pores happened too smoothly, and no clear point of mechanical failure could be identified. However, a custom measure of strength can be created and defined and used for comparison of the two materials.

To continue the work this thesis has started, data obtained from the performed mechanical tests can be used for mathematical modelling to perform finite element method (FEM) analysis and create constitutive models. The basic modelling that can be performed is FEM simulation of static testing or fitting the creep-recovery data on Burgers viscoelastic model. Also, more advanced models, that would simulate the static and dynamic mechanical behaviour of the porous scaffolds and their change during degradation can be created. These models can be used to predict the mechanical behaviour of modified scaffolds in different situations. This way, the scaffolds can be designed more efficiently.

REFERENCES

[1] L. Draghi, Static and uniaxial characterization of polymer biomaterials, in: M.C. Tanzi, S. Farè (Eds.), Characterization of Polymeric Biomaterials, Woodhead Publishing, 2017: pp. 177–202. https://doi.org/10.1016/B978-0-08-100737-2.00008-X.

[2] J.F. Mano, N.M. Neves, R.L. Reis, Biodegradable Systems in Tissue Engineering and Regenerative Medicine, in: R.L. Reis, J. San Román (Eds.), Biodegradable Systems in Tissue Engineering and Regenerative Medicine, CRC Press, 2004: pp. 127–144. https://doi.org/10.1201/9780203491232.

[3] R.K. Roeder, Mechanical Characterization of Biomaterials, in: A. Bandyopadhyay, S. Bose (Eds.), Characterization of Biomaterials, Elsevier Inc, 2013: pp. 49–104. https://doi.org/10.1016/B978-0-12-415800-9.00003-6.

[4] O.R. Vazquez, I.O. Avila, J.C.S. Díaz, E. Hernandez, An Overview of Mechanical Tests for Polymeric Biomaterial Scaffolds Used in Tissue Engineering, Journal of Research Updates in Polymer Science. 4 (2015) 168–178. https://doi.org/10.6000/1929-5995.2015.04.04.1.

[5] B. Basu, Mechanical Properties of Biomaterials, in: B. Basu, S. Ghosh (Eds.), Biomaterials for Musculoskeletal Regeneration: Concepts, Springer Singapore, Singapore, 2017: pp. 175–222. https://doi.org/10.1007/978-981-10-3059-8_6.

[6] J.A. Epaarachchi, The effect of viscoelasticity on fatigue behaviour of polymer matrix composites, Creep and Fatigue in Polymer Matrix Composites. (2011) 492–513. https://doi.org/10.1533/9780857090430.3.492.

[7] W.N. (William N. Findley, J.S. Lai, Kasif. Onaran, Creep and relaxation of nonlinear viscoelastic materials : with an introduction to linear viscoelasticity, (1989) 371.

[8] A.P.G. Castro, D. Lacroix, Micromechanical study of the load transfer in a polycaprolactone–collagen hybrid scaffold when subjected to unconfined and confined compression, Biomechanics and Modeling in Mechanobiology. 17 (2018) 531–541. https://doi.org/10.1007/s10237-017-0976-5.

[9] F. Linde, I. Hvid, The effect of constraint on the mechanical behaviour of trabecular bone specimens, Journal of Biomechanics. 22 (1989) 485–490. https://doi.org/10.1016/0021-9290(89)90209-1.

[10] J.R. Jones, L.L. Hench, Biomedical materials for new millennium: perspective on the future, Https://Doi.Org/10.1179/026708301101510762. 17 (2013) 891–900. https://doi.org/10.1179/026708301101510762.

[11] A. Dolcimascolo, G. Calabrese, S. Conoci, R. Parenti, Innovative Biomaterials for Tissue Engineering, Biomaterial-Supported Tissue Reconstruction or Regeneration. (2019). https://doi.org/10.5772/INTECHOPEN.83839.

[12] L.J. White, V. Hutter, H. Tai, S.M. Howdle, K.M. Shakesheff, The effect of processing variables on morphological and mechanical properties of supercritical CO2 foamed scaffolds for tissue engineering, Acta Biomaterialia. 8 (2012) 61–71. https://doi.org/10.1016/J.ACTBIO.2011.07.032.

[13] A. Stahl, Y.P. Yang, Regenerative Approaches for the Treatment of Large Bone Defects, Tissue Engineering Part B: Reviews. 27 (2021) 539–547. https://doi.org/10.1089/TEN.TEB.2020.0281/ASSET/IMAGES/LARGE/TEN.TEB.2020.0281_FIGURE3.JPEG.

[14] W. Xiao, M.A. Zaeem, G. Li, B. Sonny Bal, M.N. Rahaman, Tough and strong porous bioactive glass-PLA composites for structural bone repair, Journal of Materials Science. 52 (2017) 9039–9054. https://doi.org/10.1007/S10853-017-0777-3/FIGURES/14.

[15] T.A. van Vugt, J.A.P. Geurts, J.J. Arts, N.C. Lindfors, Biomaterials in treatment of orthopedic infections, Management of Periprosthetic Joint Infections (PJIs). (2017) 41–68. https://doi.org/10.1016/B978-0-08-100205-6.00003-3.

[16] D. Gorth, T.J. Webster, Matrices for tissue engineering and regenerative medicine, Biomaterials for Artificial Organs. (2011) 270–286. https://doi.org/10.1533/9780857090843.2.270.

[17] R. Francis, N. Joy, A. Sivadas, Relevance of Natural Degradable Polymers in the Biomedical Field, Biomedical Applications of Polymeric Materials and Composites. (2016) 303–360. https://doi.org/10.1002/9783527690916.CH11.

[18] R. Francis, N. Joy, A. Sivadas, Synthetic Biodegradable Polymers for Medical and Clinical Applications, Biomedical Applications of Polymeric Materials and Composites. (2016) 361–382. https://doi.org/10.1002/9783527690916.CH12.

[19] L. Jiang, J. Zhang, Biodegradable and Biobased Polymers, Applied Plastics Engineering Handbook: Processing, Materials, and Applications: Second Edition. (2017) 127–143. https://doi.org/10.1016/B978-0-323-39040-8.00007-9.

[20] A.J. (Abraham J.) Domb, Joseph. Kost, D.M. Wiseman, Handbook of biodegradable polymers, (1997).

[21] S.H. Zeng, P.P. Duan, M.X. Shen, Y.J. Xue, Z.Y. Wang, Preparation and degradation mechanisms of biodegradable polymer: A review, IOP Conference Series: Materials Science and Engineering. 137 (2016). https://doi.org/10.1088/1757-899X/137/1/012003.

[22] R. Reshmy, E. Philip, P.H. Vaisakh, R. Sindhu, P. Binod, A. Madhavan, A. Pandey, R. Sirohi, A. Tarafdar, Biodegradable polymer composites, Biomass, Biofuels, Biochemicals. (2021) 393–412. https://doi.org/10.1016/B978-0-12-821888-4.00003-4.

[23] A.S. Luyt, S.S. Malik, Can Biodegradable Plastics Solve Plastic Solid Waste Accumulation?, Plastics to Energy: Fuel, Chemicals, and Sustainability Implications. (2019) 403–423. https://doi.org/10.1016/B978-0-12-813140-4.00016-9.

[24] N. Kurokawa, F. Endo, T. Maeda, A. Hotta, Electrospinning and surface modification methods for functionalized cell scaffolds, Nanostructures for Novel Therapy: Synthesis, Characterization and Applications. (2017) 201–225. https://doi.org/10.1016/B978-0-323-46142-9.00008-6.

[25] F.R. Beltrán, M.P. Arrieta, E. Moreno, G. Gaspar, L.M. Muneta, R. Carrasco-Gallego, S. Yáñez, D. Hidalgo-Carvajal, M.U. de la Orden, J.M. Urreaga, Evaluation of the Technical Viability of Distributed Mechanical Recycling of PLA 3D Printing Wastes, Polymers 2021, Vol. 13, Page 1247. 13 (2021) 1247. https://doi.org/10.3390/POLYM13081247.

[26] K. Fukushima, Poly(trimethylene carbonate)-based polymers engineered for biodegradable functional biomaterials, Biomaterials Science. 4 (2015) 9–24. https://doi.org/10.1039/C5BM00123D.

[27] K. Deshmukh, M. Basheer Ahamed, R.R. Deshmukh, S.K. Khadheer Pasha, P.R. Bhagat, K. Chidambaram, Biopolymer Composites With High Dielectric Performance: Interface Engineering, Biopolymer Composites in Electronics. (2017) 27–128. https://doi.org/10.1016/B978-0-12-809261-3.00003-6.

[28] S.J. Langley-Hobbs, Sutures and general surgical implants, Feline Soft Tissue and General Surgery. (2014) 105–116. https://doi.org/10.1016/B978-0-7020-4336-9.00010-X.

[29] R.C. Moser, A.J. McManus, S.L. Riley, K.A. Thomas, Strength retention of 70:30 poly(L-lactide-co-D,L-lactide) following real-time aging, Journal of Biomedical Materials Research Part B: Applied Biomaterials. 75B (2005) 56–63. https://doi.org/10.1002/JBM.B.30238.

[30] L.T. Sin, A.R. Rahmat, W.A.W.A. Rahman, Overview of Poly(lactic Acid), Handbook of Biopolymers and Biodegradable Plastics: Properties, Processing and Applications. (2013) 11–54. https://doi.org/10.1016/B978-1-4557-2834-3.00002-1.

[31] A. Göpferich, Mechanisms of polymer degradation and erosion, The Biomaterials: Silver Jubilee Compendium. (1996) 117–128. https://doi.org/10.1016/B978-008045154-1.50016-2.

[32] R. Francis, D. Sakthi Kumar, Biomedical Applications of Polymeric Materials and Composites, Biomedical Applications of Polymeric Materials and Composites. (2016) 1–389. https://doi.org/10.1002/9783527690916.

[33] F. Baino, G. Novajra, C. Vitale-Brovarone, Bioceramics and scaffolds: A winning combination for tissue engineering, Frontiers in Bioengineering and Biotechnology. 3 (2015) 202. https://doi.org/10.3389/FBIOE.2015.00202/BIBTEX.

[34] R.Z. LeGeros, Properties of Osteoconductive Biomaterials: Calcium Phosphates, Clinical Orthopaedics and Related Research®. 395 (2002). https://journals.lww.com/clinorthop/Fulltext/2002/02000/Properties_of_Osteoconductive_Biomaterials_.9.aspx.

[35] H. Oonishi, H. Oonishi, S.C. Kim, L.L. Hench, J. Wilson, E. Tsuji, H. Fujita, H. Oohashi, K. Oomamiuda, Clinical application of hydroxyapatite, Bioceramics and Their Clinical Applications. (2008) 606–687. https://doi.org/10.1533/9781845694227.3.606.

[36] J. Huang, Chapter 20 - Design and Development of Ceramics and Glasses, in: Biology and Engineering of Stem Cell Niches, Elsevier Inc, 2017: pp. 315–329. https://doi.org/10.1016/B978-0-12-802734-9.00020-2.

[37] A. El-Ghannam, P. Ducheyne, 1.9 Bioactive Ceramics, in: Comprehensive Biomaterials II, Second Edition, Elsevier Ltd, 2017: pp. 204–234. https://doi.org/10.1016/B978-0-12-803581-8.10169-9.

[38] S. Aunoble, D. Clément, P. Frayssinet, M.F. Harmand, J.C. le Huec, Biological performance of a new β-TCP/PLLA composite material for applications in spine surgery: In vitro and in vivo studies, Journal of Biomedical Materials Research Part A. 78A (2006) 416–422. https://doi.org/10.1002/JBM.A.30749.

[39] E.H. Backes, L. de Nóbile Pires, H.S. Selistre-de-Araujo, L.C. Costa, F.R. Passador, L.A. Pessan, Development and characterization of printable PLA/β-TCP bioactive composites for bone tissue applications, Journal of Applied Polymer Science. 138 (2021). https://doi.org/10.1002/APP.49759.

[40] J.M. Ferri, I. Gisbert, D. García-Sanoguera, M.J. Reig, R. Balart, The effect of beta-tricalcium phosphate on mechanical and thermal performances of poly(lactic acid):, Http://Dx.Doi.Org/10.1177/0021998316636205. 50 (2016) 4189–4198. https://doi.org/10.1177/0021998316636205.

[41] R.G. Carrodeguas, S. de Aza, α-Tricalcium phosphate: Synthesis, properties and biomedical applications, Acta Biomaterialia. 7 (2011) 3536–3546. https://doi.org/10.1016/J.ACTBIO.2011.06.019.

[42] H. Chaair, H. Labjar, O. Britel, Synthesis of β-tricalcium phosphate, Morphologie. 101 (2017) 120–124. https://doi.org/10.1016/J.MORPHO.2017.06.002.

[43] L.L. Hench, J.R. Jones, Bioactive glasses: Frontiers and Challenges, Frontiers in Bioengineering and Biotechnology. 3 (2015) 194. https://doi.org/10.3389/FBIOE.2015.00194/BIBTEX.

[44] Y.C. Hu, J.P. Zhong, Osteostimulation of bioglass, Chinese Medical Journal. 122 (2009) 2386–2389. https://doi.org/10.3760/CMA.J.ISSN.0366-6999.2009.19.035.

[45] J.M. Ferri, I. Gisbert, D. García-Sanoguera, M.J. Reig, R. Balart, The effect of beta-tricalcium phosphate on mechanical and thermal performances of poly(lactic acid), Journal of Composite Materials. 50 (2016) 4189–4198. https://doi.org/10.1177/0021998316636205.

[46] R. Sergi, D. Bellucci, V. Cannillo, A Review of Bioactive Glass/Natural Polymer Composites: State of the Art, Materials (Basel). 13 (2020) 1–38. https://doi.org/10.3390/MA13235560.

[47] J.A. Killion, S. Kehoe, L.M. Geever, D.M. Devine, E. Sheehan, D. Boyd, C.L. Higginbotham, Hydrogel/bioactive glass composites for bone regeneration applications: Synthesis and characterisation, Materials Science and Engineering: C. 33 (2013) 4203–4212. https://doi.org/10.1016/J.MSEC.2013.06.013.

[48] F.S. Senatov, K. v. Niaza, A.A. Stepashkin, S.D. Kaloshkin, Low-cycle fatigue behavior of 3d-printed PLA-based porous scaffolds, Composites Part B: Engineering. 97 (2016) 193–200. https://doi.org/10.1016/J.COMPOSITESB.2016.04.067.

[49] A.M. Pinto, C. Gonçalves, I.C. Gonçalves, F.D. Magalhães, Effect of biodegradation on thermo-mechanical properties and biocompatibility of poly(lactic acid)/graphene nanoplatelets composites, European Polymer Journal. 85 (2016) 431–444. https://doi.org/10.1016/J.EURPOLYMJ.2016.10.046.

[50] M. Morreale, M.C. Mistretta, V. Fiore, Creep Behavior of Poly(lactic acid) Based Biocomposites, Materials 2017, Vol. 10, Page 395. 10 (2017) 395. https://doi.org/10.3390/MA10040395.

[51] T. Winkler, F.A. Sass, G.N. Duda, K. Schmidt-Bleek, A review of biomaterials in bone defect healing, remaining shortcomings and future opportunities for bone tissue engineering: The unsolved challenge, Bone and Joint Research. 7 (2018) 232–243. https://doi.org/10.1302/2046-3758.73.BJR-2017-0270.R1.

[52] J.J. Blaker, J.E. Gough, V. Maquet, I. Notingher, A.R. Boccaccini, In vitro evaluation of novel bioactive composites based on Bioglass®-filled polylactide foams for bone tissue engineering scaffolds, Journal of Biomedical Materials Research - Part A. 67 (2003) 1401–1411. https://doi.org/10.1002/jbm.a.20055.

[53] T.A. Saleh, Hybrid materials: fundamentals and classifications, Polymer Hybrid Materials and Nanocomposites. (2021) 147–176. https://doi.org/10.1016/B978-0-12-813294-4.00001-7.

[54] Q.Z. Chen, A.R. Boccaccini, Poly(D,L-lactic acid) coated 45S5 Bioglass®-based scaffolds: Processing and characterization, Journal of Biomedical Materials Research Part A. 77A (2006) 445–457. https://doi.org/10.1002/JBM.A.30636.

[55] R. Makkonen, Mechanical properties and preliminary in-vitro testing of 3D printed bioactive glass combined with hydrogel, (2021).

[56] A. Prasad, M.R. Sankar, V. Katiyar, State of Art on Solvent Casting Particulate Leaching Method for Orthopedic ScaffoldsFabrication,

Materials Today: Proceedings. 4 (2017) 898–907. https://doi.org/10.1016/J.MATPR.2017.01.101.

[57] F. Serio, M. Miola, E. Vernè, D. Pisignano, A.R. Boccaccini, L. Liverani, Electrospun Filaments Embedding Bioactive Glass Particles with Ion Release and Enhanced Mineralization, Nanomaterials (Basel). 9 (2019). https://doi.org/10.3390/NANO9020182.

[58] T. Distler, N. Fournier, A. Grünewald, C. Polley, H. Seitz, R. Detsch, A.R. Boccaccini, Polymer-Bioactive Glass Composite Filaments for 3D Scaffold Manufacturing by Fused Deposition Modeling: Fabrication and Characterization, Frontiers in Bioengineering and Biotechnology. 8 (2020) 552. https://doi.org/10.3389/FBIOE.2020.00552/BIBTEX.

[59] D.J. Mooney, D.F. Baldwin, N.P. Suh, J.P. Vacanti, R. Langer, Novel approach to fabricate porous sponges of poly(d,l-lactic-co-glycolic acid) without the use of organic solvents, Biomaterials. 17 (1996) 1417–1422. https://doi.org/10.1016/0142-9612(96)87284-X.

[60] J.-P. SCHERMANN, Experimental Methods, Spectroscopy and Modeling of Biomolecular Building Blocks. (2008) 129–207. https://doi.org/10.1016/B978-044452708-0.50004-6.

[61] A. Braeuer, High Pressure: Fellow and Opponent of Spectroscopic Techniques, Supercritical Fluid Science and Technology. 7 (2015) 1–40. https://doi.org/10.1016/B978-0-444-63422-1.00001-8.

[62] E. Reverchon, S. Cardea, Supercritical fluids in 3-D tissue engineering, The Journal of Supercritical Fluids. 69 (2012) 97–107. https://doi.org/10.1016/J.SUPFLU.2012.05.010.

[63] Metallic materials. Tensile testing. Part 1: Method of test at room temperature, ISO 6892-1:2019. (2019).

[64] Plastics. Determination of tensile properties. Part 1: General principles, ISO 527-1:2019. (2019).

[65] Plastics — Determination of compressive properties, ISO 604:2002. (2002).

[66] P. Vakrčka, A. Jíra, P. Hájková, Mechanical testing and numerical modelling of porous structures improving oseintegration of implants, Acta Polytechnica CTU Proceedings. 26 (2020) 127–133. https://doi.org/10.14311/APP.2020.26.0126.

[67] ISO 13314:2011(en), Mechanical testing of metals — Ductility testing — Compression test for porous and cellular metals, ISO 13314:2011. (2011).

[68] S. Calloch, D. Marquis, Triaxial tension–compression tests for multiaxial cyclic plasticity, International Journal of Plasticity. 15 (1999) 521–549. https://doi.org/10.1016/S0749-6419(99)00005-4.

[69] K. Zhao, L. Chen, R. Xiao, Z. Ding, L. Zhou, Design of a biaxial tensile testing device and cruciform specimens for large plastic deformation in the central zone, Journal of Materials Science 2019 54:9. 54 (2019) 7231–7245. https://doi.org/10.1007/S10853-019-03358-2.

[70] M.L. Oyen, Mechanical characterisation of hydrogel materials, International Materials Reviews. 59 (2014) 44–59. https://doi.org/10.1179/1743280413Y.0000000022.

[71] D. Li, L. Dong, J. Yin, R.S. Lakes, Negative Poisson's ratio in 2D Voronoi cellular solids by biaxial compression: a numerical study, Journal of Materials Science. 51 (2016) 7029–7037. https://doi.org/10.1007/S10853-016-9992-6.

[72] P. Folino, H. Xargay, Recycled aggregate concrete – Mechanical behavior under uniaxial and triaxial compression, Construction and Building Materials. 56 (2014) 21–31. https://doi.org/10.1016/J.CONBUILDMAT.2014.01.073.

[73] S. Zhao, M. Arnold, R.L. Abel, J.P. Cobb, S. Ma, U. Hansen, O. Boughton, Standardizing compression testing for measuring the stiffness of human bone, Bone & Joint Research. 7 (2018) 524. https://doi.org/10.1302/2046-3758.78.BJR-2018-0025.R1.

[74] J.M. Mansour, Biomechanics of cartilage, in: 2013: pp. 69–83.

[75] F. Boschetti, G. Pennati, F. Gervaso, G. Peretti, G. Dubini, Biomechanical properties of human articular cartilage under compressive loads, Biorheology. 41 (2004) 159–166.

[76] J.M. Patel, B.C. Wise, E.D. Bonnevie, R.L. Mauck, A Systematic Review and Guide to Mechanical Testing for Articular Cartilage Tissue Engineering, Tissue Engineering. Part C, Methods. 25 (2019) 593. https://doi.org/10.1089/TEN.TEC.2019.0116.

[77] J.M. Hodgkinson, Flexure, Mechanical Testing of Advanced Fibre Composites. (2000) 124–142. https://doi.org/10.1533/9781855738911.124.

[78] P. Hajikarimi, F. Moghadas Nejad, Mechanical models of viscoelasticity, Applications of Viscoelasticity. (2021) 27–61. https://doi.org/10.1016/B978-0-12-821210-3.00003-6.

[79] L. de Nardo, S. Farè, Dynamico-mechanical characterization of polymer biomaterials, in: M.C. Tanzi, S. Farè (Eds.), Characterization of Polymeric Biomaterials, Woodhead Publishing, 2017: pp. 203–232. https://doi.org/10.1016/B978-0-08-100737-2.00009-1.

[80] C. Xue, H. Gao, Y. Hu, G. Hu, Experimental test and curve fitting of creep recovery characteristics of modified graphene oxide natural rubber and its relationship with temperature, Polymer Testing. 87 (2020) 106509. https://doi.org/10.1016/J.POLYMERTESTING.2020.106509.

[81] C. Zhang, Z. Zhang, Z. Qiu, Analysis of mixed lubrication of dynamically loaded journal bearings including non-Newtonian effects and mass conserving cavitation, Tribology Series. 34 (1998) 175–186. https://doi.org/10.1016/S0167-8922(98)80072-2.

[82] J.A. Epaarachchi, The effect of viscoelasticity on fatigue behaviour of polymer matrix composites, Creep and Fatigue in Polymer Matrix Composites. (2011) 492–513. https://doi.org/10.1533/9780857090430.3.492.

[83] J. Adhikari, P. Saha, A. Sinha, Surface modification of metallic bone implants—Polymer and polymer-assisted coating for bone in-growth, Fundamental Biomaterials: Metals. (2018) 299–321. https://doi.org/10.1016/B978-0-08-102205-4.00014-3.

[84] N.E. Dowling, Fatigue of Materials: Introduction and Stress-Based Approach, in: N.E. Dowling (Ed.), Mechanical Behavior of Materials, 4th ed., Pearson Higher Education, 2012: pp. 416–490.

[85] N.E. Dowling, Strain-Based Approach to Fatigue, in: N.E. Dowling (Ed.), Mechanical Behavior of Materials, 4th ed., Pearson Higher Education, 2012: pp. 745–801.

[86] J. Antonio Travieso-Rodriguez, M.D. Zandi, R. Jerez-Mesa, J. Lluma-Fuentes, Fatigue behavior of PLA-wood composite manufactured by fused filament fabrication, Journal of Materials Research and Technology. 9 (2020) 8507–8516. https://doi.org/10.1016/J.JMRT.2020.06.003.

[87] Y. Bai, W.-L. Jin, Simplified Fatigue Assessment, Marine Structural Design. (2016) 527–535. https://doi.org/10.1016/B978-0-08-099997-5.00027-7.

[88] E. Suhir, R. Ghaffarian, S. Yi, Probabilistic Palmgren–Miner rule, with application to solder materials experiencing elastic deformations, Journal of Materials Science: Materials in Electronics. 28 (2017) 2680–2685. https://doi.org/10.1007/S10854-016-5845-Y.

[89] S. Karjalainen, Static and dynamic mechanical behavior of biomaterials in dry and simulated physiological conditions, (2016).

[90] N. Dusunceli, N. Theilgaard, Effects of temperature on the relaxation behavior of poly (lactic acid), (2016) 1–4. https://doi.org/10.2417/SPEPRO.006761.

[91] O. Korhonen, Foaming of biopolymer/bioactive glass composites using supercritical carbon dioxide, (2020).

[92] A.R. Boccaccini, V. Maquet, Bioresorbable and bioactive polymer/Bioglass® composites with tailored pore structure for tissue engineering applications, Composites Science and Technology. 63 (2003) 2417–2429. https://doi.org/10.1016/S0266-3538(03)00275-6.

[93] L.D. Kimble, D. Bhattacharyya, In Vitro Degradation Effects on Strength, Stiffness, and Creep of PLLA/PBS: A Potential Stent Material, Http://Dx.Doi.Org/10.1080/00914037.2014.945203. 64 (2014) 299–310. https://doi.org/10.1080/00914037.2014.945203.

[94] P. Merloz, R. Minfelde, C. Schelp, F. Lavaste, J. Huet-Olivier, C. Faure, J. Butel, In vitro study of the properties of bioresorbable lactic acid polymer materials, Revue de chirurgie orthopédique et réparatrice de l'apparell moteur. 81 (1995) 433.

[95] E.A.R. Duek, C.A.C. Zavaglia, W.D. Belangero, In vitro study of poly(lactic acid) pin degradation, Polymer (Guildf). 40 (1999) 6465–6473. https://doi.org/10.1016/S0032-3861(98)00846-5.

[96] L.C. Gerhardt, A.R. Boccaccini, Bioactive glass and glass-ceramic scaffolds for bone tissue engineering, Materials. 3 (2010) 3867–3910. https://doi.org/10.3390/MA3073867.

[97] M. Razavi, S.-Q. Wang, Why Is Crystalline Poly(lactic acid) Brittle at Room Temperature?, (2019). https://doi.org/10.1021/acs.macromol.9b00595.

[98] M. Jamshidian, E.A. Tehrany, M. Imran, M. Jacquot, S. Desobry, Poly-Lactic Acid: Production, applications, nanocomposites, and release studies, Comprehensive Reviews in Food Science and Food Safety. 9 (2010) 552–571. https://doi.org/10.1111/J.1541-4337.2010.00126.X.

[99] D. Qin, L. Sang, Z. Zhang, S. Lai, Y. Zhao, Compression Performance and Deformation Behavior of 3D-Printed PLA-Based Lattice Structures, Polymers 2022, Vol. 14, Page 1062. 14 (2022) 1062. https://doi.org/10.3390/POLYM14051062.

A. COMPLETE STRESS-STRAIN CURVES

A.1. Tensile testing

A.1.1. Week 0

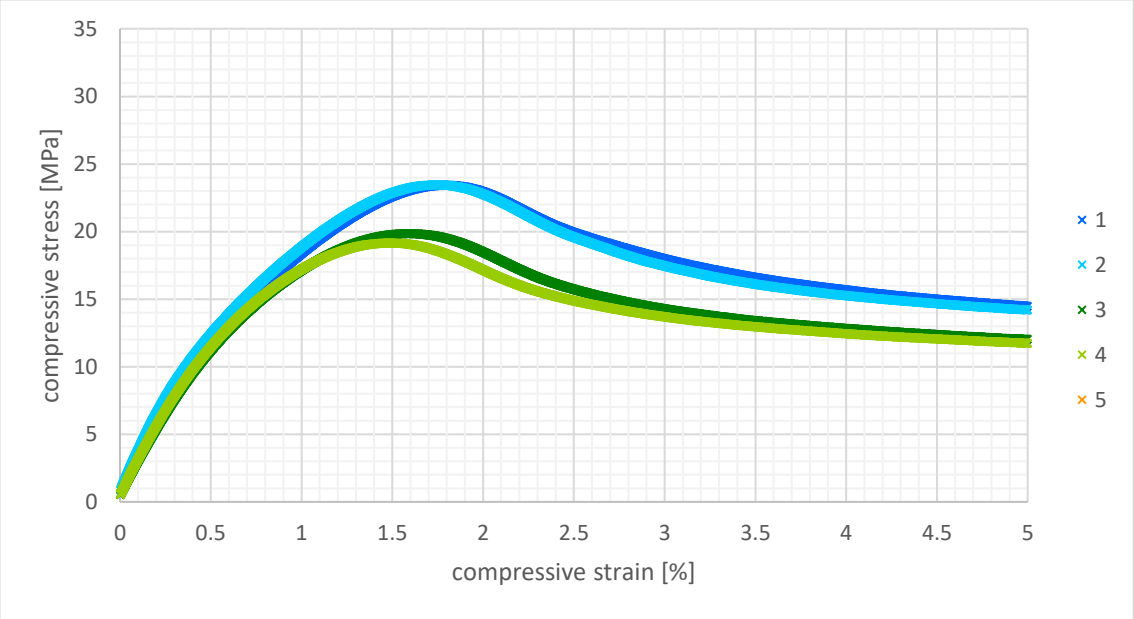

Figure i. Stress-strain curve from BaG composite tensile testing, week 0.

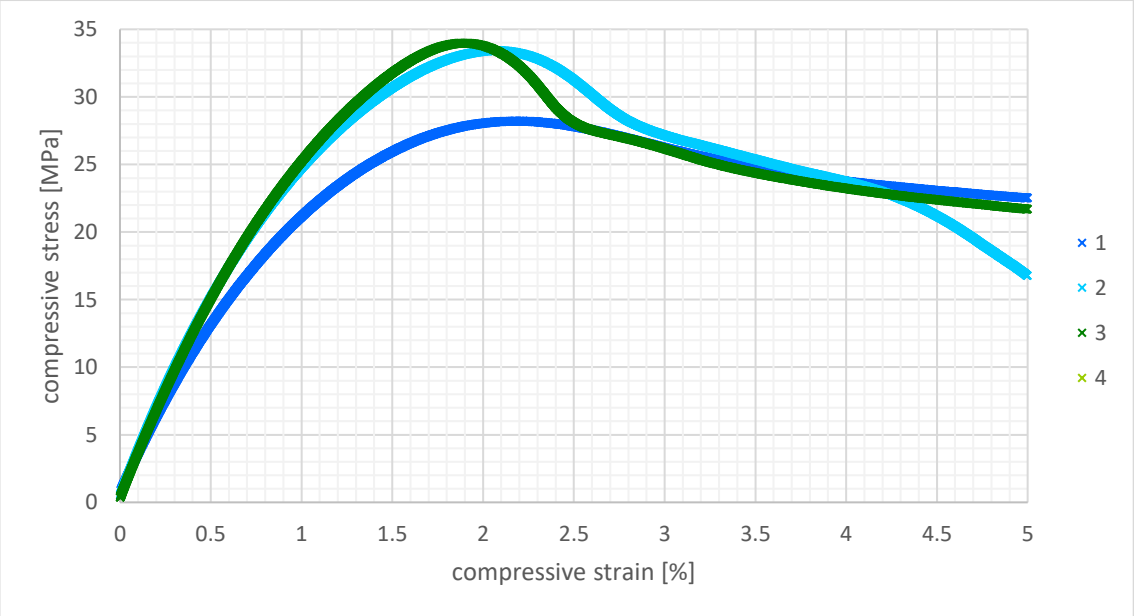

Figure ii. Stress-strain curve from TCP composite tensile testing, week 0.

A.1.2. Week 4

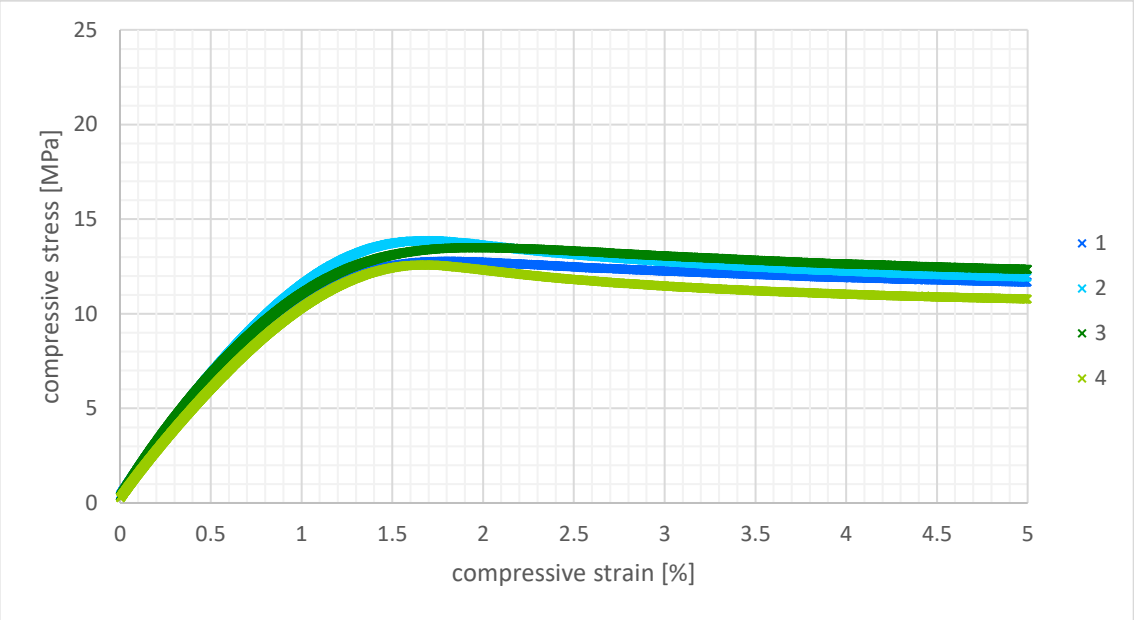

Figure iii. Stress-strain curve from BaG composite tensile testing, week 4.

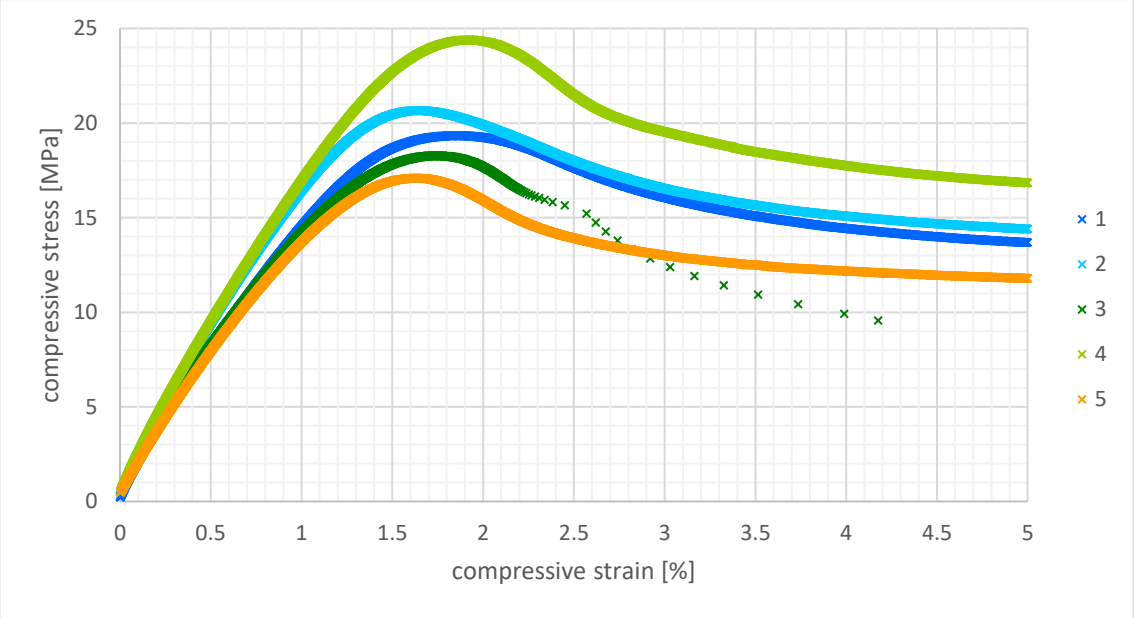

Figure iv. Stress-strain curve from TCP composite tensile testing, week 4.

A.1.3. Week 8

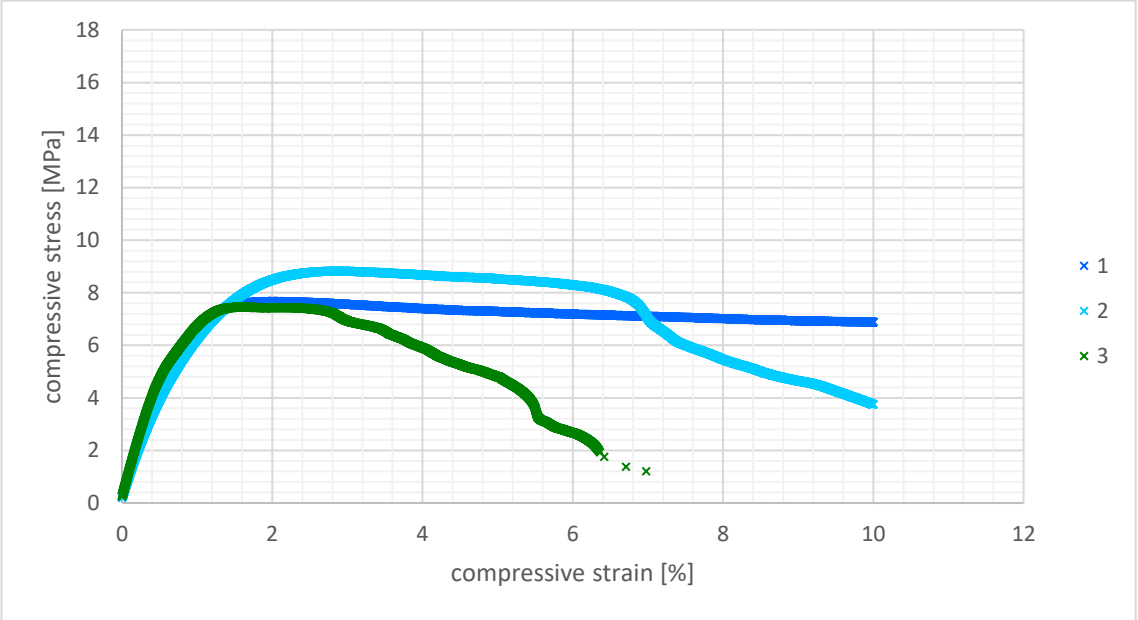

Figure v. Stress-strain curve from BaG composite tensile testing, week 8.

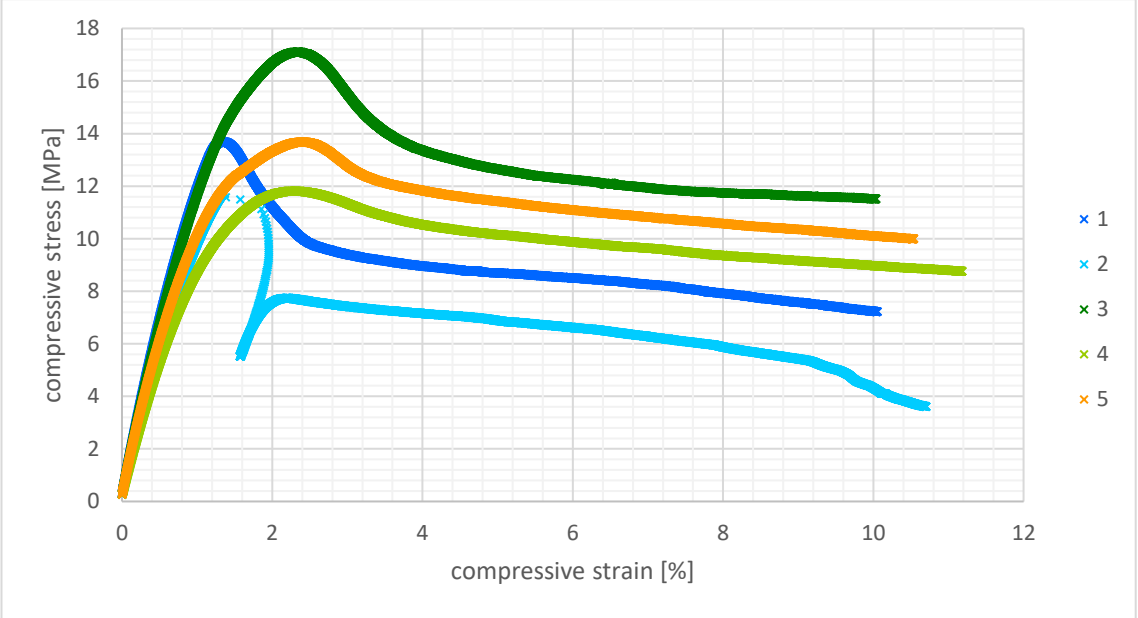

Figure vi. Stress-strain curve from TCP composite tensile testing, week 8.

A.1.4. Week 12

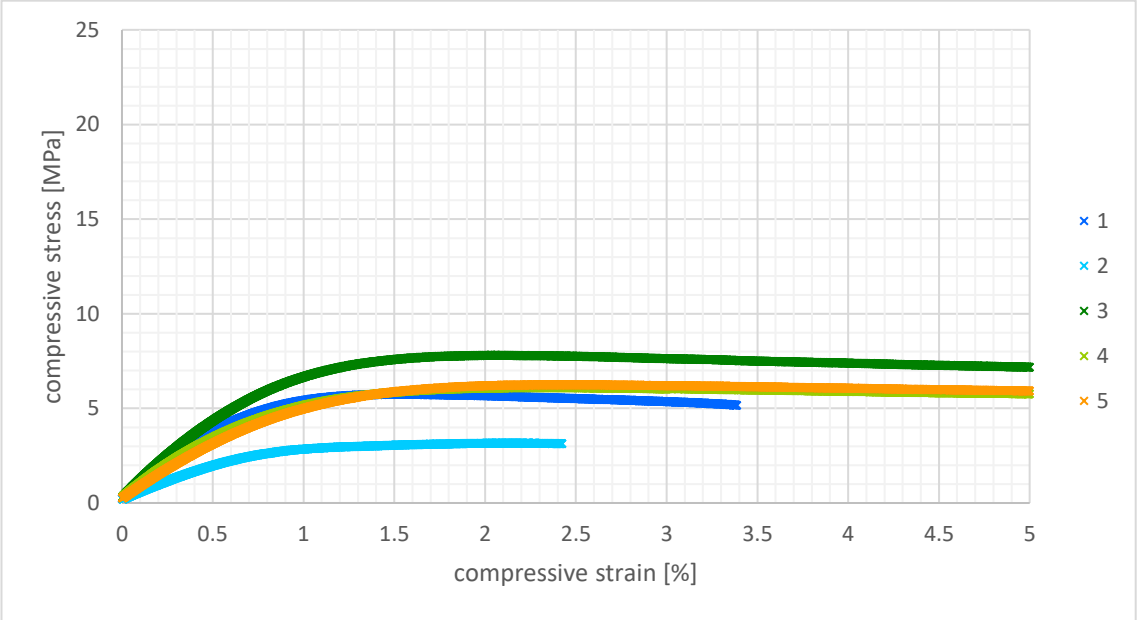

Figure vii. Stress-strain curve from BaG composite tensile testing, week 12.

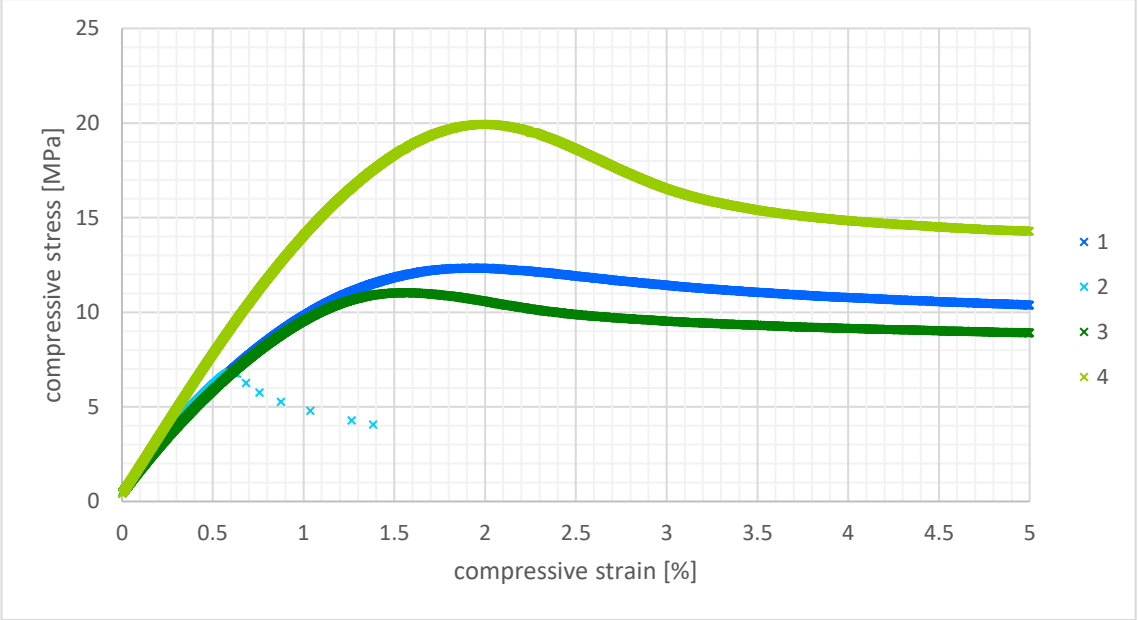

Figure viii. Stress-strain curve from TCP composite tensile testing, week 12.

A.2. Unconfined compression testing

A.2.1. Week 0

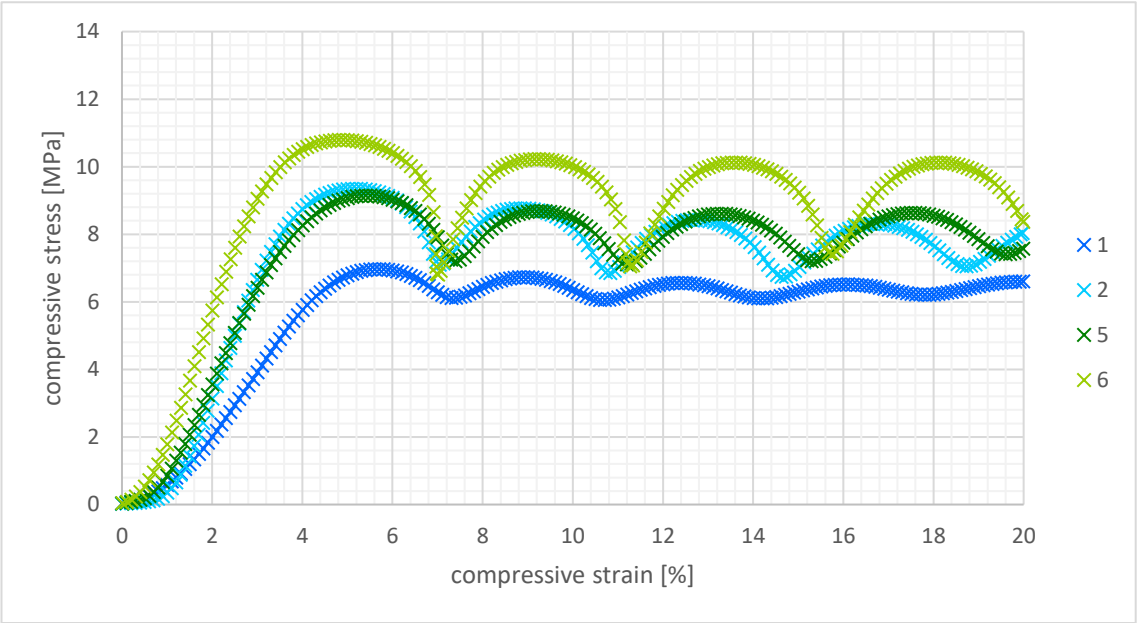

Figure ix. Stress-strain curve from BaG composite unconfined compression testing, week 0.

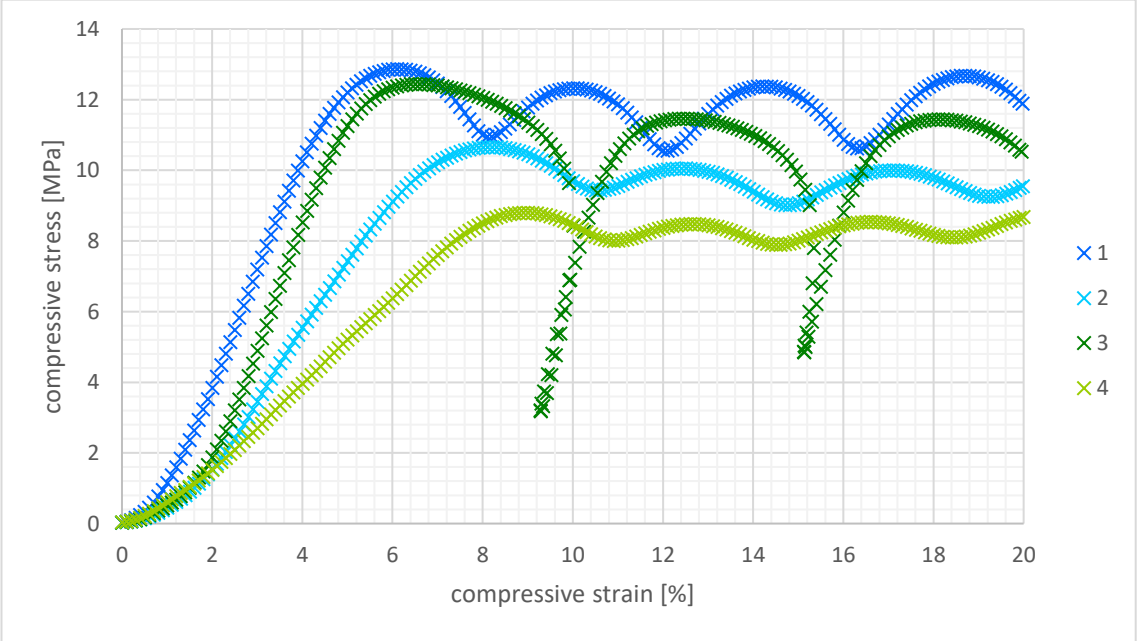

Figure x. Stress-strain curve from TCP composite unconfined compression testing, week 0.

A.2.2. Week 4

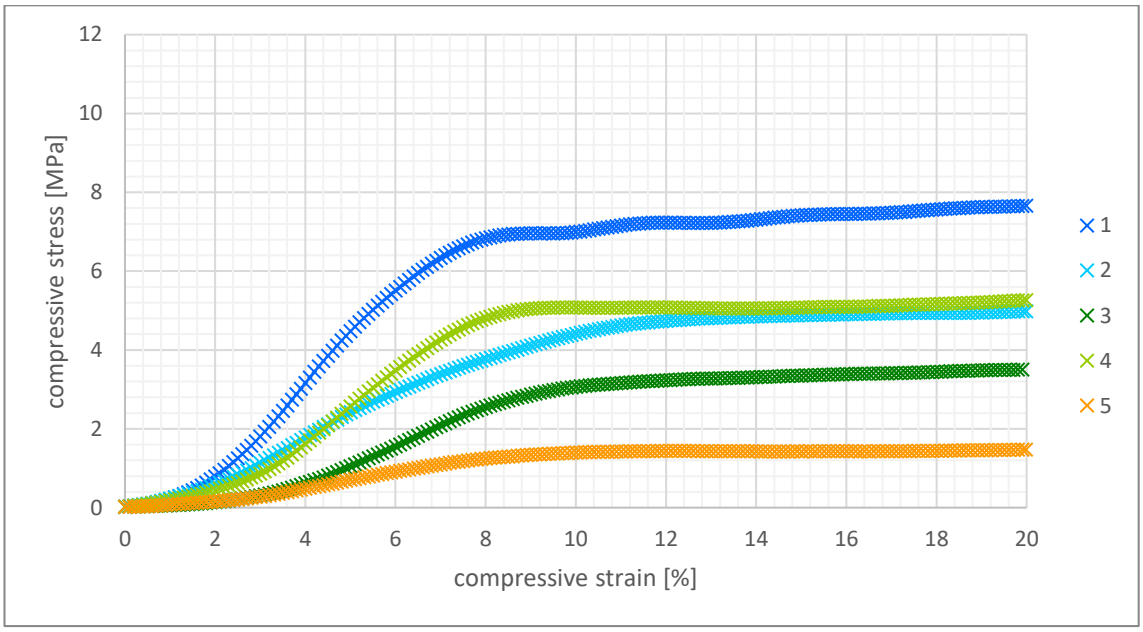

Figure xi. Stress-strain curve from BaG composite unconfined compression testing, week 4.

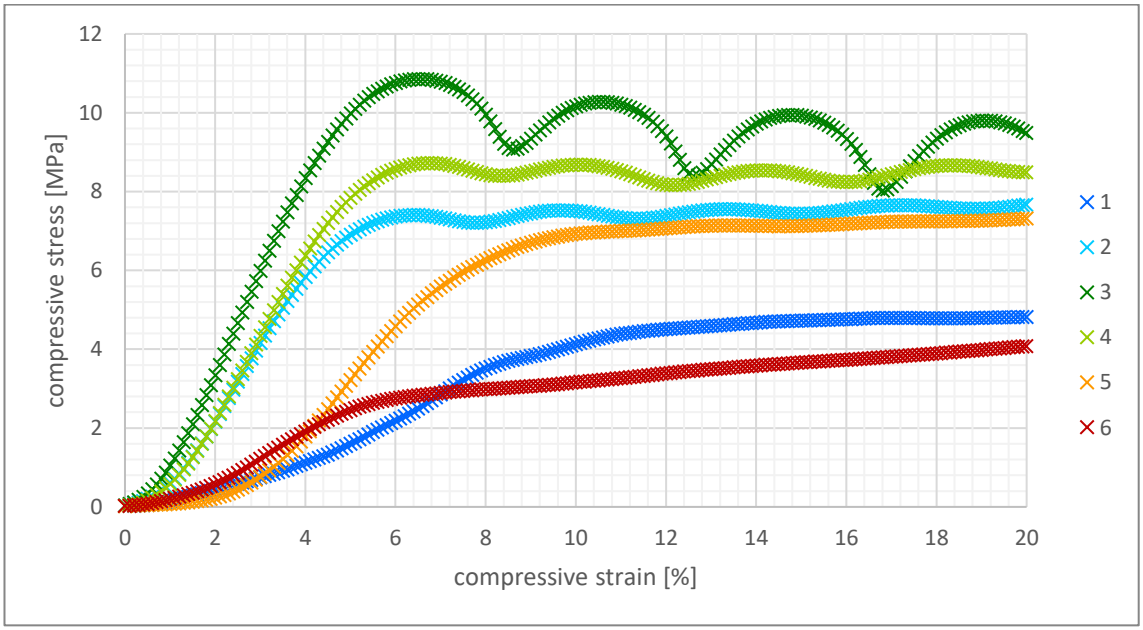

Figure xii. Stress-strain curve from TCP composite unconfined compression testing, week 4.

A.2.3. Week 8

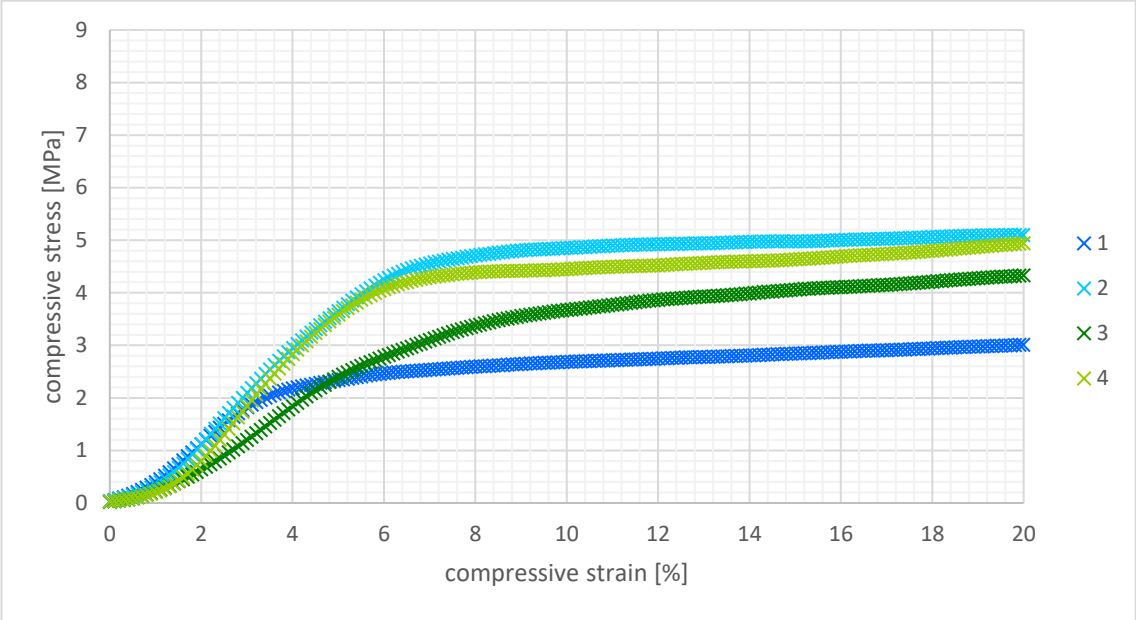

Figure xiii. Stress-strain curve from BaG composite unconfined compression testing, week 8.

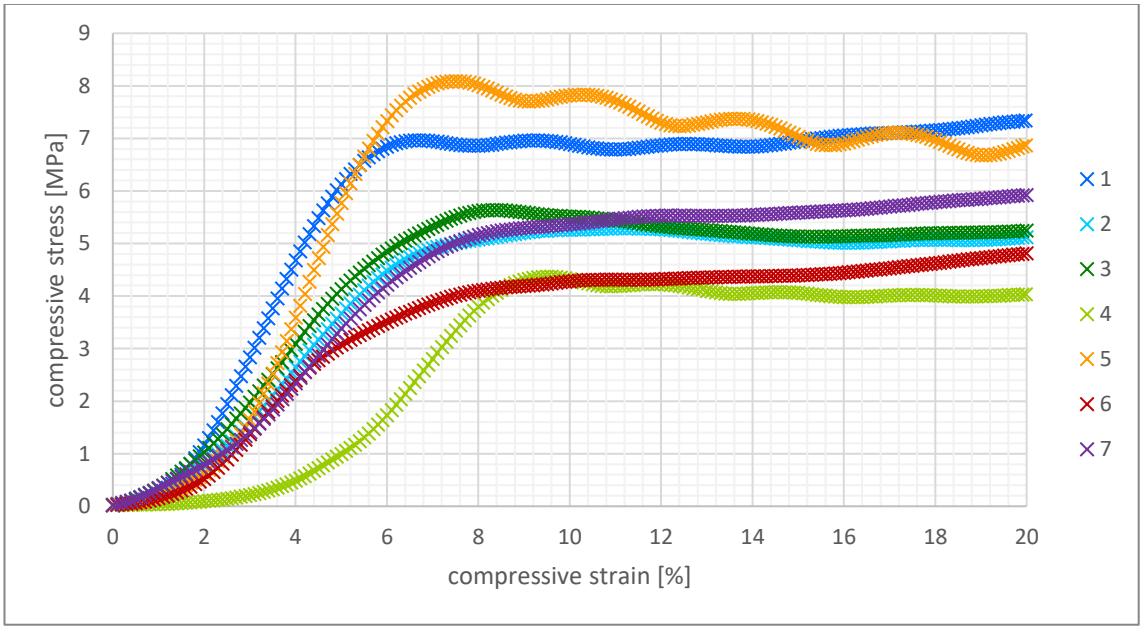

Figure xiv. Stress-strain curve from TCP composite unconfined compression testing, week 8.

A.2.4. Week 12

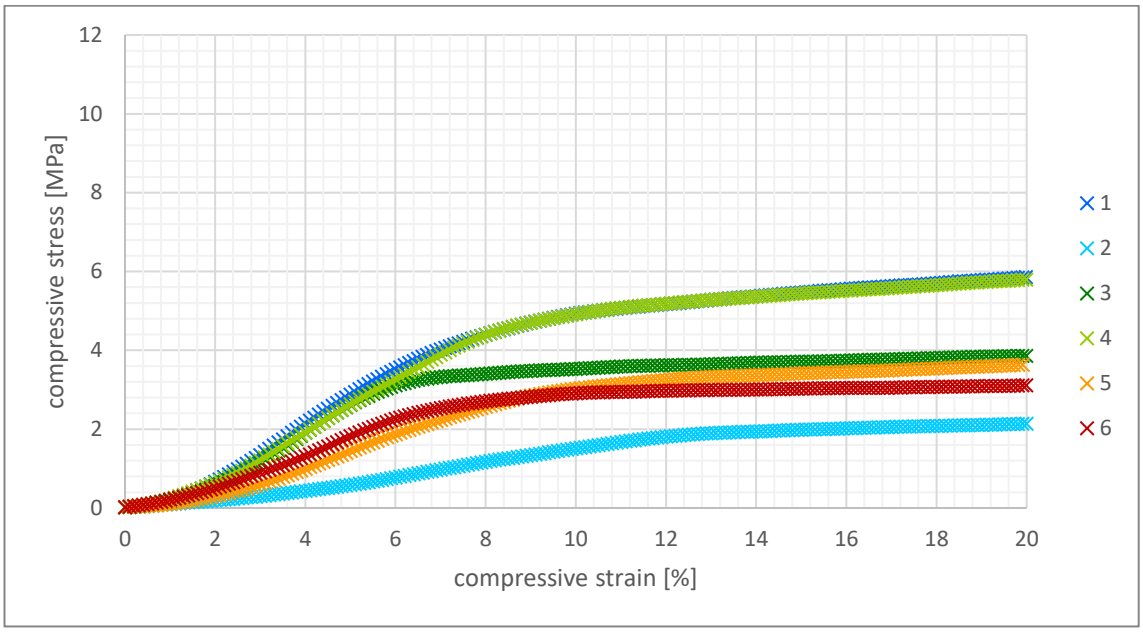

Figure xv. Stress-strain curve from BaG composite unconfined compression testing, week 12.

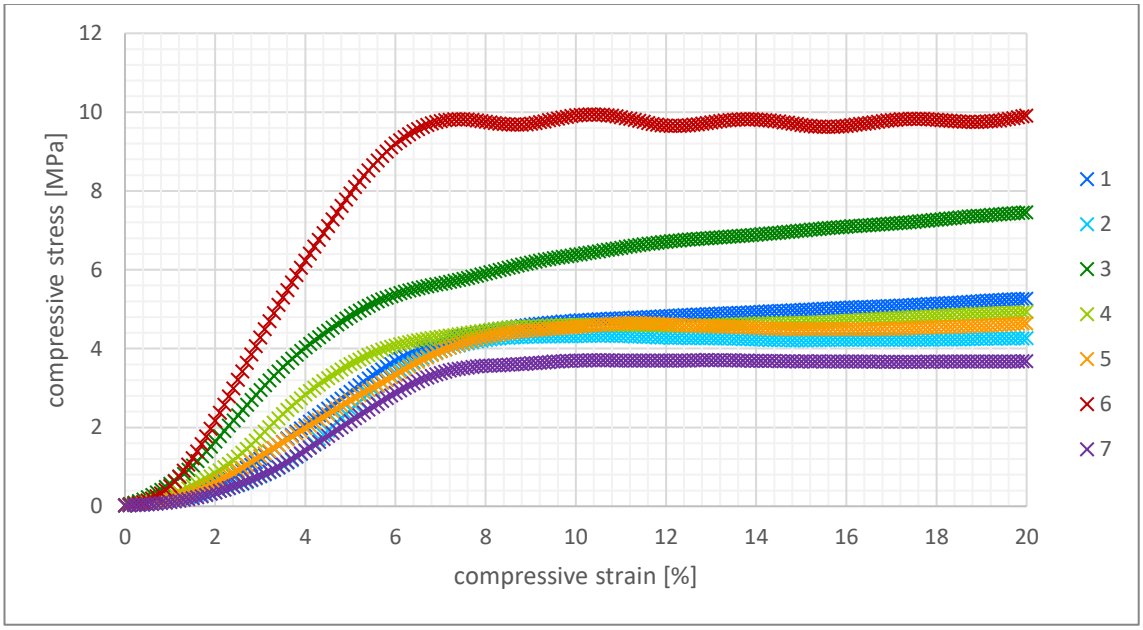

Figure xvi. Stress-strain curve from TCP composite unconfined compression testing, week 12.

A.3. Confined compression

A.3.1. Week 0

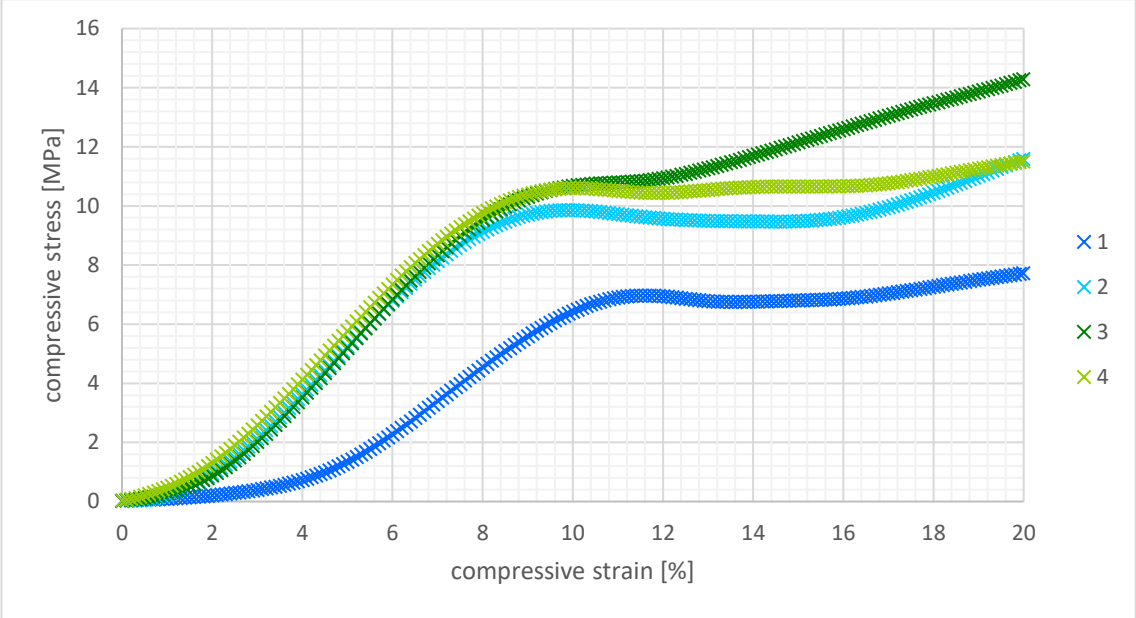

Figure xvii. Stress-strain curve from BaG composite confined compression testing, week 0.

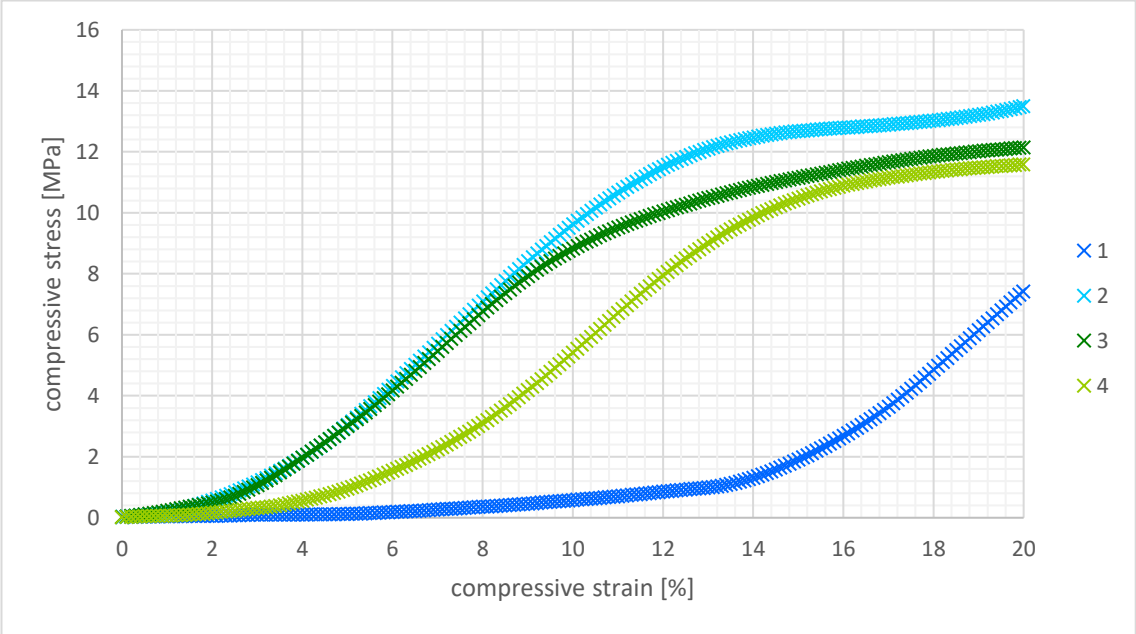

Figure xviii. Stress-strain curve from TCP composite confined compression testing, week 0.

A.3.2. Week 4

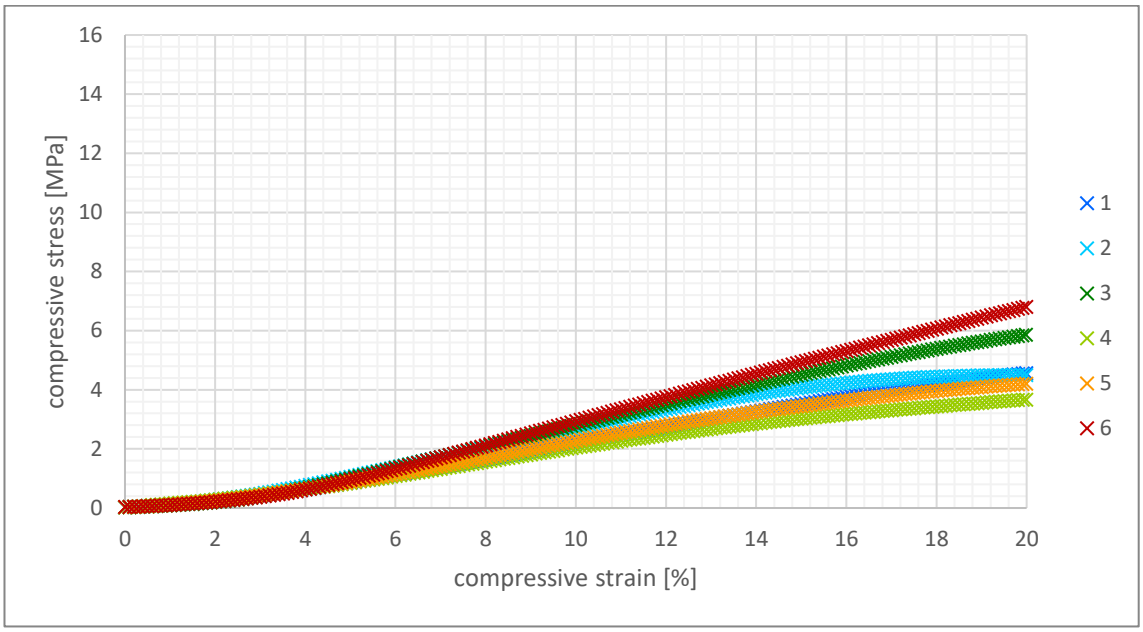

Figure xix. Stress-strain curve from BaG composite confined compression testing, week 4.

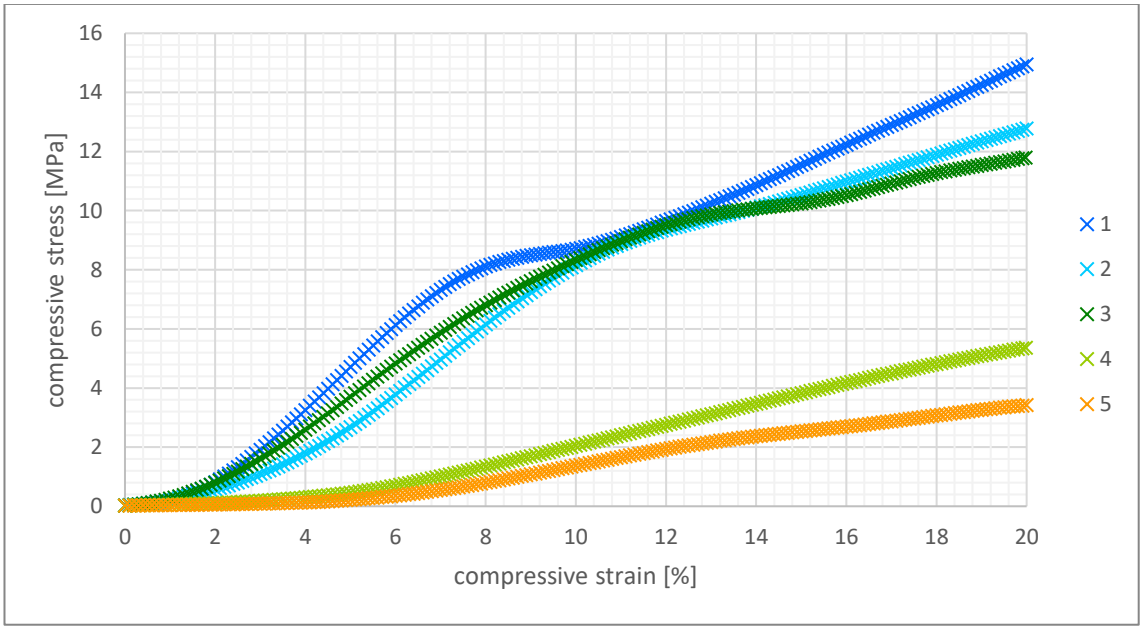

Figure xx. Stress-strain curve from TCP composite confined compression testing, week 4.

A.3.3. Week 8

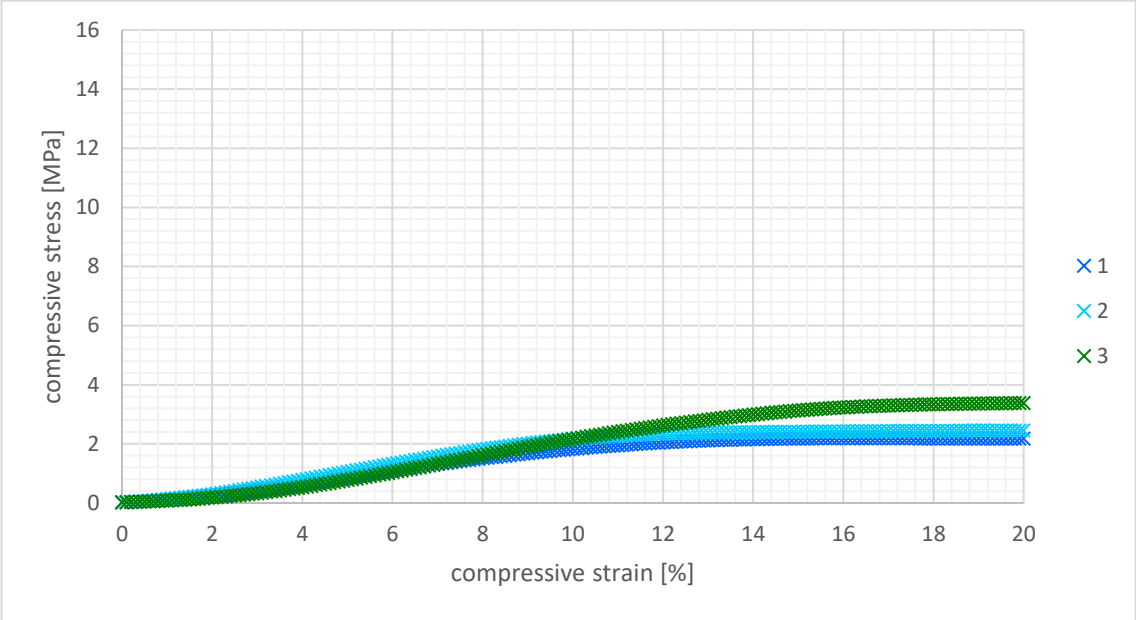

Figure xxi. Stress-strain curve from BaG composite confined compression testing, week 8.

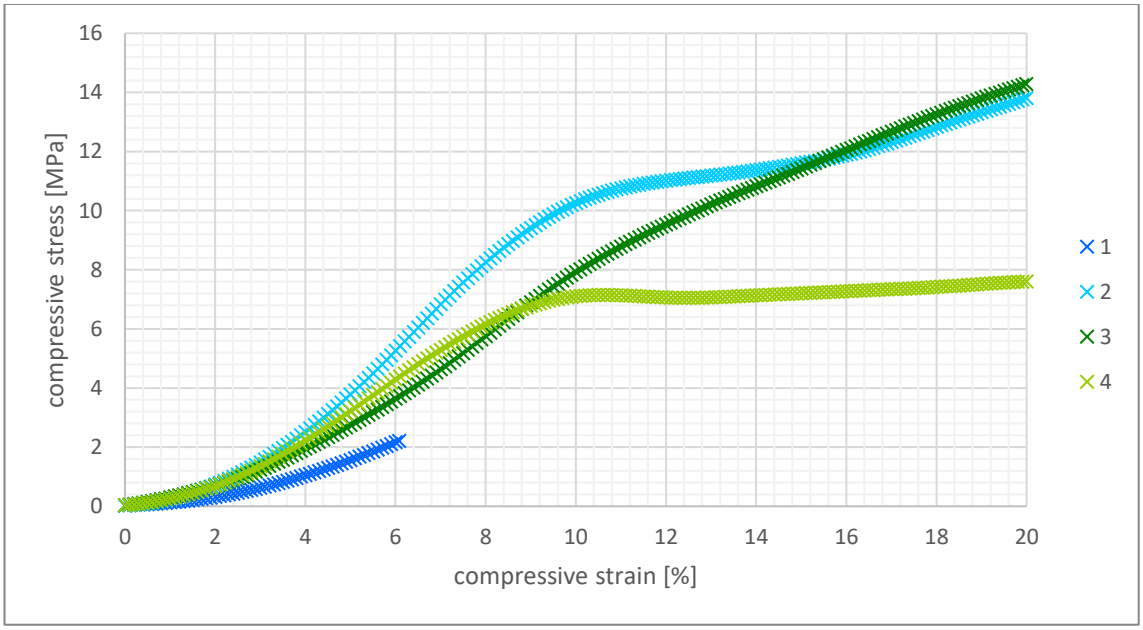

Figure xxii. Stress-strain curve from TCP composite confined compression testing, week 8.

A.3.4. Week 12

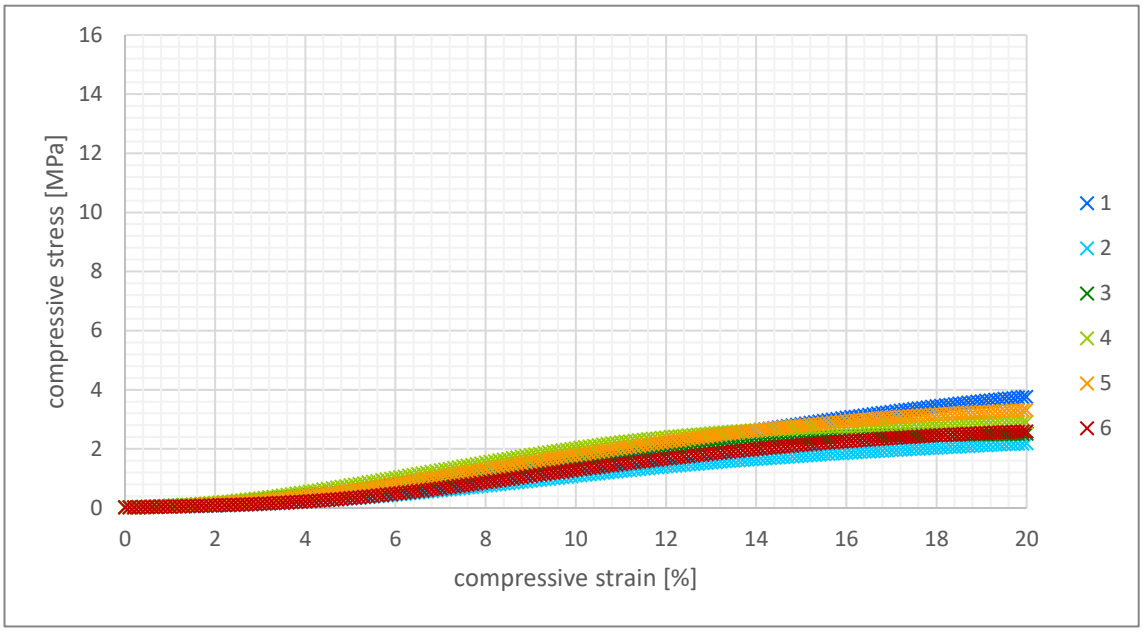

Figure xxiii. Stress-strain curve from BaG composite confined compression testing, week 12.

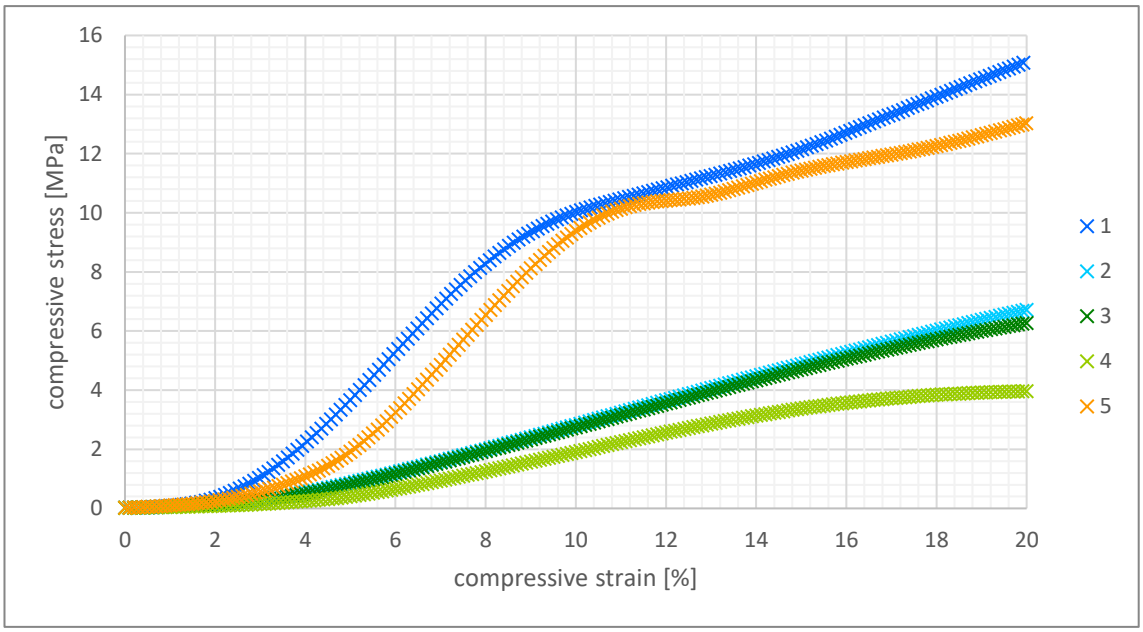

Figure xxiv. Stress-strain curve from TCP composite confined compression testing, week 12.